VTT WORKING PAPERS 157

Tero Sundström, Ari Kevarinmäki, Stefania Fortino & Tomi Toratti

Shear resistance of glulam beams under varying humidity conditions

ISBN 978-951-38-7498-8 (URL: http://www.vtt.fi/publications/index.jsp)
ISSN 1459-7683 (URL: http://www.vtt.fi/publications/index.jsp)

JULKAISIJA – UTGIVARE – PUBLISHER

VTT, Vuorimiehentie 5, PL 1000, 02044 VTT
puh. vaihde 020 722 111, faksi 020 722 4374

VTT, Bergsmansvägen 5, PB 1000, 02044 VTT
tel. växel 020 722 111, fax 020 722 4374

VTT Technical Research Centre of Finland, Vuorimiehentie 5, P.O. Box 1000, FI-02044 VTT, Finland
phone internat. +358 20 722 111, fax +358 20 722 4374

Series title, number and
report code of publication

VTT Working Papers 157
VTT-WORK-157

Author(s)

Tero Sundström, Ari Kevarinmäki, Stefania Fortino & Tomi Toratti

Title

Shear resistance of glulam beams under varying humidity conditions

Abstract

The research programme of this study included tests of 104 glulam beams. The aim of the experiments was to find out whether the variation of humidity affects the shear strength of large size glulam sections. It is known that moisture gradients are induced in dynamic humidity variations, and these produce internal stress distributions to wood members. The target of this study was to find out if these stress distributions have an effect on the shear strength of a glulam beam. The beams were divided into five test series and they were stored for different time periods in specific moisture conditions before testing. Beams were first conditioned in moist air (RH 90%) and then in dry air (RH 30%). The effect of different coatings was also studied since coatings may affect the moisture variations of a wood member caused by varying humidity. The results showed that moisture gradients caused by varying humidity conditions had no effect on the shear strength. Solely the actual mean moisture content of the beam seemed to affect the shear strength. The coatings applied were discovered to have only minor effects on the induced moisture gradients and no effect at all to the shear strength of the beams. The results give no evidence to the recommended crack factor (k_{cr} = 0,67) recently added to EN1995-1-1 design procedures for the reduction of shear resistance.The high initial moisture scatter between the material provided by one producer (out of four) disturbed the interpretation of test results especially when considering moisture content effects. The deviation in the moisture content measurement results was significant even when the moisture scatter from one producer was not taken into account. The differences in shear strengths between manufacturers had also an effect to the analysis of the results. The effects of moisture induced stresses could have been easier to observe if the material had been more homogenous. Finite element calculations were conducted to evaluate the moisture induced stresses in the beam. Calculations supported the obtained results that moisture gradients and moisture induced stresses do not decrease the shear strength of glulam beams. The calculated moisture induced stresses were small in those directions that had highest stresses in the actual loading. The visual examination of failure planes together with finite element calculations suggested that shear failure occurred because shear strengths in τ_{rl} and τ_{tl} directions of the local wood coordinate system were exceeded. Calculated moisture induced shear stresses were however small and local in those directions.

ISBN
978-951-38-7498-8 (URL: http://www.vtt.fi/publications/index.jsp)

Series title and ISSN		Project number
VTT Working Papers 1459-7683 (URL: http://www.vtt.fi/publications/index.jsp)		17546
Date January 2011	Language English	Pages 125 p. + app. 12 p.
Name of project Improved glued wood composites – modelling and mitigation of moisture induced stresses	Commissioned by	
Keywords Glulam, shear strength, moisture induced stresses	Publisher VTT Technical Research Centre of Finland P.O. Box 1000, FI-02044 VTT, Finland Phone internat. +358 20 722 4520 Fax +358 20 722 4374	

Preface

The present report documents research performed in the project: Improved glued wood composites – modelling and mitigation of moisture-induced stresses, which is a European project within the Woodwisdom-net program and funded by Tekes, VTT and the Building with Wood group (for the Finnish sub-project). The test material was donated by the Glulam Association of Finland.

The contributions and funding from the above mentioned parties is gratefully acknowledged.

The authors

Contents

Preface 4

1. Introduction 7

2. Moisture induced stresses in glulam beams 9
   - 2.1 Humidity conditions 9
   - 2.2 Moisture transport in wood 10
   - 2.3 Moisture induced stresses 14

3. Experimental programme 21
   - 3.1 Pre-test arrangements 22
     - 3.1.1 X-ray examination 22
   - 3.2 Test Humidity arrangements 26
   - 3.3 Coatings 27
   - 3.4 Test setup and loading arrangements 27
   - 3.5 Moisture content monitoring 31

4. Evaluation of shear stresses and elastic and shear moduli 33
   - 4.1 The effect of cross-section to shear strengths 33
   - 4.2 Calculation of stresses using Eurocode 5 and Euler-Bernoulli beam equation 34
   - 4.3 Calculation of elastic modulus from strain measures 36
   - 4.4 Calculation of shear modulus from strain measures 43
   - 4.5 Calculation of stresses using finite element method 46
     - 4.5.1 Elastic strains and stresses 47
     - 4.5.2 Strains and stresses from moisture content changes 57

5. Results 74
   - 5.1 Test series S1 77
     - 5.1.1 Strengths of test specimens 78
     - 5.1.2 Failure modes 80
     - 5.1.3 Moisture properties of test specimens 80
   - 5.2 Test series S2 81
     - 5.2.1 Strengths of test specimens 81
     - 5.2.2 Failure modes 84
     - 5.2.3 Moisture properties of test specimens 84
   - 5.3 Test series S3 85
     - 5.3.1 Strengths of test specimens 86
     - 5.3.2 Failure modes 88
     - 5.3.3 Moisture properties of test specimens 88
   - 5.4 Test series S4 89
     - 5.4.1 Strength of test specimens 89
     - 5.4.2 Failure modes 91
     - 5.4.3 Moisture properties of test specimens 92

5.5 Test series S5 93
5.5.1 Strength of test specimens 93
5.5.2 Failure modes 95
5.5.3 Moisture properties of test specimens 96
5.6 Results for the shrinkage in height direction 97
5.7 Results of the X-ray examination for all test series 99

6. Analysis of the results 101
6.1 Comparison of results of test series 101
6.1.1 Average moisture content 101
6.1.2 Moisture content gradient 105
6.1.3 Shear resistance 107
6.2 Effect of moisture induced stresses to the shear resistance 110
6.3 Effect of coatings 114
6.4 Relationship between elastic modulus and failure type 115
6.5 Effect of defects in beams 116
6.5.1 Defects in tension side of beams 116
6.5.2 Knots in the shear zone of beams 117

7. Conclusions 121

Acknowledgements 123

References 124

Appendices

Appendix A: Product information of used coatings
Appendix B: Measured variables of the specimens in the pre-test phase and the ultimate loads
Appendix C: Measured values of moisture content for all specimens

1. Introduction

This research programme is a part of the Improved Moisture research project which is included in the WoodWisdom-Net programme [1]. The objective of the Improved Moisture project is: "To find ways to manage the performance of load bearing timber structures in variable humidity conditions which these are exposed to by nature in their true environment. This includes developing design methods, detailing methods (including connections) and building instructions in such a way that the adverse effects related to moisture can be avoided and/or controlled. A good example is the control of cracking of glulam structures. The research will facilitate the understanding of the nature of moisture induced stresses, and new computational tools are developed to assess the strength of structures, and cracking of wood under weather exposure. The ultimate goal is to develop innovative wood composites which are significantly less sensitive to moisture variations." [2]

The shear resistance of timber and glulam beams has been under discussion in Europe. The winter 2005–2006 was snowy in Central Europe and over 50 roof failures took place in Germany, Austria and Poland [10]. Of course only a few of those broken roof structures were made of wood. However, the safety of wood structures was in the headlines of the media as in two failures that led to fatalities the roof structure was made of wood. In Germany there were few cases of failure where glulam beams, which were under high permanent actions and varying humidity conditions, had shear failures. Because of these failures concept of effective width was added to design of timber members in shear according to EN 1995-1-1. Relevant effective width is calculated from the nominal width by multiplying it with factor k_{cr}. For glulam and solid timber the recommended value of k_{cr} is 0,67 and for other wood-based products in accordance with EN 13986 and EN 14374 the recommended value for k_{cr} is 1,0. This increases calculated shear stress for certain loading up to 50%.

A glulam product is made by gluing timber boards together. The grain direction of the boards is aligned parallel to the longitudinal direction of the produced structural element. The cross-section dimensions of the boards vary; usually the thickness of the boards is approximately 45 mm and the width is no more than 215 mm. Timber boards, lamellas, are normally glued together from their faces. Glulam enables large timber cross-sections and reduces the effect of defects in timber.

This research programme includes a total of 104 glulam beams. The beams were supplied by 4 Finnish glulam manufacturers. The beams were grouped to 5 series. 4 main series consisted of 24 specimens and one reference series consisted of 8 specimens. The meaning of the reference series was to find out the shear resistance of real size Finnish glulam beams in the test setup chosen for this study. The results of the other series can then be compared to the results of the beams that had no moisture induced stresses. The main series were stored different time periods in specific moisture conditions. Part of the beams had different kind of coatings on them. Every main series had the same amount of coated and uncoated beams to see how the coatings affect the shear resistance. The reference series was uncoated.

2. Moisture induced stresses in glulam beams

2.1 Humidity conditions

The moisture content of wood depends on the relative humidity (RH) of the surrounding air. Glulam beams are used in many kinds of conditions. Most common conditions are like normal indoor conditions: no massive moisture sources and temperatures of approximately 20 °C. However, conditions can be very different, for example conditions in an indoor ice-skating ring or an indoor swimming pool.

In indoor circumstances the RH varies greatly especially in those countries that have yearly seasons. Cold air cannot contain much water. Outdoor air is cold and has big RH in the winter, but the absolute moisture content of air is actually quite small. After warming the outdoor air, the RH of air decreases greatly and this leads to low RH in indoor air.

Usually the RH of heated air is increased by different residential activities, but this is not always the case. The year-round average RH of indoor air in Helsinki with different residential related moisture regains is shown in Figure 1. The difference in RH between the moistest and driest period can be seen to be approximately 40% at greatest.

Glulam structure, just like any other structure, can also be exposed to liquid water in addition to air humidity. Usually this happens as a result of a construction defect. Exposure to liquid water can easily and rapidly increase the moisture content of wood.

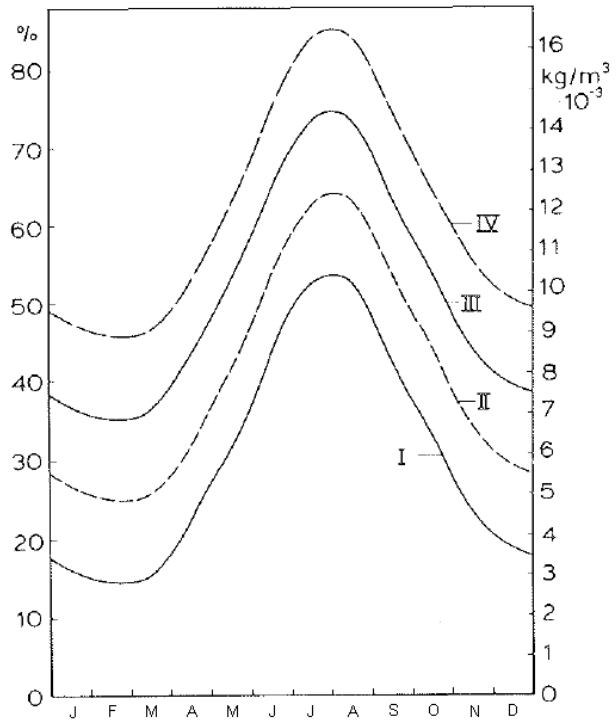

Figure 1. Average relative humidity of indoor air in Helsinki with different residential related moisture regains, indoor air temperature is 22°C. Moisture regains: I = 0 g/m³, II = 2 g/m³, III = 4 g/m³ and IV = 6 g/m³.

2.2 Moisture transport in wood

The transfer of water in wood is usually modelled in three ways; surface flow through cell walls due to a gradient in adsorbed amount between different locations, capillary flow due to a gradient in capillary pressure and gaseous diffusion of water vapour due to a gradient in partial vapour pressure [6].

Some mathematical models have been generated to describe the moisture transfer in wood. The simplest one is the Fick's law of diffusion which describes the evening out of the concentration differences because of thermal radiation of molecules [4]. The problem with the Fick's law is that it examines the phenomena only inside wood, and therefore it does not take into account what happens between the surface of the wood and the surrounding air. This means that there is a need for an additional theory for surface flow.

One-dimensional Fick's first law gives the diffusion flux in a concentration field and can be written as follows:

$$J = -D\frac{\partial \phi}{\partial x} \tag{1}$$

where J is the diffusion flux, $\frac{kg}{m^2 s}$

D is the material depending diffusion coefficient, $\frac{m^2}{s}$

ϕ is the concentration, $\frac{kg}{m^3}$

x is the position coordinate, m.

The minus sign in equation 1 shows that the flux is aligned towards the smaller concentration. Fick's second law predicts how concentration field changes in function of time. It can be derived from equation 1 as follows:

$$\frac{\partial \phi}{\partial t} = -\frac{\partial J}{\partial x} = \frac{\partial}{\partial x}\left(D \frac{\partial \phi}{\partial x} \right) \tag{2}$$

If diffusion coefficient D is kept constant, equation 2 can be simplified into form:

$$\frac{\partial \phi}{\partial t} = D \frac{\partial^2 \phi}{\partial x^2} \tag{3}$$

Keeping the diffusion coefficient D constant means that the direction dependence and nonlinearity of the moisture transport are not taken into account. In case of two or more dimensions, Fick's second law can be written as follows:

$$\frac{\partial \phi}{\partial t} = D \Delta \phi \tag{4}$$

where Δ is Laplace operator.

Equation 4 is analogous to Fourier's heat equation which describes the behaviour of a specific heat distribution over time.

The moisture transfer inside the wood is not the only matter that should be noticed when considering moisture transport in wood. A theory for moisture flow from the air to the surface of the wood and vice versa is as well needed. The moisture flow from the air to the surface can simply be defined as in equation 5 [11]:

$$q_n = \rho_0 \cdot S \cdot \left(u_{air} - u_{surf} \right) \tag{5}$$

where q_n is the value of the flow across the boundary
ρ_0 is the density of wood in absolute dry conditions
S is the surface emissivity
u_{air} is the equilibrium moisture content of wood corresponding to the air humidity
u_{surf} is the moisture content of the wood surface.

Moisture transfer in wood depends on the species of wood and the direction in which the transfer is examined. Heartwood and sapwood have different moisture transfer properties as well. If exposed to liquid water, the water absorption rate is much greater in the longitu-

dinal direction than in the perpendicular directions. When exposed to air humidity the difference is smaller. The dimension of timber in longitudinal direction is usually multiple times longer compared to dimensions perpendicular to grain and therefore longitudinal air humidity absorption can usually be ignored.

Spruce and pine have minor structural differences when considering moisture transport. The longitudinal water receptivity of spruce is lower than that of pine, especially if examining sapwood [5]. Figure 2 shows wood moisture content change in longitudinal direction when the other end perpendicular to grain of the test specimen was kept below water surface [5]. The longitudinal faces of the test specimens were carefully treated with dense moisture barrier lacquer, so that water would not migrate trough those faces. As can be seen, moisture content change was significantly slower in spruce. However, the difference between spruce and pine sapwood decreased after continuing the experiment over 7 days. Clear difference between spruce and pine heartwood could still be seen.

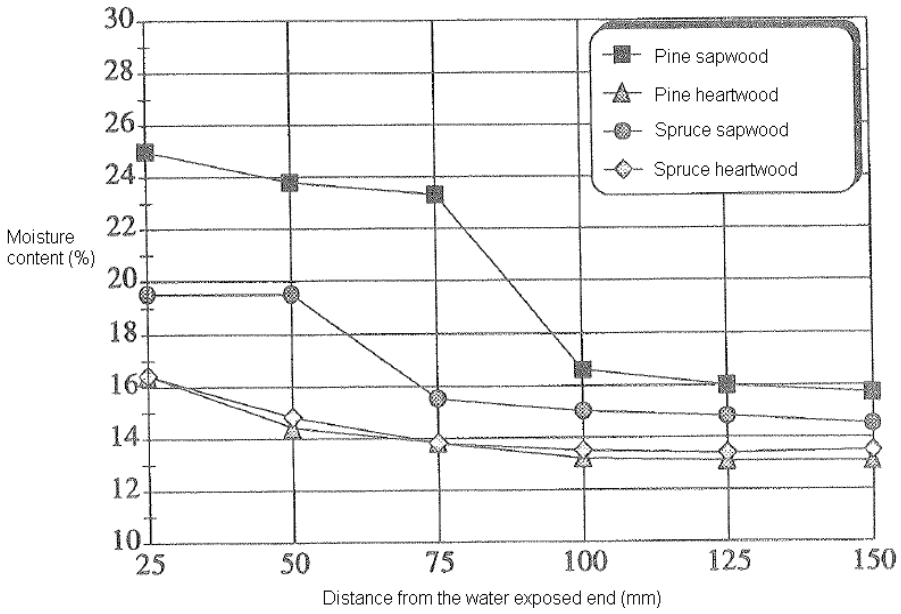

Figure 2. Moisture content in longitudinal direction after 2 hours expose to water [5].

Fortunately, in most cases glulam is rarely exposed to liquid water. Usually the moisture exposure is generated by air humidity. Moisture content variation in surfaces of wood specimens under cyclic varying humidity from RH 65% to RH 90% and vice versa is shown in Figure 3. The duration of one humidity cycle was 7 days [5]. Values were measured from longitudinal faces of the specimens. The moisture content of the surface varies approximately 4% between cycles as can be seen from the Figure 3.

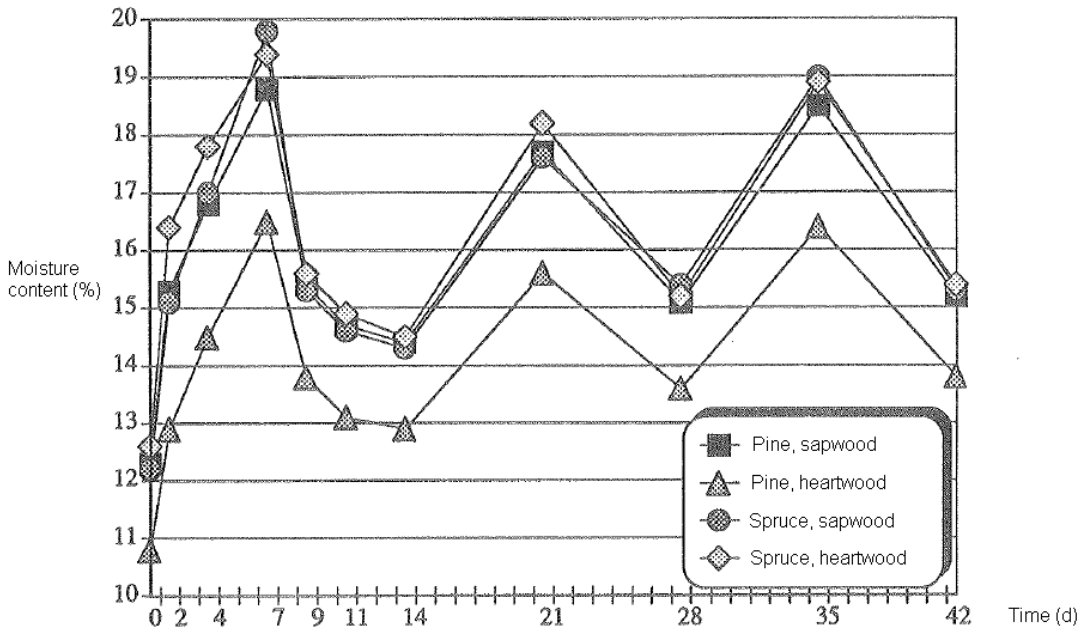

Figure 3. Moisture content of pine and spruce under cyclic varying humidity [5].

Moisture content variation in different depths of curved glulam beams under cyclic varying humidity is shown in Figure 4. The length of the humidity cycles was 4 weeks and the variation of RH was from 40% to approximately 85% [3]. Moisture content was measured with electrical resistance method on longitudinal faces of beams. The moisture content values were not supposed to be defined with a known accuracy, but the amplitude of moisture content during the cycles was assumed to be quite reliable. The difference between maximum and minimum moisture content values was about 3% in the depth of 10 mm and 1% in the depth of 45 mm. The moisture transport can be seen to be quite slow. However, the normal humidity cycles are longer than 4 weeks. The RH is high circa 4 months and low circa 6 months in normal conditions, as can be seen from Figure 1. The RH is near the annual average RH in rest of the months. Despite of the slow changes the moisture content change is a problem in the whole cross-section due to long humidity cycles.

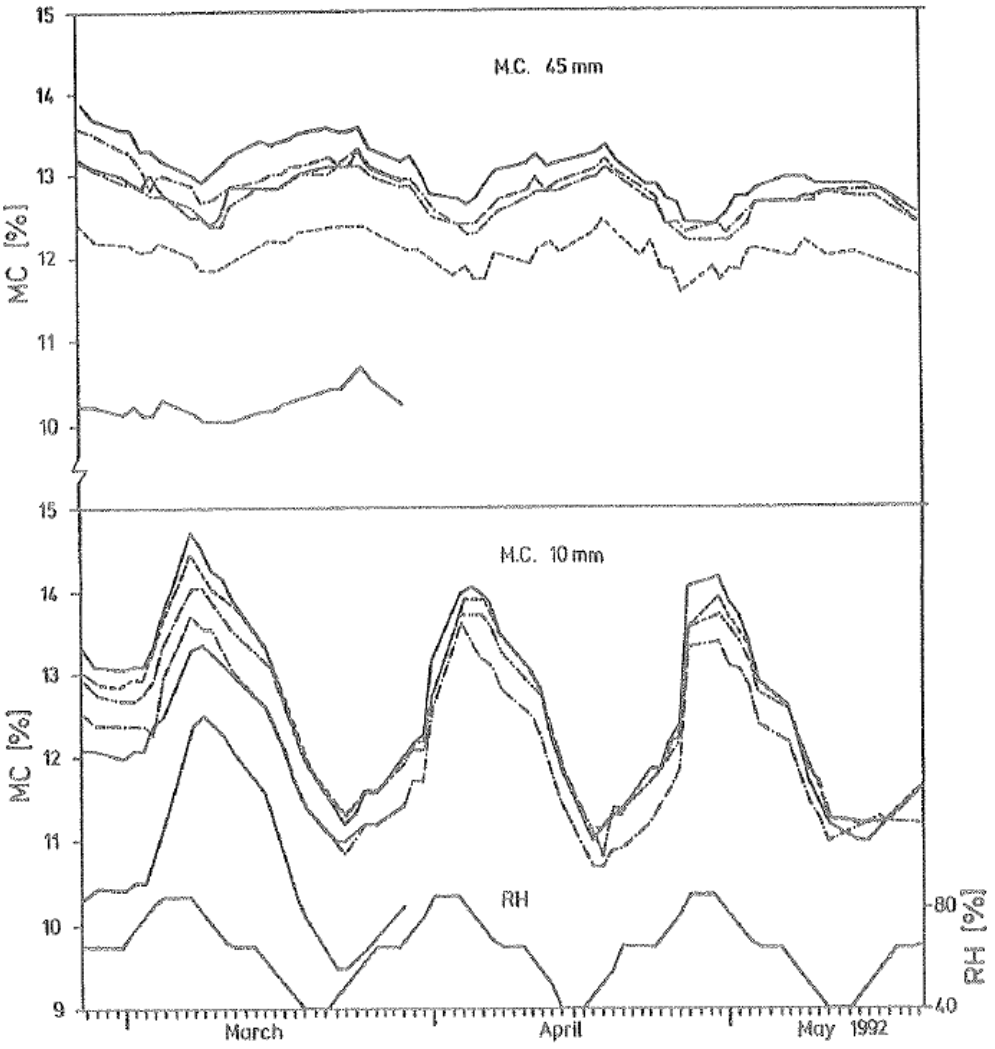

Figure 4. Moisture content in different depths of glulam timber beams under varying humidity [3].

2.3 Moisture induced stresses

The cross-sections of glulam beams are usually as in Figure 5 which shows the end face of a test specimen. The lamellas in the middle part of the beam are usually oriented so that adjacent lamellas have similar alignments if considering the place of the pith in the log from which they are made of. Alignment different than the previous one is used only between one of the outermost lamellas and the lamella next to it. The outermost lamellas are always aligned in such a way that the pith side is faced out from the beam.

Different moisture induced deformations in tangential and radial directions induce stresses to lamellas. If a glulam beam with an initial moisture content of 12% is exposed to a relative humidity of 90% for an adequate time, its average moisture content in the whole cross-section will increase to approximately 20%. This moisture content change will cause

deformations and stresses to the cross-section. The stresses will decrease over time due to the creep but they do not disappear totally from the cross-section. If the beam is then exposed to drier climate, there will be new stresses developed again.

The free deformations induced by moisture content change in a piece of wood can be calculated from equation 6:

$$\Delta x = x \cdot S \cdot \frac{\Delta MC}{fsp} \tag{6}$$

where Δx is the change in the considered dimension, mm
x is the considered dimension, mm
S is the total shrinkage percentage from green to oven-dry, %
ΔMC is the change in moisture content, %
fsp is the fibre saturation point, about 30% with spruce, %.

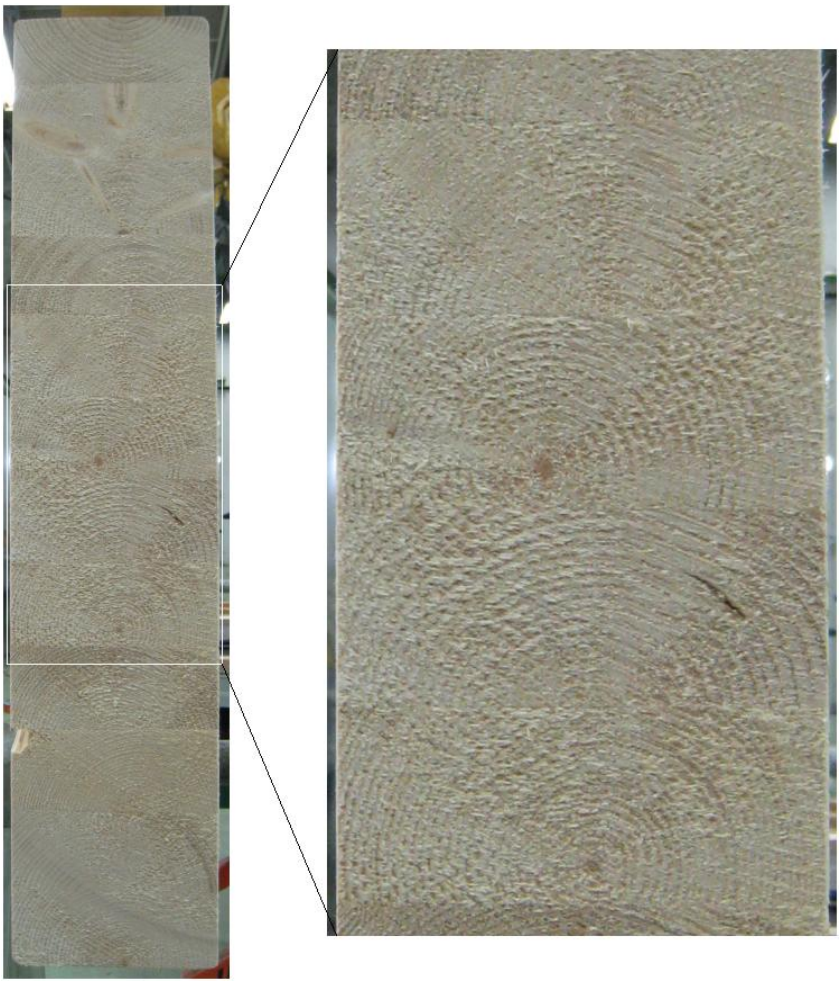

Figure 5. End face of a glulam beam, typical orientation of lamellas.

The free deformation of adjacent lamellas in tangential and radial directions can be calculated from equation 6. With a decrease of 8% MC, the width of lamellas with 115 mm nominal width changes about -1,1 mm in radial direction and -2,4 mm in tangential direction. The changes in the vertical direction of a lamella would be similar but approximately half of the changes in horizontal direction. This is due to the fact that the height of lamella is approximately half of its width. However, when lamellas are glued together, the free deformations cannot fully occur which results in moisture induced stresses to lamellas.

Moisture induced stresses affect also the stress state of a lamella because of different deformations in tangential and radial direction. This can be seen from the cross-section of a sawed log. Cracks parallel to radial direction can be seen quite soon after the drying of the log has started.

Lamellas of glulam timber are usually sawn from quite small logs near the pith. That is why lamellas have edges that are in both radial and tangential directions. It is easy to justify when considering moisture induced stresses in such a complex structure as a glulam timber, there should be a good material model and numerical methods to obtain proper evaluations of the stresses. The finite element method has been used generally in calculation of stresses.

Two different local coordinate systems used in the previous studies are shown in Figures 6 and 7 [4] [11]. The difference between these coordinate systems is that the system in Figure 6 does take into account neither the spiral grain nor conical angle.

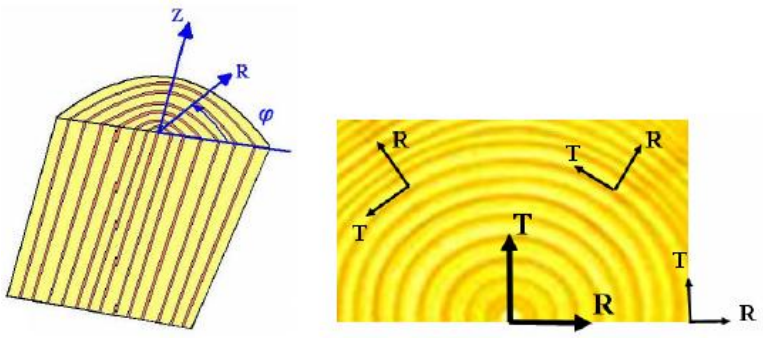

Figure 6. Local coordinate system [11].

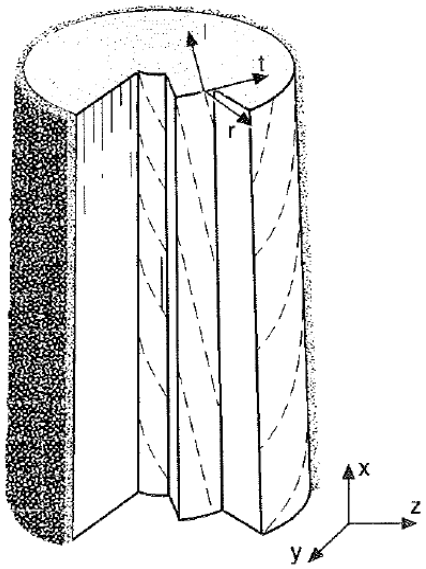

Figure 7. Local and global coordinate systems [4].

A material model should take into account different deformations, including elastic ε_e, moisture-induced ε_w, mechano-sorptive $\varepsilon_{w\sigma}$ and creep ε_c deformations. Equation 7 shows a way to calculate total strain:

$$\varepsilon = \varepsilon_e + \varepsilon_w + \varepsilon_c + \varepsilon_{w\sigma} + \varepsilon_{w\sigma}^{irr} \tag{7}$$

where $\varepsilon_{w\sigma}^{irr}$ is the irrecoverable part of the mechano-sorptive strain.

Equation 7 was used in a VTT project [11] and it is used in this study as well in the calculation of moisture induced stresses. The mechano-sorptive deformation is divided into recoverable and irrecoverable parts. A similar approach for the material model was used in a Swedish doctoral thesis [4] as well.

The elastic part, stresses are assumed to relate to elastic strains by Hooke's law. Relations of elastic deformations and stresses for an orthotropic material such as wood can be represented as follows:

$$\begin{aligned}
\varepsilon_l^e &= \frac{\sigma_l}{E_l} - \nu_{rl}\frac{\sigma_r}{E_r} - \nu_{tl}\frac{\sigma_t}{E_t}, \gamma_{lr}^e = \frac{\tau_{lr}}{G_{lr}} \\
\varepsilon_r^e &= \frac{\sigma_r}{E_r} - \nu_{lr}\frac{\sigma_l}{E_l} - \nu_{tr}\frac{\sigma_t}{E_t}, \gamma_{lt}^e = \frac{\tau_{lt}}{G_{lt}} \\
\varepsilon_t^e &= \frac{\sigma_t}{E_t} - \nu_{lt}\frac{\sigma_l}{E_l} - \nu_{rt}\frac{\sigma_r}{E_r}, \gamma_{rt}^e = \frac{\tau_{rt}}{G_{rt}}
\end{aligned} \tag{8}$$

where ε_l^e, ε_r^e and ε_t^e are the elastic normal strains in the orthotropic directions of the local coordinate system

γ_{lr}^{e}, γ_{lt}^{e} and γ_{rt}^{e} are the elastic shear strains in the orthotropic planes l-r, l-t and r-t in the local coordinate system

E_l, E_r and E_t are the elastic moduli in the orthotropic directions of the local coordinate system

G_{lr}, G_{lt} and G_{rt} are the shear moduli in the orthotropic planes l-r, l-t and r-t in the local coordinate system

ν_{lr}, ν_{rl}, ν_{lt}, ν_{tl}, ν_{rt} and ν_{tr} are the Poisson's ratios in the orthotropic directions

σ_l, σ_r and σ_t are the normal stresses in the orthotropic directions in the local coordinates

τ_{lr}, τ_{lt} and τ_{rt} are the shear stresses in the orthotropic planes l-r, l-t and r-t in the local coordinate system.

Equations in equation 8 can be expressed as matrices as follows:

$$\bar{\varepsilon}_e = \begin{bmatrix} \varepsilon_l^e \\ \varepsilon_r^e \\ \varepsilon_t^e \\ \gamma_{lr}^e \\ \gamma_{lt}^e \\ \gamma_{rt}^e \end{bmatrix}, \bar{\sigma} = \begin{bmatrix} \sigma_l \\ \sigma_r \\ \sigma_t \\ \tau_{lr} \\ \tau_{lt} \\ \tau_{rt} \end{bmatrix}, \bar{C} = \begin{bmatrix} \frac{1}{E_l} & -\frac{\nu_{rl}}{E_r} & -\frac{\nu_{tl}}{E_t} & 0 & 0 & 0 \\ -\frac{\nu_{lr}}{E_l} & \frac{1}{E_r} & -\frac{\nu_{tr}}{E_t} & 0 & 0 & 0 \\ -\frac{\nu_{lt}}{E_l} & -\frac{\nu_{rt}}{E_r} & \frac{1}{E_t} & 0 & 0 & 0 \\ 0 & 0 & 0 & \frac{1}{G_{lr}} & 0 & 0 \\ 0 & 0 & 0 & 0 & \frac{1}{G_{lt}} & 0 \\ 0 & 0 & 0 & 0 & 0 & \frac{1}{G_{rt}} \end{bmatrix}, \bar{\varepsilon}_e = \bar{C}\bar{\sigma} \qquad (9)$$

The compliance matrix $\bar{C}$ is usually assumed to be symmetric. Because of this Poisson's ratios are related with each other as follows:

$$\nu_{rl} = \frac{E_r}{E_l}\nu_{lr},\ \nu_{tl} = \frac{E_t}{E_l}\nu_{lt},\ \nu_{tr} = \frac{E_t}{E_r}\nu_{rt} \qquad (10)$$

The magnitudes of shear and elastic moduli depend on moisture content and temperature as mentioned before. The influence of temperature and moisture content is usually assumed to be linear. If variations of the moisture content and the temperature are observed, equations 9 are functions of time since then moisture content and temperature are time related.

Moisture induced strains can be modelled in the same way as mentioned before in equation 6. Because the definition of strain is the change of examined dimension divided by the original dimension, moisture induced strains can be expressed as matrices as follows:

$$\bar{\varepsilon}_w = \begin{bmatrix} \varepsilon_l^w \\ \varepsilon_r^w \\ \varepsilon_t^w \\ \gamma_{lr}^w \\ \gamma_{lt}^w \\ \gamma_{rt}^w \end{bmatrix}, \quad \bar{\alpha} = \begin{bmatrix} \frac{S_l}{fsp} \\ \frac{S_r}{fsp} \\ \frac{S_t}{fsp} \\ 0 \\ 0 \\ 0 \end{bmatrix}, \quad w = MC, \quad \bar{\varepsilon}_w = \bar{\alpha} w \tag{11}$$

where ε_l^w, ε_r^w and ε_t^w are the normal strains in the orthotropic directions of the local coordinate system

γ_{lr}^w, γ_{lt}^w and γ_{rt}^w are the shear strains in the orthotropic planes l-r, l-t and r-t in the local coordinate system

S_l, S_r and S_t are the total shrinkage percentage from green to oven-dry, %

fsp is the fibre saturation point, about 30 % with spruce, %

MC is the moisture content, %.

As can be seen from the zero values in matrix α it is assumed that a moisture content change does not cause shear strains. For an orthotropic material such as wood this simplified assumption is not precisely correct, because shrinkages are direction dependent. Therefore this assumption causes some error to the calculations. Nevertheless, this kind of simplified assumption is used in both of the previous studies [4] [11].

Mechano-sorptive creep is the difference of deformations between a specimen in varying humidity and in constant humidity, when the loading arrangements are otherwise similar. The equations used in the modelling of the mechano-sorptive creep are complicated and are not shown in this study. The equations applied can be found for example from references 10 and 18.

Viscoelastic creep deformations are time-dependent strains that develop when exposing the specimen under constant stresses in fixed environmental conditions. The creep strain is direction dependent and highly influenced by moisture content, temperature and stress level. The handling of the creep is quite similar to the handling of mechano-sorptive creep, at least in the two studies [4] and [11]. Creep is usually divided to recoverable and irrecoverable strains. The recoverable part of the strain will recover in some time after the load is removed. That is to say, the recovery is not instant but is time dependent.

Because mechano-sorptive and viscoelastic creep are time dependent also environmental conditions should be expressed as a function of time. Then, the moisture induced strain is also a function of time and if the elastic and the shear moduli are modelled as function of temperature and moisture content, the elastic strains are also functions of time.

The previous equations are defined in the local coordinates. In practice the loads interact in directions of the global coordinate system and there is a need to make a coordinate system transformation. This can also be quite complicated, at least if spiral grain and conical angle are taken into consideration. That is probably why coordinate system in the VTT study [4] was a simplified version of the Swedish study [11], see Figures 6 and 7.

3. Experimental programme

The aim of the experimental programme was to determine the shear resistance of straight glulam beams under varying humidity conditions. A total of 104 glulam beams were supplied by 4 Finnish glulam manufacturers for the programme.

The beams were divided to 5 series after their arrival. The beams were numbered, photographed and also X-ray photographed. After this, the beams were conditioned in 65% relative humidity and in ca. 20°C temperature. Four main samples, S2–S5, consisted of 24 beams each and initial reference sample, S1, had 8 beams. The nominal dimensions were; length 3200 mm, width 115 mm and height 540 mm. Beams had 12 lamellas. Beams had different coatings; 1 layer of AQUATOP 2600 varnish from Teknos Ltd, 2 layer of AQUATOP 2600 varnish and one layer of Linogard Underhållsolja from Linotech LTD. There were also beams with no coating for reference.

The manufacturers who supplied the beams were Kestopalkki LPJ Ltd, Late Rakenteet Ltd, PRT-Lami Ltd and Versowood Ltd. Every manufacturer supplied 26 beams. Both Late Rakenteet Ltd and Versowood Ltd supplied 12 beams which were coated with one layer of AQUATOP 2600 varnish, 12 beams which were coated with two layers of AQUATOP 2600 varnish and 2 beams which were uncoated. Both Kestopalkki LPJ Ltd and PRT-Lami Ltd supplied 26 uncoated beams, from which total of 24 beams were coated with one layer of Linogard Underhållsolja in VTT before other pre-test arrangements were carried out. 28 of the beams Kestopalkki LPJ Ltd and PRT-Lami Ltd supplied were left uncoated.

In every main test series, S2–S5, there were 6 specimens with two layer of AQUATOP 2600 varnish, 6 specimens with one layer of AQUATOP 2600 varnish, 6 specimens with one layer of Linogard Underhållsolja and 6 uncoated specimens. Each of these groups of 6 specimens (treated the same way) were formed so that three of the specimens were made by one manufacturer and the other three were made by another manufacturer. Thus every main test series had 3 beams treated/untreated in a certain way from one manufacturer. The reference test series, S1, had 8 uncoated specimens, two from every manufacturer.

The purpose of the reference test series S1 was to create material for comparing the results of the moisture strained series. The beams for the reference test series were chosen to

be from every manufacturer participating in the project. This way the quality differences of wood and differences in manufacturing can be determined. The average value obtained for the shear resistance from the test sample S1 covers the differences between manufacturers. Glulam manufacturers usually use timber near the factory and because the habitat of tree affects e.g. its density, there can be quite considerable density differences between the manufacturers. Density correlates with the strength properties and therefore it should be noticed. The possible strength grading differences are another matter that makes divergence between products of different manufacturers. There should not be great differences in strength grading but still differences are possible. Qualities of finger joints have also divergence as well as the moisture content of the product. These differences lead to the need of reference test series.

3.1 Pre-test arrangements

Pre-test arrangements started by choosing the bottom edge of beam. The bottom edges were chosen not to have big knots or joints in the middle of beam to avoid bending failures. The beams were weighed and marked up. The main dimensions of the beams were also measured. Length was taken with a tape measure. Width was measured from both upper and bottom edges in both ends of the beam. Height of the beam was measured from both ends. Width and height were measured with a slide gauge. After dimensions were measured both faces and ends were photographed and also X-ray examination was made to every beam. After pre-test arrangements the beams were stored in a relative humidity of 65% and in approximately 20°C.

Marking of the beams was done so that in every main test series beams 1–3 and 7–9 are coated with two layers of AQUATOP 2600 varnish, beams 4–6 and 10–12 are coated with one layer of AQUATOP 2600 varnish, beams 13–15 and 19–21 are coated with one layer of Linogard linseed oil and beams 16–18 and 22–24 are uncoated. The results from pre-test measurements are in Appendix B.

3.1.1 X-ray examination

As noted before, X-ray examination was done to every beam before conditioning. X-ray examination enables to see behind the surface of the beam. Properties of the beams can be studied in more detail.

X-ray examination is based on the ability of X-ray photons to transmit through different materials. Part of the X-ray photons is absorbed into the material under examination while the rest of the X-ray photons transmit all the way to the X-ray detector. The portion of absorbed X-ray photons depends mainly from the density and the thickness of the part under examination. When a beam with constant dimension in the studied direction is radiated with constant intensity throughout its length, the density differences in the beam can be

seen in the detector where transmitted intensities are detected. A picture is formed from the measurements in the detector.

The X-ray examination reveals knots, year rings, defects, finger joints and density differences between lamellas easily. Figure 8 shows an example picture of an X-rayed beam.

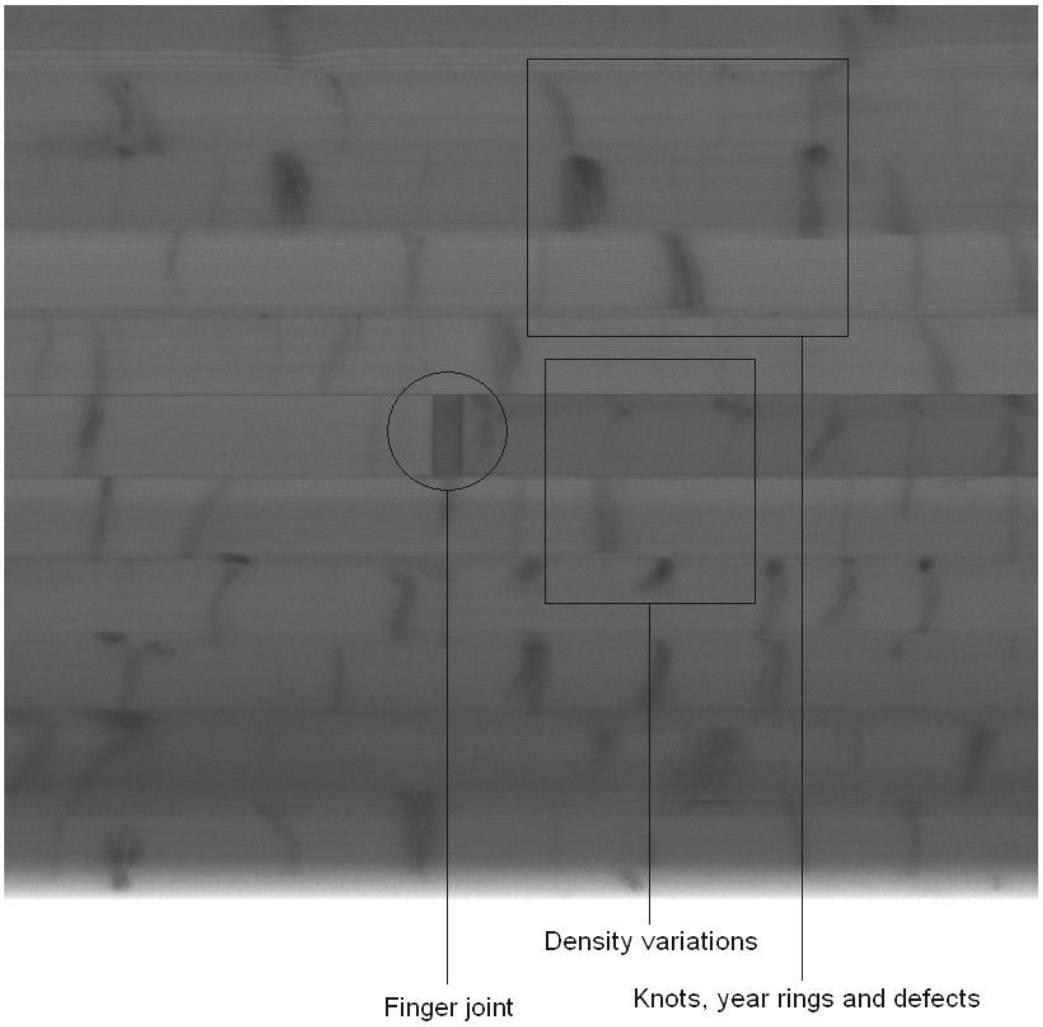

Figure 8. Part of a X-ray examined beam.

Inspex X-ray inspection system was used in the X-ray examination. The system has 235 kV X-ray source, two different detectors with pixel sizes of 0,4 mm and 1,5 mm and high resolution digital RGB line camera for documenting outer surfaces. A 0,4 mm detector was used in the examinations. There is also a conveyor system that moves the part that is being examined with constant velocity through the X-ray machine. The detector is of a linear type and examines one line at time. The velocity of the conveyor system and the speed of the detector are synchronized so that the generated picture is continuous.

The X-ray instrumentation was not able to picture the whole height of the beam. Therefore little less than one lamella in upper edge of the beam was not pictured. Another problem with the inspection system used was that the X-ray source was a point type one and had a limiter that aligned the X-ray photons linearly. This means that X-ray photons do not meet the examined part perpendicularly if the part is not straight below the source. This is a troublesome feature when examining materials that have quite low density since X-ray photons scatter into different directions especially when they do not meet the part examined perpendicularly. When hitting the material perpendicularly there is significantly less scattering. The density of wood is so small that the scattering effect occurs. This means that the X-rays scattered in the edges of the beam so that the accuracy of the picture is decreased. The scattering phenomena can be seen in the lower edge of Figure 8. The whole height of the beam was thus not properly pictured. Yet from the important middle part of the beam, if considering shear strength, the pictures were of good quality. However, the picture quality was sufficient also in the edges so that e.g. the defects in the tension side edge were seen quite well.

X-ray pictures were analysed with image processing software ImageJ. The analyzed variable was Mean Grey Value which was defined to a specific area. Each pixel in the analysed pictures has its own grey tone and the specific tone has its own value. X-ray pictures were 16 bit type so that there were 14262 different tones for grey in every pixel. Small grey value means that pixels tone is close to black and big value means that the tone is close to white. Mean Grey Value is the average value of the grey tone values in a certain area.

A mean Grey Value was defined for every beam so that the area analysed from the picture was as big as it could be without any distortion in the area. Distortion in the picture is caused by scattering and the fact that the beam has to be supported somehow to the conveyor. Figure 9 shows a typical X-ray picture from the whole examined area. The darker rectangles in the ends of the beam are a part of the holder of the beam. The scattering phenomenon can be noticed in the lower edge of the picture when one knows that the lower edge of the beam was in fact equal to the lower edge of the picture. The white sector in the lower edge is due to the scattering. The analysed area was approximately 90% of the actual face area of the beam.

Figure 9. Typical X-ray picture.

The weight and the main dimensions of all beams were measured before the X-ray examination. Thus the average densities of the beams were known on the examination moment. The correlation between average wet density and Mean Grey Value of a beam was studied with x-y plot. The results can be found in chapter 6.6.

Another examined variable was the proportion of knots in a lamella. It was determined from an X-ray picture by defining first the Mean Grey Value (MGV) for the whole investigated area including knots and defects. Then the MGV was defined for clear wood in the whole investigated area by defining MGV from small areas in which there were no signs of knots and defects. The MGV value for clear wood was determined for about 5 small areas inside the whole investigated area. Average of those values was used as the value of MGV for the clear wood. Figure 10 shows the method of defining the proportion of knots in principle.

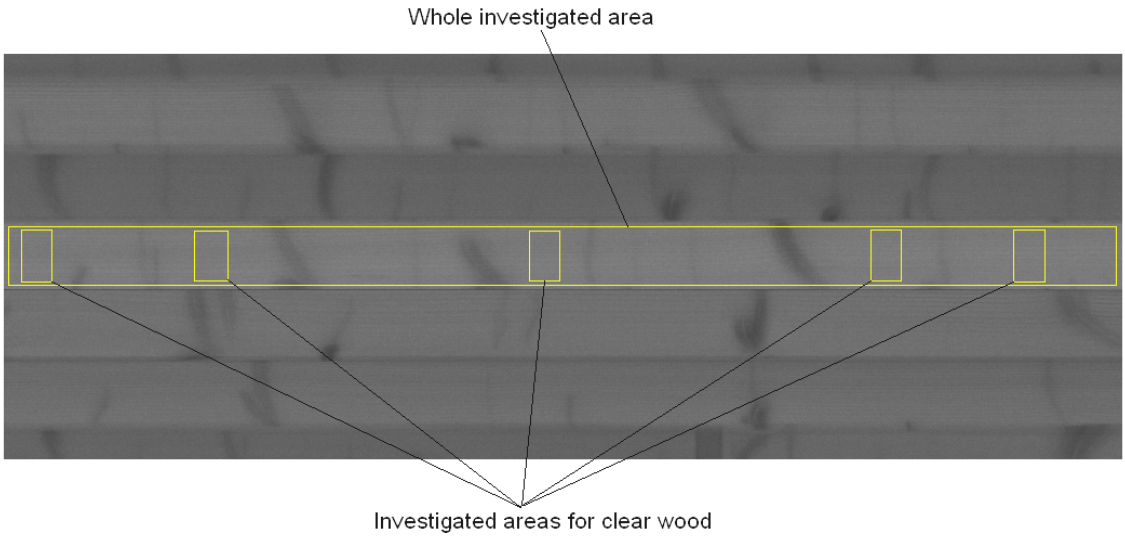

Figure 10. Method for defining the proportion of knots in principle.

The defined values of MGV for wood with defects and clear wood were modified to corresponding densities according to equation 48. The proportion of knots was derived from simplified relationship between average density, clear woods density and knots density shown in equation 12.

$$\rho_{ave} = x \cdot \rho_{knot} + (1 - x)\rho_{cw} \tag{12}$$

where ρ_{ave} is the density defined for the whole investigated area
ρ_{cw} is the density defined for clear wood inside the investigated area
ρ_{knot} is the average density of knot
x is the proportion of knots.

The proportion of knots can be derived from equation 12 as follows:

$$x = \frac{\rho_{ave} - \rho_{cw}}{\rho_{knot} - \rho_{cw}} \cdot 100\% \quad (13)$$

The value used for ρ_{knot} was defined from X-ray picture by defining the MGV values for knots in a beam. Average value of the MGV values of the knots was calculated and equation 48 was used to obtain a value for average density of the knots. The value obtained was 551,6 kg/m^3. The result for the proportion of knots depends greatly from the density used for the knots. That is why the calculated proportions should not be kept as actual proportions. However, differences in proportion values that have been calculated with same knot density can be compared. Results for the examination of the proportion of knots can be found from chapter 6.5.2

3.2 Test Humidity arrangements

All test specimens were first conditioned in RH 65% for about a month so that the moisture content of the specimens would normalize to equilibrium. Test series S1 was tested after this RH 65% conditioning. Further conditioning of the other test series can be seen from Table 1.

Table 1. Conditioning of the test specimens.

Test series	Conditioning
S1	1 month RH 65% -> testing
S2	1 month RH 65% -> 1 month RH 90% -> testing
S3	1 month RH 65% -> 3 months RH 90% -> testing
S4	1 month RH 65% -> 3 months RH 90% -> 1 month RH 30% -> testing
S5	1 month RH 65% -> 3 months RH 90% -> 3 months RH 30% -> testing

Conditioning of specimens was quite extreme compared to the conditions normally faced by load-bearing structures. The wet and dry periods in conditioning were both chosen so that indoor load-bearing structures do not usually expose to worse conditions. Outdoor conditions can be similar to the conditions of the wet test period. Relative humidity is usually high in Finland, even over 90% in winter time for long periods. On the other hand RH does not usually drop below 50% in outdoor conditions, not even in summer time. Indoors RH can drop even below 20% at winter time, as can be seen from Figure 1, but usually there are use related moisture regains that increase RH. However, load-bearing structures can be exposed to very varying conditions because of construction defects or accidents.

3.3 Coatings

The beams of the reference test series S1 were uncoated, but the other series S2–S5 had also coated beams. Three different coatings were used but only two different agents. The agents were AQUATOP 2600 varnish from Teknos Ltd and Linogard Underhållsolja from Linotech Ltd. The different coatings were one layer of AQUATOP 2600 varnish, two layers of AQUATOP 2600 varnish and one layer of Linogard Underhållsolja. AQUATOP coatings were applied by the beam manufacturers in their factories, but Linogard Underhållsolja was applied by the research group few days before the beams were photographed and X-rayed.

AQUATOP 2600 is acrylic water-borne varnish which is used as weather-resistant varnish. Product information of AQUATOP 2600 is in Appendix A. Coating version with two layers of AQUATOP 2600 was made so that the second layer was applied after the first layer had completely dried. Every surface of beam was treated.

Linogard Underhållsolja is made from cold-pressed linseed oil. It is used in indoors and outdoors as water-proofing impregnating oil. Product information of Linogard Underhållsolja is in Appendix A. The oil was first applied to every surface of the beam with a brush and after about 30 minutes the surfaces were wiped dry.

3.4 Test setup and loading arrangements

Experimental determination of shear strengths of structural elements like beams is not standardized by CEN, the European Committee for Standardization. The test for material shear strength of wood is standardized, but shear strength of a small piece of wood with variable amount of defects is not the same as shear strength of a real size glulam beam with different amount of defects and glued joints.

Different types of tests have been made to determine the correct value for structural elements, including glulam beams. In determining of shear strength the test specimens should of course fail due to a shear failure, otherwise the maximum shear strength capacity can not be attained. Failure mechanism in shear failure can be explained as follows: the middle part of the beam breaks and enables the lower and upper parts of the beam to slide relative to each other in the longitudinal direction. This results in a radical decrease in the capacity of the beam. Another typical failure type of beams is a bending failure which is actually caused by tension failure in the tension side of the beam. Of course when the test specimen fails for example by a bending failure, it can be said that the shear strength is at least the amount that the specimen persisted. Though, it cannot be said how many percent of the maximum shear strength the attained strength was. Therefore it is of course better the more specimens fail in shear. Shear and bending/tension failures are the most typical failures in straight glulam beams. One could say that they are also the only failure types that can cause the collapse of the beam. Local compression perpendicular to grain failures caused

by too small support areas can also occur but they do not usually cause a collapse of the beam. Lateral-torsional buckling can also happen but only without proper supports. However, compression failure in grain direction is almost impossible to obtain with symmetric cross-sections.

Shear failure is not always easy to achieve with glulam beams. Big knots or reaction wood in lowest lamellas can easily cause bending/tension failure before shear stress reaches the shear strength. Proper test setup for determining shear strength of glulam beams has been under discussion in International conferences. Different loading types like symmetric and asymmetric three-point loading, asymmetric four-point loading and symmetric five-point loading have been studied. Also, the effect of different span depth ratios has been studied as well as the shape of the cross-section of the beam. The symmetric five-point loading has been recommended by a Japanese study [8]. Also an American study recommends symmetric five-point loading [9]. Ratio of shear and tension stress is bigger in five-point loading than in other loading types.

Different types of cross-section manipulation have also been conducted in various studies; rectangular cross-sections have been machined to I-cross-sections to reduce the shear resistance of a beam and to easily attain shear failure.

Nevertheless, symmetric three-point loading was chosen for this experimental program. Height of the beam was chosen big enough to obtain a size effect. The height of the cross-section is so big that a beam of that size could generally be used in structures. Because of the chosen height a five-point loading specimen would be so long that it would have been impractical and laborious to work with, especially because the number of the specimens is high in this programme.

The probability to bending failure in symmetric three-point loading was attempted to decrease when ordering the specimens from manufacturers. Manufacturers were asked to produce the test specimens so that a few lowest lamellas would not have finger joints. However all manufacturers did not realize this wish.

Test setup was chosen to be a symmetric three-point loading to reduce the need of the length of the beam. Test setup is shown in Figures 11, 12 and 13. The important dimensions, support types and places of gauges can be seen from Figure 13.

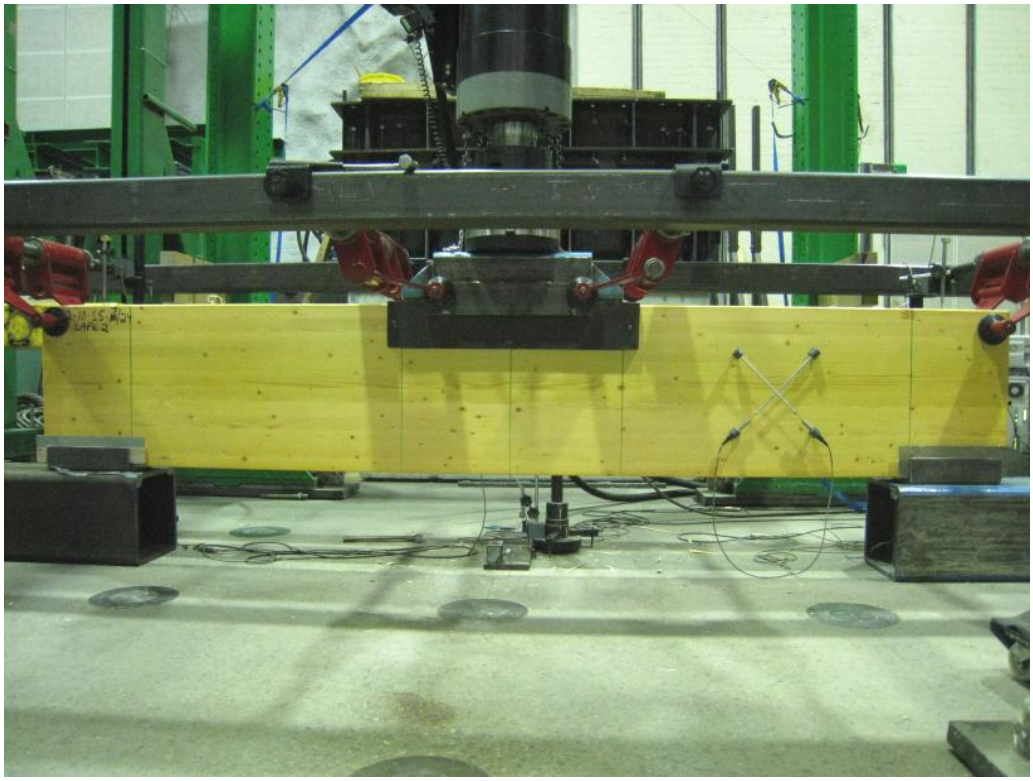

Figure 11. The test setup used in the shear experiments of this study.

Figure 12. The test setup at the support.

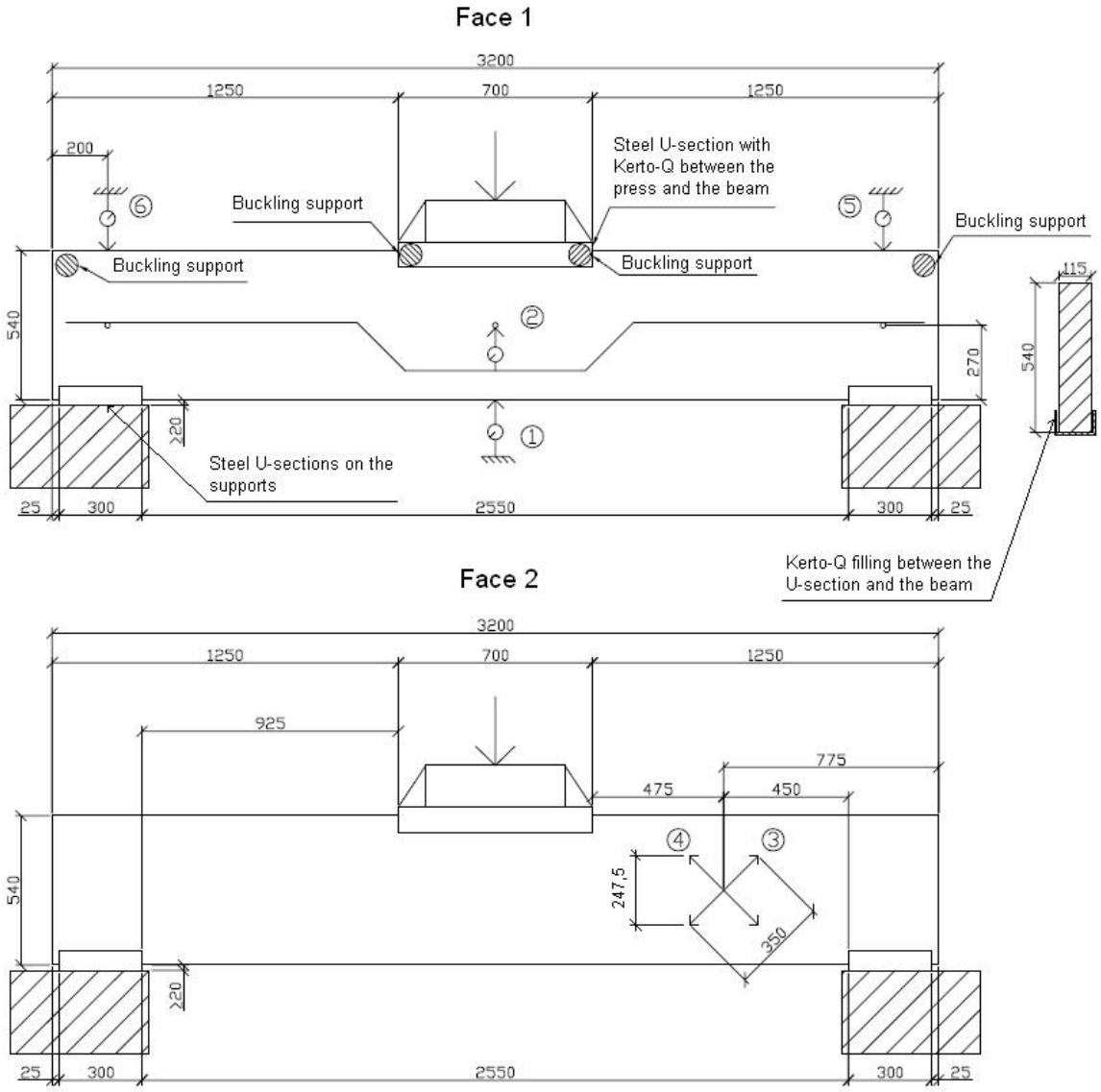

Figure 13. Test setup, dimensions and numbering of gauges, dimensions are in millimetres.

The deformations of the beams were automatically measured with six gauges shown in Figure 13. Gauge 1 measures the deformation of the lower edge of the beam in the centre of the span. Gauge 2 measures the deformation of the centre line of the beam in the centre of the span. Cross-measure was monitored by gauges 3 and 4 and deformations in supports were measured with gauge 5 and 6. Accuracy of the gauges were: gauge 1 0,08 mm, gauge 2 0,05 mm, gauge 3 0,05 mm, gauge 4 0,09 mm, gauge 5 0,08 mm and gauge 6 0,07 mm. The load was also automatically measured. Accuracy of the force transducer was 40 N.

Four lateral supports were applied to prevent lateral buckling. The supports were of a pivoting type which allowed the specimen to deflect without significant frictional resistance. Hydraulic actuator was also hinge-supported. One more measurement taken was the

position of the head of the hydraulic actuator. The force in the hydraulic actuator was also monitored. The target rate of loading was 60 kN/min for test series S1. For other test series the target rate was changed so that it was 80 kN/min until the load was 220 kN and 40 kN/min after that. The change was done in order to see more easily which of the failure types appeared in the tested specimen.

The beams were supported with specific hinged supports as usual. Even so, the supports were not completely rigid but only rigid levels on which the beam rested. This kind of support was chosen to reduce bending moment in the middle of the beam at least slightly. In both supports and loading point there was an open channel section and the beam was placed inside it. There was also a plywood filling between the beam and the flanges of the open channel section. This kind arrangement was made to reduce the plastic deformation from perpendicular to grain forces. Compression strength of wood perpendicular to grain was exceeded very easily so this arrangement was necessary to prevent massive deformations and breakage in the beam.

First two tested beams in test series S1 were tested with a little different test setup. The length of the supports was smaller, 250 mm, and also the length of the loading point was smaller, only 500 mm. There also was no open channel section in the loading point when testing the first beam. However, the open channel section was added before testing the second beam. When testing the first beam there were buckling supports only in the ends of the beam. Buckling supports were added also to the middle of the beam when testing the second beam, but at first they were not stiff enough. After modifying buckling supports stiffer the testing was almost successful. There was still a need to increase the length of the profile in the loading point and in the supports. This was done before continuing the tests. After these changes, the test setup was like in Figures 11, 12 and 13.

3.5 Moisture content monitoring

The moisture content distribution in cross-section was monitored by taking a test piece of the specimen after the testing of the specimen to failure. The test piece was taken from approximately one quarter of the length measured from the end of a beam. It was taken from approximately the mid height of the beam. This place was chosen because the coinciding maximum shear stress. The test piece was divided into five similar smaller pieces in width direction, pieces being about 20 mm in width. The pieces were weighed within moments after testing and after that they were dried in an oven and then weighed again. The moisture content distribution in the cross-section could then be defined with an accuracy of about 20 mm in width. Figure 14 shows the division of the piece sawed from the specimens.

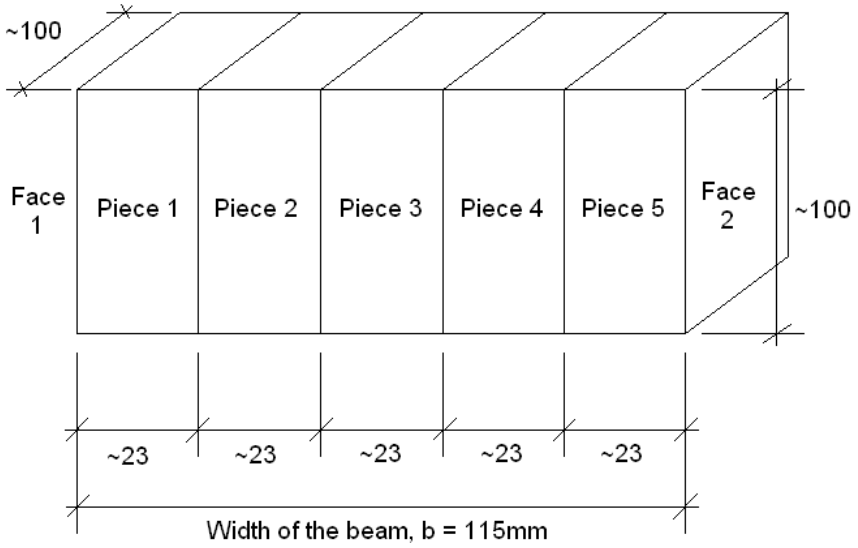

Figure 14. Moisture content test piece division.

The approximate value for the dry mass of a whole specimen was calculated from the wet mass of the specimen and the moisture content in the cross-section. The wet mass of the specimen was measured in the test situation. The average moisture content was calculated after drying the specimen in the oven. After knowing the dry mass of a specimen, the change in the average moisture content was examined using the weighing results which were measured at different times during the handling process of a specimen. Weight was measured in the pre-test situation and in the test situation. None of particular specimens were weighed more than twice so exact average moisture content in function of time for a specimen cannot be presented. However, the test groups (of 6 specimens with the same coating) were tested in every stage of conditioning. Thus, a statistical average moisture content alteration in function of time for a test group can be approximated.

4. Evaluation of shear stresses and elastic and shear moduli

4.1 The effect of cross-section to shear strengths

The affect of different test setups to the shear resistance and strength was studied in a Swedish Master's Dissertation [12]. They tested beams with unsymmetrical three point loadings with small differences, and also with one five point loading. Test series were small: there were only four beams in every series. Two of the test setups were otherwise similar but cross-sections were different, the other had a rectangular cross-section while other had I-section. The I-section was made from the rectangular cross-section by cutting.

The maximum shear stresses from the ultimate loads of the Swedish study were calculated simply with a linear elastic material model and with the Euler-Bernoulli beam equation. Results showed different strength between rectangular and I-section, even though the material was the same. Average strength for rectangular beams was 4,57 MPa. and for I-section 6,06 MPa. The ultimate load for I-section was approx. 70% of the ultimate load for rectangular cross-section. An increase of ca. 25% in strength for I-section is quite significant. One thing that may affect the results is that deformations and stresses do not comply with Hooke's law with the ultimate load levels. This could produce some error to the outcome of the above. However, it is difficult to evaluate how much it affects. One thing that clearly affects the result is that two of the rectangular beams had bending failure with quite low loading. Only one beam with I-section failed with bending. However, if beams with bending failure are ignored the average shear strength for rectangular beams is about 4,9 MPa, which is still much lower than with I-section.

There were also few other test setups in the Swedish study, but these beams were all with I-sections. In one setup the beam was supported similarly as in previous setups but it also had 450 mm long overhangs in both ends. Average shear strength of this setup was 6,21 MPa. even though two out of four beams had bending failure. Another test setup was a symmetrical five point loading in which average shear strength was 7,20 MPa.

It seems that the shape of the cross-section and the choice of the test setup affects the results.

4.2 Calculation of stresses using Eurocode 5 and Euler-Bernoulli beam equation

The selected coordinate system is shown in Figure 15.

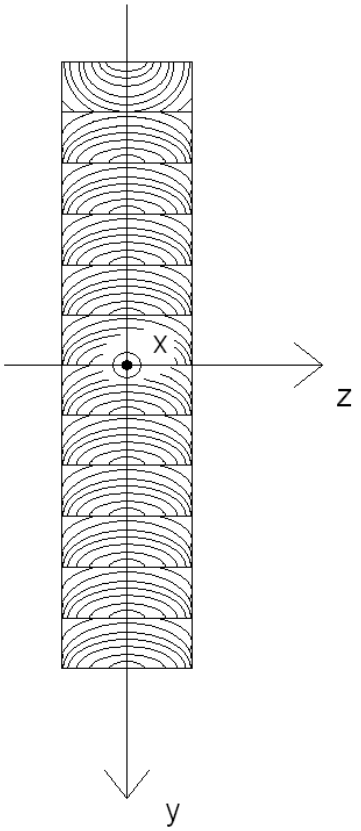

Figure 15. Coordinate system of the cross-section.

The average shear stresses in a cross-section can be calculated from equations 14 and 16.

$$\tau_{xy}(y) = \frac{V_y}{I_z b} S_z(y) \tag{14}$$

$$\tau_{xz}(z) = \frac{V_z}{I_y h} S_y(z) \tag{15}$$

where V_y and V_z are the shear forces in directions shown by subscripts
I_y and I_z are the moments of inertia around y- and z-axis
b is the width of the cross-section
h is the height of the cross-section
S_y and S_z are the static moments around y- and z-axis.

According to Eurocode 5 (EN 1995-1-1:2004 + A1:2008 + AC:2006) effective width should be used in the calculation shear stress. Effective width is calculated from nominal cross-section dimension by multiplying it with factor k_{cr}. The recommended value for k_{cr} is given as 0,67 for glued laminated timber. Shear stress resultant in a point of the cross-section can be calculated from equation 16.

$$\tau = \sqrt{\tau_{xy}^{\ 2} + \tau_{xz}^{\ 2}} \tag{16}$$

Since $V_z = 0$ in the test setup, the term $\tau_{xz} = 0$ as well. Thus, the shear stress resultant is same as τ_{xy}. Static moment for rectangular cross-sections can be calculated from equation 17 and moment of inertia around z-axis for rectangular cross-section can be calculated from equation 18.

$$S_z(y) = \int_A y dA = \frac{1}{2} b\left(\left(\frac{h}{2}\right)^2 - y^2\right) \tag{17}$$

$$I_z = \int_A y^2 dA = \frac{1}{12} bh^3 \tag{18}$$

Substituting equations 17 and 18 to equation 14 and noting that A = bh, the shear stress distribution of a rectangular cross-section can be calculated from equation 19.

$$\tau_{xy}(y) = 6\frac{V_y}{A}\left(\frac{1}{4} - \frac{y^2}{h^2}\right) \tag{19}$$

Shear stress distribution in the cross-section, calculated with nominal dimensions of the cross-section when the load is 380kN, can be seen from Figure 16. Distribution in Figure 16 is from the part of the beam where the shear force is highest; that is to say near the ends of the beam. It can be seen that shear stress is zero in the edges and that it rises quite quickly to the maximum value in the middle of the cross-section. Shear stress is within 80% of the maximum value in almost half of the height of the beam in the middle part of the cross-section. That is why a shear failure can appear quite close to upper and lower edges of the beam even though the expected failure location is the middle of cross-section. There are significant differences in strengths of the lamellas and glue bonds and because shear stress is high in quite a big part of a cross-section the weakest place in the beam is usually found inside quite a large area in vertical direction of the beam. The heterogeneity of wood as material affects the possible locations of the failure planes.

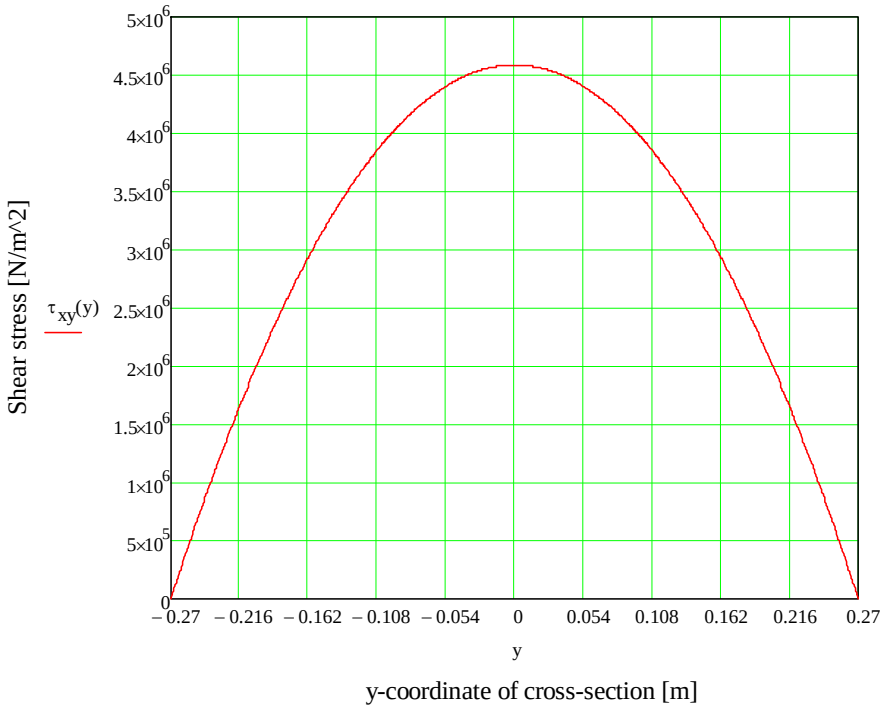

Figure 16. Shear stress distribution in the beam cross-section.

The dimensions of the cross-section affect linearly the result of the shear stress. This is why it should be taken into account that the dimensions of the cross-section alternate depending on the moisture content of the beam. In this study the main dimensions of the beams were measured in the pre-test phase. The shrinkage coefficient of the beams in the height direction was studied with measuring the height of the beams in the test series S5 before testing. When the differences in average moisture content between pre-test and test phases were known the shrinkage coefficient could be defined. All stresses shown in the results are calculated with nominal dimensions taking moisture content induced changes in dimensions into account. Factor kcr has not been used in the calculations of shear stress values.

4.3 Calculation of elastic modulus from strain measures

European standard EN 408:2003 defines the determination of a few mechanical properties such as local and global modulus of elasticity, shear modulus and bending strength for structural and glue laminated timber. In most methods the test specimen should be a beam with length about 18 times the height of the beam. In this study the length of the beams is only about 6 times the height so the methods in the standard do not apply. The results in this study are not completely comparable. However, the difference might not be that great, and some conclusions can be done.

Calculation of elastic modulus is based on an elastic material model. Hooke's law $\sigma = E\varepsilon$, in which the stress σ is directly proportional to the strain ε in some direction, is usually applied as it is simple and describes the behaviour of most materials accurately.

To calculate the elastic modulus, a model for the deformation of the beam under loading is needed. Two simple models to describe this are the Euler-Bernoulli beam theory and the Timoshenko beam theory. The difference between these two models is that in the Euler-Bernoulli beam equation any cross-section perpendicular to the longitudinal axis in a non-deformed state will remain perpendicular to longitudinal axis also in the deformed state, while in Timoshenko beam equation cross-section in deformed state does not have to be perpendicular to longitudinal axis in the deformed state. This small difference does not appear to be dramatic, but actually this is the case because it takes into account the effect of shearing force to the deformation of the beam. Figure 17 shows the conceptual difference between Euler-Bernoulli and Timoshenko theories.

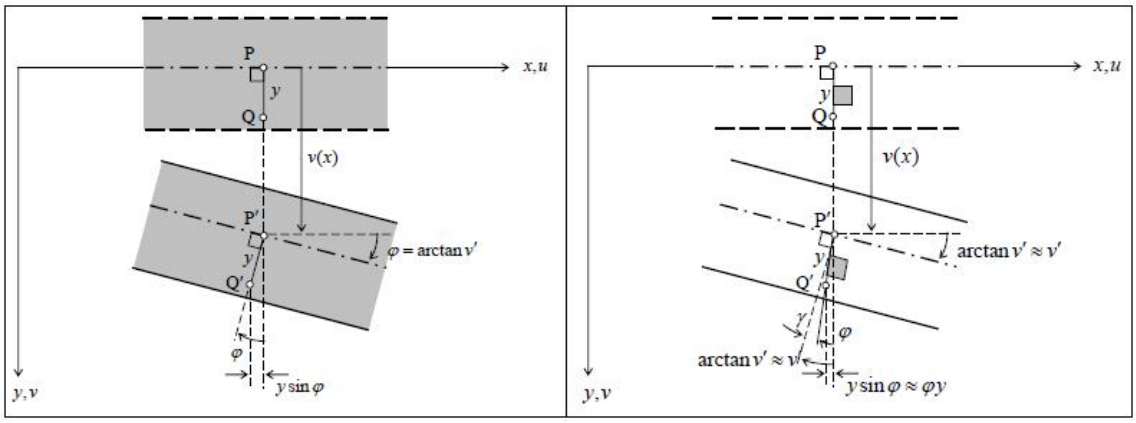

Figure 17. Variables in Euler-Bernoulli (left) and Timoshenko (right) beam theories.

where y and x are the cross-section coordinates, coordinate system similar to Figure 15

v and u are the deformations in direction of y and x coordinates

φ is the rotation of angle of line PQ that is perpendicular to longitudinal coordinate axel before deformation

γ is the shear strain/angle of slide in deformed state, the difference of line P´Q´ and a line that is perpendicular to longitudinal coordinate axel and goes through point P´ or Q´.

The relation between rotation φ and deformation v in Euler-Bernoulli beam equation can be derived from the rotation of the longitudinal axis of the beam based on the condition that the line P´Q´ remains perpendicular to longitudinal axis after deformation. The slope of deformation line v(x) can be calculated from the derivative of v´(x), which leads to equation 20.

$$\varphi(x) = \arctan v'(x) \tag{20}$$

With normal deformations rotation φ can be assumed to be <<1 and therefore $\varphi \approx \tan\varphi$. The relation between rotation φ and deformation v can be written as follows:

$$\varphi(x) = v'(x) \tag{21}$$

In case of Timoshenko beam theory the corresponding equation can be seen from Figure 17 to be as follows:

$$v'_\gamma(x) = \varphi(x) + \gamma(x) \tag{22}$$

where subscript γ in $v'_\gamma(x)$ refers to the using of Timoshenko beam theory.

The relation of shear force V and shear strain γ is in Timoshenko beam theory assumed to be as follows:

$$V(x) = \frac{1}{\zeta} GA\gamma(x) \Leftrightarrow \gamma(x) = \zeta \frac{V(x)}{GA} \tag{23}$$

where G is the shear modulus
A is the cross-section area
ζ is the displacement factor.

The displacement factor ζ can be calculated from equation 24.

$$\zeta = \frac{A}{I_z^2} \int_A \frac{S(y)^2}{b(y)^2} dA \tag{24}$$

where I_z is the moment of inert.ia around z-axis.

For rectangular cross-section ζ = 1,2. The relation of bending moment and deformation v can be derived in Euler-Bernoulli beam theory to be as follows:

$$v''(x) = -\frac{M(x)}{EI_z} \tag{25}$$

where M(x) is the expression of bending moment
E is the elastic modulus.

The expression of deformation v can be integrated from equation 25. When considering the Timoshenko beam theory the v(x) is calculated from equations 26 and 27.

$$v'_\gamma(x) = \varphi(x) + \zeta \frac{V(x)}{GA} \tag{26}$$

$$\varphi'(x) = -\frac{M(x)}{EI_z} \tag{27}$$

First, the φ(x) is calculated from equation 27 by integrating it. After that φ(x) is inserted into equation 26 which is again integrated to get v(x).

To define to expressions of bending moment and shear a static model as shown in Figure 18 is used. The supports of the test setup are difficult to define in the static model so that these reflect the real situation. The supports in the test setup are not hinged and do not make possible the free rotation on the supports. However, the supports are not absolutely rigid and cannot be modelled as rigid supports in the static model. Probably the best way to model the support would be some kind of helical spring support. However, defining the spring ratio would need specific measurements which were not conducted. In this work the manual calculations are done with a model with hinged supports accepting that there is little inaccuracy in the model. The model in the FEM-calculations does however observe the special support type. The static model of the test setup is shown if Figure 18.

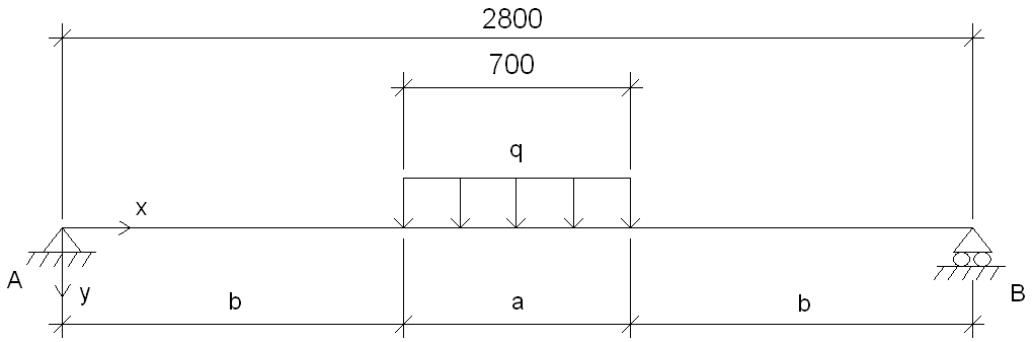

Figure 18. Static model of the test setup.

The support reactions can be easily calculated from equilibrium condition:

$$A_y = \frac{qa}{2}, B_y = \frac{qa}{2}, A_x = 0 \tag{28}$$

where A_y is the support reaction in y-direction in support A
A_x is the support reaction in x-direction in support A
B_y is the support reaction in y-direction in support B
q is the uniform load
a and b are the dimensions shown in Figure 18.

The expressions of bending moment and shear force can also be calculated from equilibrium conditions:

$$\begin{array}{lll} 0 \le x < b: & b \le x < b+a: & b+a \le x \le 2b+a: \\ V(x) = A_y & V(x) = A_y - q(x-b) & V(x) = -B_y \\ M(x) = A_y x & M(x) = A_y x - \frac{q}{2}(x-b)^2 & M(x) = B_y(2b+a-x) \end{array} \tag{29}$$

The piecewise specified expression of deformation v(x) for Euler-Bernoulli beam theory can then be solved from equation 25.

$$
\begin{aligned}
v_1(x) &= -\frac{1}{EI}\left(\frac{A_y}{6}x^3 + C_1 x + C_2\right), 0 \le x < b \\
v_2(x) &= -\frac{1}{EI}\left(-\frac{q}{24}x^4 + \frac{A_y + bq}{6}x^3 - \frac{qb^2}{4}x^2 + C_3 x + C_4\right), b \le x < b + a \\
v_3(x) &= -\frac{1}{EI}\left[-\frac{B_y}{6}x^3 + \frac{B_y(2b+a)}{2}x^2 + C_5 x + C_6\right], b + a \le x \le 2b + a
\end{aligned}
\tag{30}
$$

where C_1, C_2, C_3, C_4, C_5 and C_6 are constants of integration.

In the same way the piecewise specified expression of deformation $v_\gamma(x)$ for Timoshenko beam theory can then be solved from equations 26 and 27.

$$
\begin{aligned}
v_{1\gamma}(x) &= -\frac{1}{EI}\left(\frac{A_y}{6}x^3 + C_1 x\right) + \zeta\frac{A_y}{GA}x + C_2, 0 \le x < b \\
v_{2\gamma}(x) &= -\frac{1}{EI}\left(-\frac{q}{24}x^4 + \frac{A_y + bq}{6}x^3 - \frac{qb^2}{4}x^2 + C_3 x\right) + \frac{\zeta}{GA}\left[-\frac{q}{2}x^2 + (A_y + qb)x\right] + C_4, b \le x < b + a \\
v_{3\gamma}(x) &= -\frac{1}{EI}\left[-\frac{B_y}{6}x^3 + \frac{B_y(2b+a)}{2}x^2 + C_5 x\right] - \frac{\zeta}{GA}B_y x + C_6, b + a \le x \le 2b + a
\end{aligned}
\tag{31}
$$

In both cases constants of integration can be solved from boundary conditions and continuity conditions.

$$
\begin{aligned}
v(0) = 0 \qquad & v_1(b) = v_2(b) \qquad v_2(b+a) = v_3(b+a) \\
v(2b+a) = 0 \qquad & v_1'(b) = v_2'(b) \qquad v_2'(b+a) = v_3'(b+a)
\end{aligned}
\tag{32}
$$

Figure 19 shows the calculated deflections of centre line of the beam when the load is $0{,}1F_{max}$ or $0{,}4F_{max}$ and when the characteristic material values of GL32c are used. F_{max} refers to the obtained average maximum load in the tests of this study which was 357,74 kN. Thus, $0{,}1 \cdot F_{max} = 51{,}1kN$ and $0{,}4 \cdot F_{max} = 204{,}4kN$. The symbol v refers to the result of Euler-Bernoulli beam theory and v_γ to the result of Timoshenko beam theory. It can be seen that there is quite a significant difference between the Euler-Bernoulli and the Timoshenko beam theories in this kind of test setup. When bending moment caused by a load is small compared to shear force caused by the same load, the deflection from shear forces should observed. This is usually the case with e.g. short beams.

Figure 20 shows the calculated deflections together with realized deflections of the centre line in the beams of test series S1. The Timoshenko beam theory seems to describe the realized deflection quite well. Instead, the Euler-Bernoulli beam theory underestimates the deflection. The calculated deflections are done using characteristic values of GL32c.

With Timoshenko beam theory there is almost insignificant difference in the deflections within the elastic zone of the beam. The plastic deformations in the beams results in differences in the measured and calculated deflections.

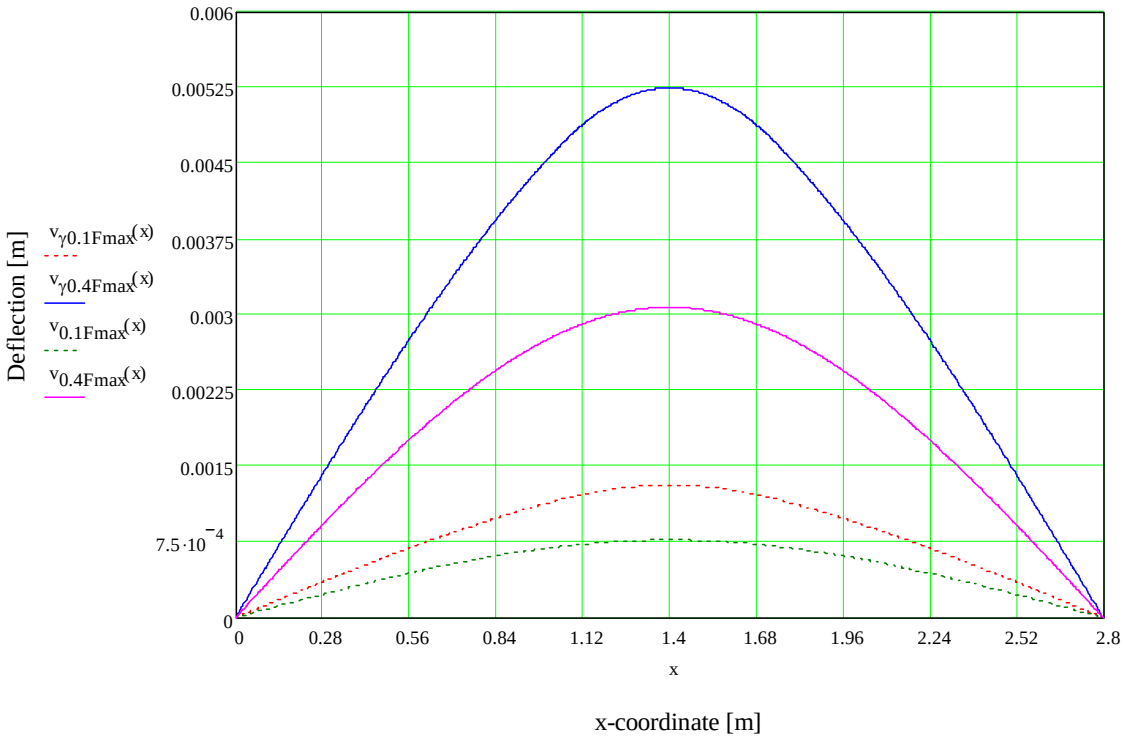

Figure 19. The calculated deflection of the centre line of the beam when the load is $0{,}1F_{max}$ or $0{,}4F_{max}$.

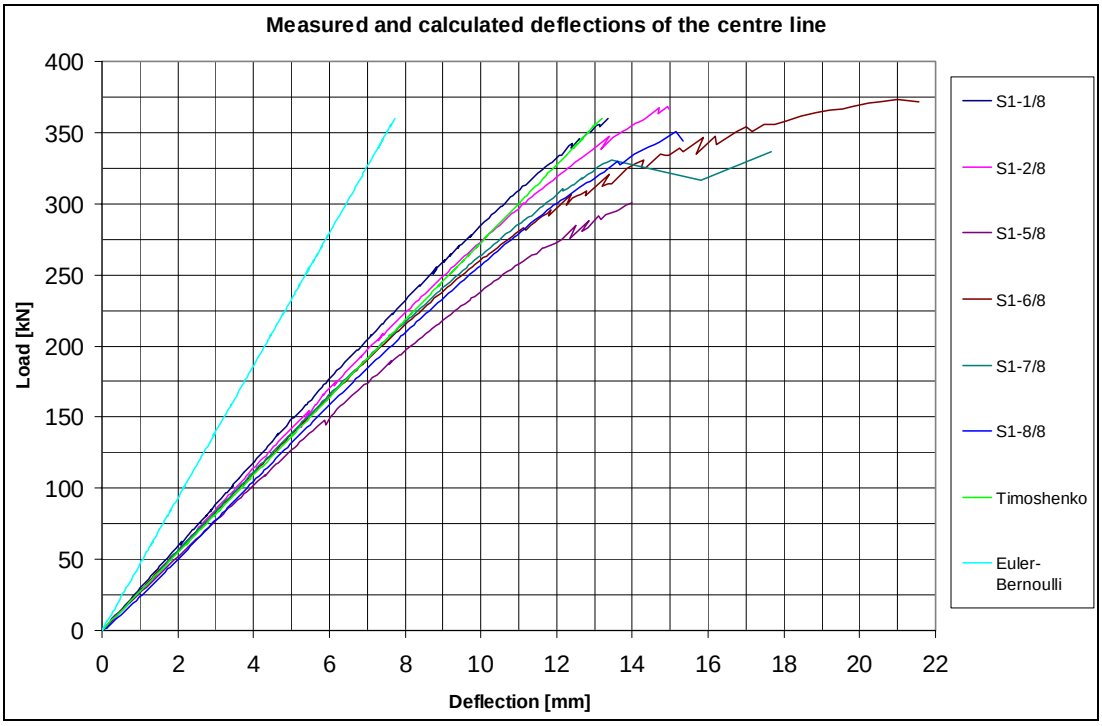

Figure 20. Measured and calculated deflections.

Elastic modulus is solved from the expression of the deflection v(x) as a function of the measured load and the corresponding measured deflection. The investigated interval for the deflection and load is from $0,1F_{max}$ to $0,4F_{max}$. The beam is supposed to work elastically within this interval. This kind of interval is used also in EN 408:2003 where regression analysis is taken from the longest possible section of the data that gives a correlation coefficient of 0,99 or better.

Generally, the results for measured elastic modulus are divided into two cases, local and global elastic modulus, depending on the measuring method. The test setup in tests that are done according to EN 408:2003 is a symmetrical four-point loading. Thus, the middle part of the test specimen, aligning between loading points, does not have any shear force influencing it. According to EN 408 the local modulus of elasticity is calculated from the deflection that is measured between the loading points. Thus, no part of the deflection is caused by shear force. The global elastic modulus, on the other hand, is calculated from the deflection that occurs in the whole length of the beam so part of the deflection is caused by shear forces. According to EN 408 both moduli of elasticity are calculated using Euler-Bernoulli beam equation which alone does not take into account the deflection from shear force. This is why global elastic modulus is usually smaller than local elastic modulus.

The global elastic modulus is also called the apparent modulus of elasticity. The difference between local and global elastic modulus is that the local elastic modulus is calculated from deflection which is not increased by deformations due shear force, because there is no shear force acting to the part of beam in which the deflection is measured. The global elastic modulus is calculated from the total deflection containing the deformation from the bending moment and shear force.

The test setup in this study is a symmetrical three-point loading so there is no part of the beam that does not have a shear force affecting it. Thus, local elastic modulus can not be directly calculated from any measurements. However, the test setup highlights the deformations caused by shear force so the values obtained for global elastic modulus are clearly smaller than characteristic value of GL32c, 13700 N/mm^2. Local elastic modulus can be calculated from the measurements if deflection caused by shear force is taken into consideration. This can be done using Timoshenko beam equation by assuming some value for the shear modulus. As can be seen from Figure 20 the deflection calculated from Timoshenko beam equation by using characteristic values follows quite accurately the measured deflection. This result encourages calculating the value for local elastic modulus by using Timoshenko beam theory and assuming that the shear modulus is equal to the characteristic value. The values for local elastic modulus shown in the “Results” part of this study (chapter 5) are calculated from Timoshenko beam theory using characteristic value of 780 N/mm^2 for the shear modulus.

The inaccuracy in the static model will result in a systematic error in the results of both elastic moduli. The result for the elastic moduli calculated from the expressions of v(x) and

$v_\gamma(x)$ made with inaccurate static model will give values for elastic moduli that are greater than the real values. The difference, however, is not very substantial.

4.4 Calculation of shear modulus from strain measures

European standard EN 408:2003 defines two ways to determine the shear modulus. Both of the methods are based on determination of elastic moduli first. In one method there is a need to first determine both local and global elastic moduli for a specimen. In the other method global elastic moduli are determined from four specimens with different spans but similar cross-sections. Thus, the shear modulus is determined using the measured elastic moduli.

Shear modulus can be determined also directly from strain measurements as is done in this study. The results obtained this way are not necessarily comparable with methods of EN 408. When the shear modulus is calculated directly from strain measurements, its value should be more realistic than a modulus calculated using measured elastic moduli.

The shear deformation was measured with crossed gauges 3 and 4 shown in Figure 13. Gauges were placed in the middle of free length between load press and support where shearing force can be assumed to have its greatest value in the beam. Shear force distribution can also be expected to be constant in the longitudinal direction between the test points of the gauges. Gauges were aligned centrally in the height direction of the beam. The height between the test points of the gauges was approximately c = 247,5 mm. The height c defines the part of the beam where the shear deformations are measured. The part of the beam which is between the gauges is approximately 45,8% of the total height of the beam. However, because of the shape of the shear stress distribution shown in Figure 16, the part of the beam between the test points of the gauges bears about 63,9% of the total shear force.

The relationship between shear modulus G_{xy}, shear force V_y and shear strain γ_{xy} can be derived using the energy balance method as was done in a Finnish study done at VTT [14]. The deduction of the relationship is conducted similarly in this study. Figure 21 illustrates a situation in which shear force effects to a rectangular cross-section. The figure follows the Timoshenko beam theory in which it is assumed that a straight line perpendicular to the length axis of an undeformed beam remains straight in the deformed beam. This means that the magnitude of shear strain is constant in the height direction of a specific cross-section.

The strain energy W_τ for an element of unit length dx = 1 can be calculated from shear stresses as follows when using Hooke's law for shear strain $\tau = G\gamma$:

$$W_\tau = \frac{1}{2}\int_A \tau_{xy}\gamma_{xy}\,dA = \frac{1}{2}\int_A \tau_{xy}\frac{\tau_{xy}}{G_{xy}}\,dA = \frac{1}{2G_{xy}}\int_{-b/2}^{b/2}\int_{-c/2}^{c/2}\tau_{xy}^2\,dz\,dy \qquad (33)$$

where τ_{xy} is shear stress in the cross-section.

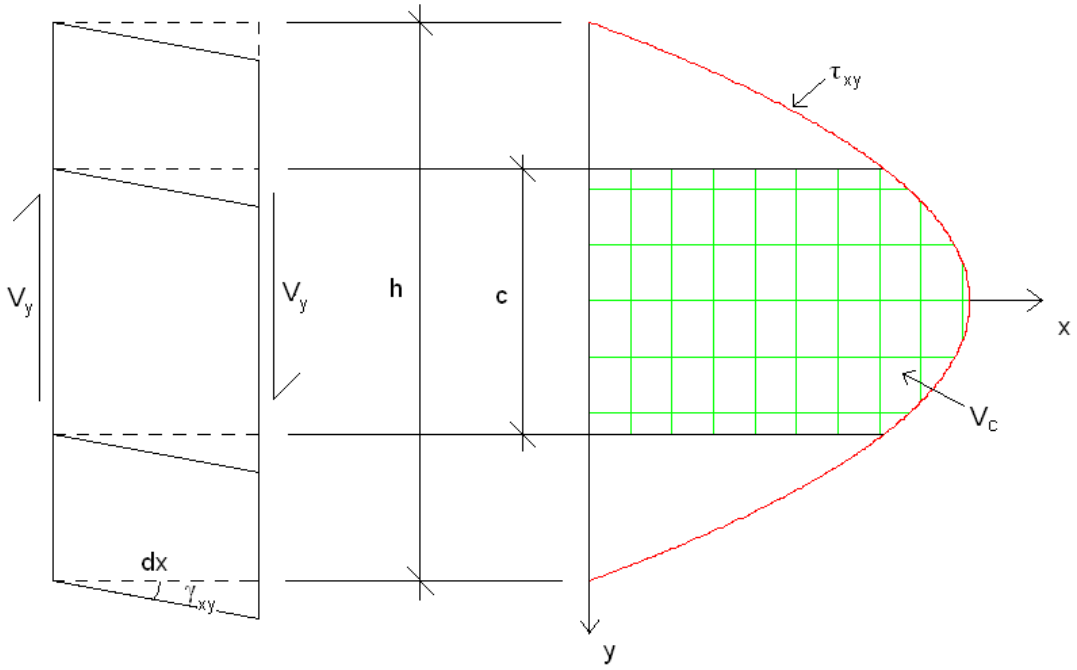

Figure 21. Effects of shear force V_y in rectangular cross-section, rigid body motion excluded.

One should notice that the strain energy above is calculated for the part of the cross-section that is between the measuring points of the crossed gauges. When the expression of shear stress, equation 19, is inserted to equation 33 and the integral is calculated, strain energy in shear can be written as follows:

$$W_\tau = \frac{1}{2G_{xy}} \int_{-b/2}^{b/2} \int_{-c/2}^{c/2} \left[6\frac{V_y}{A}\left(\frac{1}{4} - \frac{y^2}{h^2}\right)\right]^2 dzdy = \frac{18V_y^2}{G_{xy}A^2} b \int_{-c/2}^{c/2} \left(\frac{1}{4} - \frac{y^2}{h^2}\right)^2 dy = \frac{18V_y^2}{G_{xy}A^2} b \cdot c\left(\frac{1}{16} - \frac{1}{24}\left(\frac{c}{h}\right)^2 + \frac{1}{80}\left(\frac{c}{h}\right)^4\right) \quad (34)$$

where c is the height between the test points of the gauges
b is the width of the beam.

From Figure 21 it can be seen that the work W_V, which is done for an element of unit length dx = 1 by the part of the shear force that is carried by the part of the beam between the gauges, can also be written as follows:

$$W_V = \frac{1}{2} V_c \gamma_{xy} \quad (35)$$

where V_c is the part of shear force carried by the part of the beam between the gauges
γ is the shear strain resulting from the shear force V.

V_c can be calculated from equation 36.

$$V_c = b \int_{-c/2}^{c/2} \tau_{xy} dy = \frac{3}{2} V_y \frac{c}{h}\left[1 - \frac{1}{3}\left(\frac{c}{h}\right)^2\right] \quad (36)$$

After inserting equation 36 to equation 35 can the work W_V be written as:

$$W_V = \frac{3}{4} V_y \frac{c}{h}\left[1 - \frac{1}{3}\left(\frac{c}{h}\right)^2\right] \cdot \gamma_{xy} \tag{37}$$

The definitions of work W_V and strain energy W_τ can be assumed to describe the same internal work. This means that they are equal, i.e. $W_V = W_\tau$. Thus, the shear strain can be solved from the assumed balance as follows:

$$\gamma_{xy} = \frac{\frac{3}{2} - \left(\frac{c}{h}\right)^2 + \frac{3}{10}\left(\frac{c}{h}\right)^4}{1 - \frac{1}{3}\left(\frac{c}{h}\right)^2} \cdot \frac{V_y}{G_{xy} A} = \psi \frac{V_y}{G_{xy} A} \tag{38}$$

The shear modulus can be easily solved from equation 38 if shear strain and shear force are known. The deformation of square shaped element exposed to shear force can be assumed to be as in Figure 22 when deformations are small, which usually is the case. Also, the gauges 3 and 4 form this kind of an element and therefore shear strain can be calculated from these measurements.

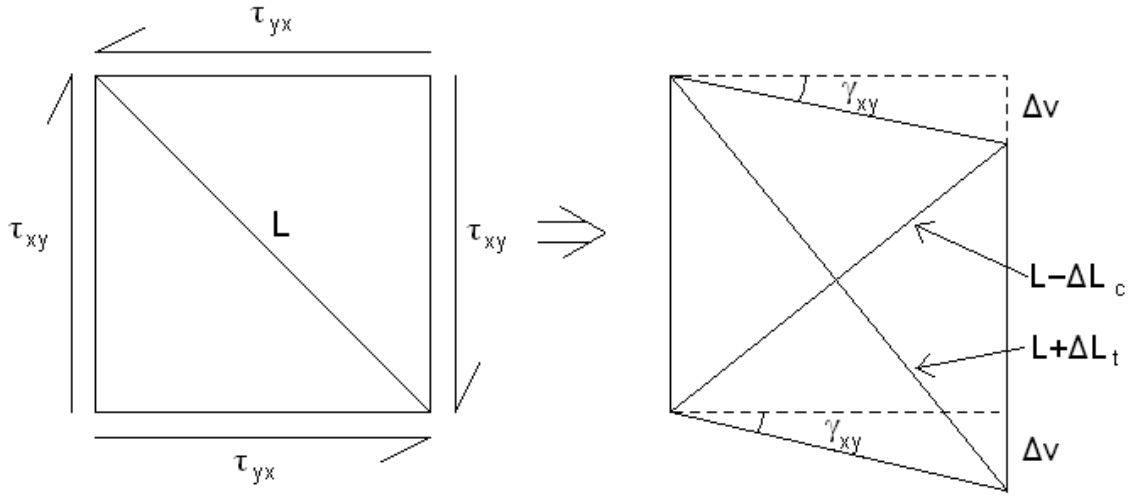

Figure 22. Deformation of square shaped element exposed to shear stresses.

The expression of shear strain can be seen from Figure 22 to be as follows:

$$\tan\gamma_{xy} = \Delta v \div \frac{L}{\sqrt{2}} = \frac{\Delta v}{L}\sqrt{2},\ \tan\alpha \approx \alpha\ when\ \alpha << 1\ \Rightarrow\ \gamma_{xy} = \sqrt{2}\frac{\Delta v}{L} \tag{39}$$

where L is the diagonal length of the square shaped element
Δv is the vertical displacement depending on the shear strain.

The equation for Δv can solved from equations 40 and 41 which are derived from the relations of right-angled triangles in Figure 22.

$$\left(\frac{L}{\sqrt{2}}+\Delta v\right)^2+\left(\frac{L}{\sqrt{2}}\right)^2=(L+\Delta L_t)^2 \tag{40}$$

$$\left(\frac{L}{\sqrt{2}}-\Delta v\right)^2+\left(\frac{L}{\sqrt{2}}\right)^2=(L-\Delta L_c)^2 \tag{41}$$

where ΔL_t and ΔL_c are the absolute values of the displacements in gauges 3 and 4, gauge 4 being the tensile one and gauge 3 being the compressed one.

The second powers of Δv are solved from both equations 40 and 41 and after that the results are equated and Δv is solved from the resulting equated equation.

$$\Delta v=\frac{\Delta L_t+\Delta L_c}{\sqrt{2}}=\sqrt{2}\Delta L_{34mean} \tag{42}$$

where ΔL_{34mean} is the average of the absolute values of the displacements in the gauges 3 and 4.

Equation 42 can be inserted to equation 39 in order to obtain a relationship between shear strain γ and displacement of gauges 3 and 4.

$$\gamma_{xy}=2\frac{\Delta L_{34mean}}{L} \tag{43}$$

The shear modulus can be solved from equation 38 by inserting equation 43 to it.

$$G_{xy}=\psi\frac{L}{2A}\frac{V_y}{\Delta L_{34mean}},\ \psi=\frac{\frac{3}{2}-\left(\frac{c}{h}\right)^2+\frac{3}{10}\left(\frac{c}{h}\right)^4}{1-\frac{1}{3}\left(\frac{c}{h}\right)^2} \tag{44}$$

4.5 Calculation of stresses using finite element method

Simple manual calculations do not always model the real situation very well, especially when examining an orthotropic material as wood. Also for example non-typical supporting of structure can make manual calculations laborious. The supports used in the test setup of this study to reduce bending moment in the middle of the beam complicate manual calculation. The static model used should have a spring in the hinged supports in the M_z direction to make the results more accurate. However, then the value of spring rate should be examined with additional tests. This is the reason why analysis softwares are nowadays used more and more in design, at least when the structure under examination is complicated.

There are different softwares available that can handle also orthotropic materials. The software used in this study is Abaqus version 6.8 finite element software. Examination of the stresses was conducted in two different ways. First, only the elastic strains were studied without the effects of moisture and time. After that the effects of moisture and time were studied so that beam did not have any external mechanical loads. The first case relates to the short test event and the second one to the conditioning of the beams.

4.5.1 Elastic strains and stresses

The model used in Abaqus elastic strain calculations was composed of a beam part of full width, full height and only half of the length of the real beam. Mid length symmetry was used to decrease the amount of elements used in calculation. Supports and loading head were modelled to be stiff steel parts. The interface of beam and steel parts was modelled to have frictional contact. The buckling supports and the flanges of the open channel sections were modelled with a boundary condition that prevented strains in Z-direction in a certain area of the beam surface. Similar boundary conditions were set in both sides of the beam. The beam was composed of 12 lamellas all of which had their own cylindrical coordinate system. Lamellas had rigid contact to each other. The model is shown in Figure 23.

The local cylindrical coordinate systems of the lamellas were aligned so that the pith was centred in width direction. In height direction the pith was aligned in the lower edge of the lamella in all but the uppermost lamella. The pith was aligned in the upper edge in the uppermost lamella. Figure 23 shows the alignment of cylindrical coordinate systems in lamellas. Alignment of the lamellas is the same as in Figure 15. On the other hand, the alignment of the lamellas is then like an idealised model from a typical alignment shown in Figure 5. Notation of the local coordinate system in Abaqus differs from the notation used previously in this study. The Abaqus notation shows in some pictures and may confuse the reader. The Abaqus notations correspond to the previous notations as follows: R-direction = r-direction, T-direction = t-direction and Z-direction = l-direction.

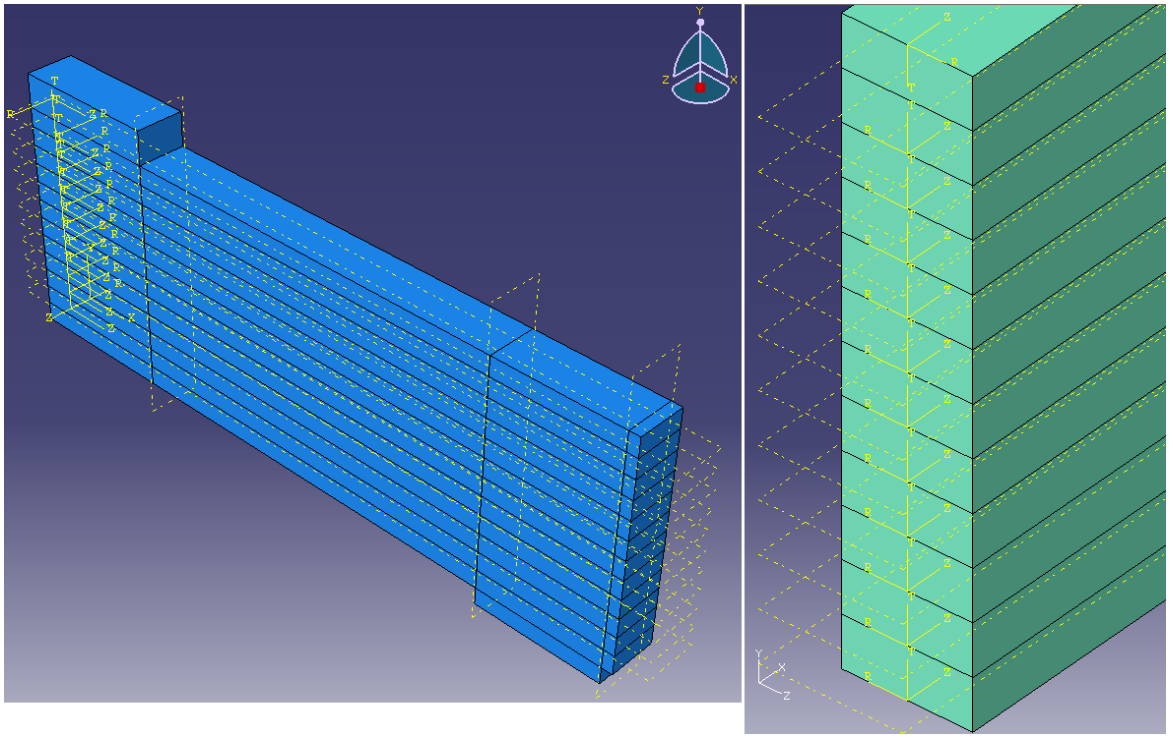

Figure 23. Model for Abaqus calculations.

Material properties used in the elastic strain analysis are shown in Table 2. These values were chosen because they have been noticed to correlate quite well in previous calculations and studies done to glulam at VTT. Similar properties have been used also in other European research centres/universities that have been cooperating with VTT.

One should notice that the Poisson's ratio v_{rt} is more than 0,5 (Table 2). It is generally known that Poisson's ratio for actual materials is between 0,0 and 0,5. In this case the ratio has been chosen to be bigger than 0,5. This means that the volume of a deformed element is smaller than the volume of the same, but undeformed element.

Table 2. Material properties used in the elastic strain analysis.

Property	Value	Unit
E_r	817	MPa
E_t	420	MPa
E_l	11900	MPa
G_{rt}	42,5	MPa
G_{rl}	743	MPa
G_{tl}	624	MPa
v_{rt}	0,555	-
v_{rl}	0,038	-
v_{tl}	0,014	-
ρ	450	kg/m^3

The elastic deformations were first calculated with four different loads: 50 kN, 100 kN, 200 kN and 350 kN. Then the calculated strains were compared to the measured deformations. Table 3 shows the calculated and measured deformations in the midpoint of the centre line. The difference between the measured and calculated deflections is also visualized in Figure 24 in which there are six measured load-deflection curves from the test series S1.

Table 3. Calculated and measured deformations.

	The deflection of the midpoint of the centre line	
Load [kN]	Calculated [mm]	Measured [mm]
50	1,53	1,5–2,0
100	3,06	3,1–4,0
200	6,11	6,3–8,2
350	10,68	11,5–19,5

Figure 24. Difference between Abaqus calculations and measured deflections.

It can be seen from Figure 24 that the modelled beam in Abaqus is stiffer than the six beams of the test series S1. The used material properties should have been optimized to the test results if there had been a need for better correlation of calculated and measured de-

flections. A few beams from all the tests series were approximately as stiff in their elastic part of the load-deflection curves as the Abaqus model was. Plastic deformations result in a difference in the elastic Abaqus calculations after the load exceeds approximately 150 kN.

The calculated displacements with 350 kN load are shown in Figure 25. The displacements in Figure 25 are scaled to be approximately 11 times bigger than in reality. The displacements were noticed to correlate quite well with the real deformations. The boundary conditions that modelled the open channel sections caused the bulging that can be seen below the loading head and above the support. This kind of bulging was noticed also in the tests. On the other hand, the slip in the support shown in Figure 25 was not noticed in the test.

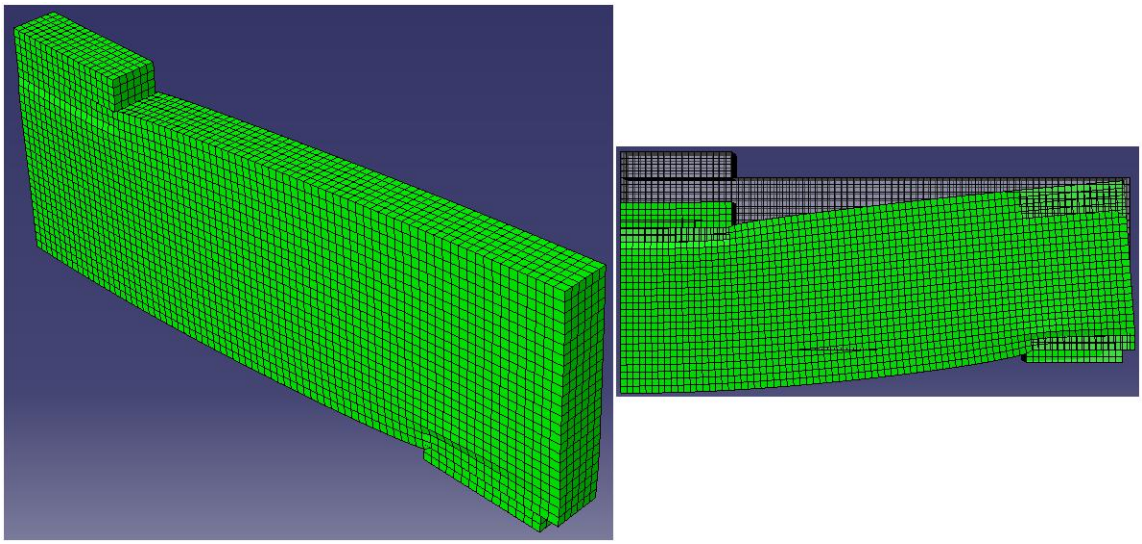

Figure 25. The strained state of the modelled beam, 350kN.

Directions of the principal stresses in the elastic loading are illustrated in Figures 26 and 27. It can be seen that the local coordinate system does not affect to the directions of principal stresses. Projections of principal stresses in plane perpendicular to global X-axis shown in Figure 26 meet the direction of Y-axis. According to Mohr's circle the maximum shear stresses are found on the planes that form a 45° angle with the directions of minimum and maximum principal stresses. In the mid height of the beam, where the minimum and maximum principal stresses form an x-shape, these planes can be seen to meet approximately the planes that are perpendicular to X- and Y-axis. Therefore the directions of maximum shear stresses are approximately equal to the directions of global shear stresses τ_{xy} and τ_{yx} in that area. The value of the highest principal stress was 29,3 MPa. It was situated in the middle of the span and in the lower edge of the beam.

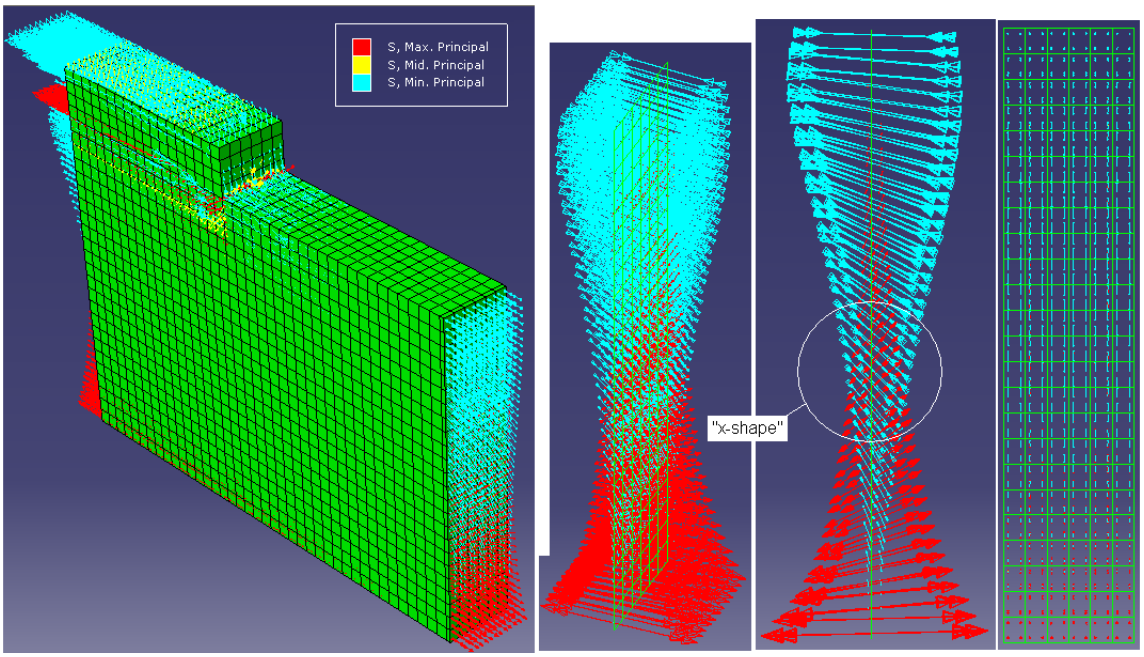

Figure 26. The directions of the principal stresses in the beam.

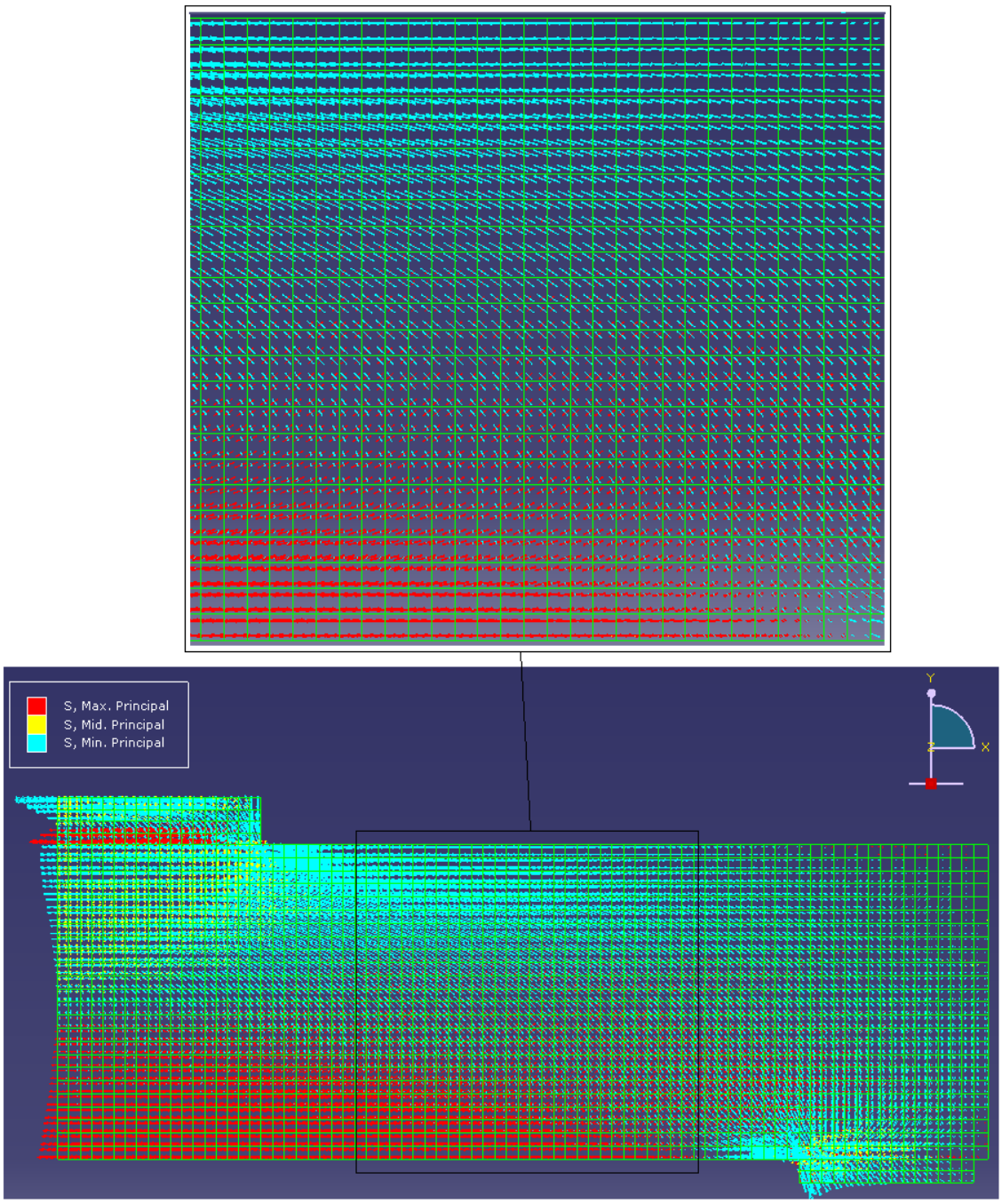

Figure 27. The directions of the principal stresses in the beam.

Results for the calculated elastic stresses in local coordinate system when load corresponds to 350 kN are illustrated in the following figures. The numbers in the subscripts refer to the local coordinate system of Abaqus shown in Figure 23 as follows: 1 = R-direction, 2 = T-direction and 3 = Z-direction. The height of every lamella is two elements in the figures presenting the results of elastic stresses.

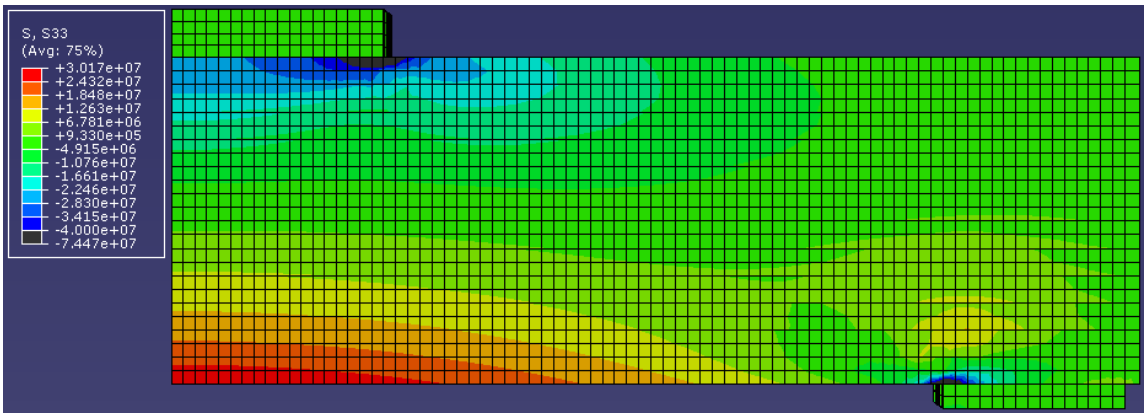

Figure 28. Normal stress σ_l. The unit of the results is N/m^2.

The normal stress in l-direction is quite evenly distributed in the width direction. The maximum tension stress in the lowest lamella is approximately 30,2 N/mm^2. The value was approximately equal to the value of the greatest principal stress in the middle of the beam. This is logical because the direction of the greatest principal stress is approximately parallel to the l-direction of the local coordinate system. The maximum compression stress is affected by the local interference of the loading head and support. If the interference is ignored one can notice that compression stress is approximately equal to tension stress. Tension stress in parallel to grain direction can be seen to be large considering the characteristic tension strength in grain direction of glulam GL32c, 19,2 N/mm^2. It is no wonder why some of the beams had bending/tension failure in the tests.

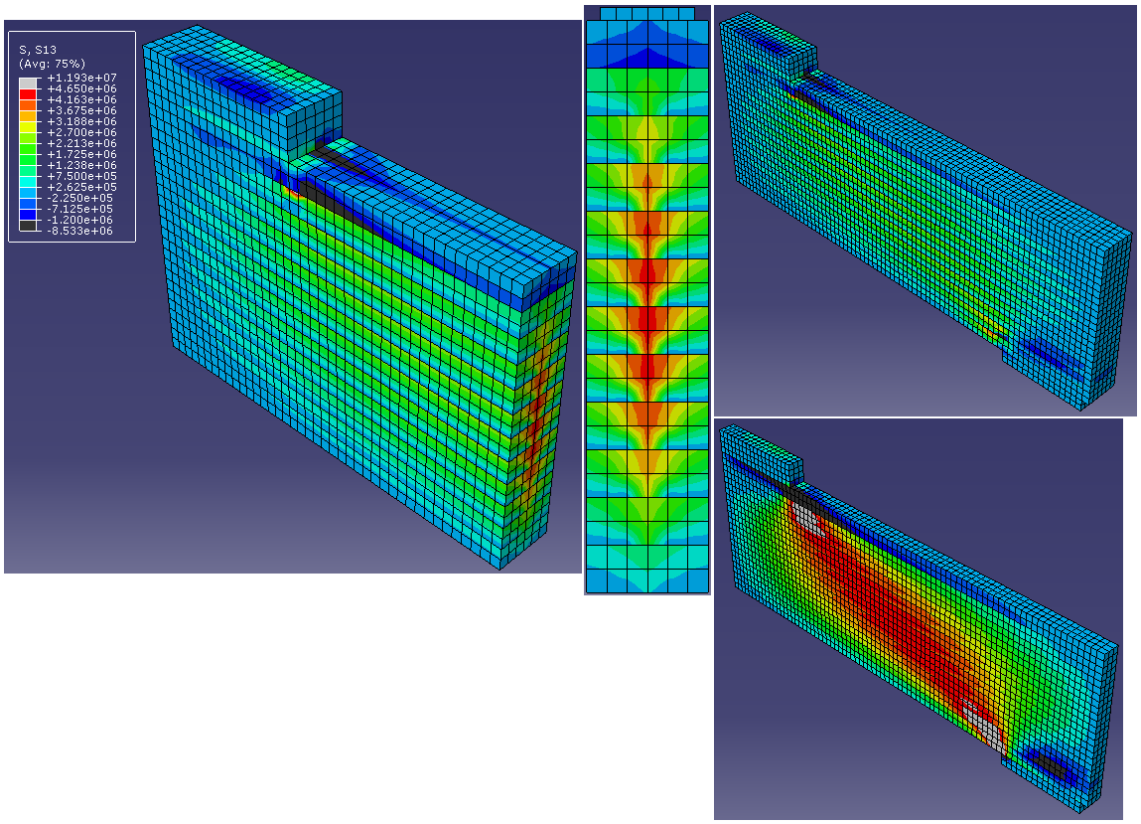

Figure 29. Shear stress τ_{rl}. The unit of the results is N/m^2.

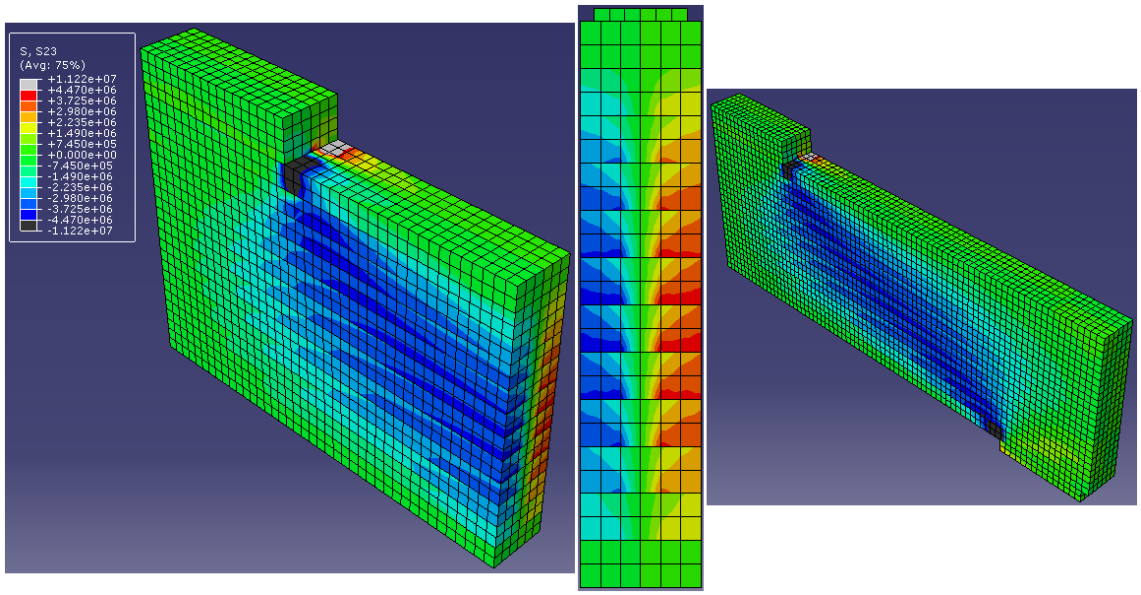

Figure 30. Shear stress τ_{tl}. The unit of the results is N/m^2.

The distributions of shear stresses τ_{rl} and τ_{tl} can be seen from Figures 29 and 30. Both stresses are of the same magnitude. Local interference affects greatly the maximum values of both stresses. If the interference is ignored the maximum value for τ_{rl} is approximately 4,65 N/mm^2 and ±4,47 N/mm^2 for τ_{tl}. In both cases the maximum values are obtained from the mid height of the beam, but shear stresses are rather high in quite a great part of the cross-section. τ_{rl} is over 3,7 N/mm^2 and τ_{tl} over ±3,5 N/mm^2 in some parts of every six middlemost lamella. Shear stresses τ_{rl} and τ_{tl} are in special focus when considering the failure mechanism in the shear failure. Failure planes in the shear failures of this study usually followed growth rings.

Shear properties of Norway spruce were examined in reference [15]. The shear moduli were determined with video extensometry and FEM calculations and also shear strengths for clear wood were reported. Figure 32 shows these obtained strengths. Shear strength in rl-direction can be seen to be between 4 and 8 N/mm^2. Shear strength in tl-direction is between 3 and 6 N/mm^2. Compared to the capacity of clear wood, knots in the lamella will probably increase the shear capacity in tl- and rl-directions. However, the calculated shear stresses τ_{rl} and τ_{tl} can be seen to be near the capacity of the lamellas.

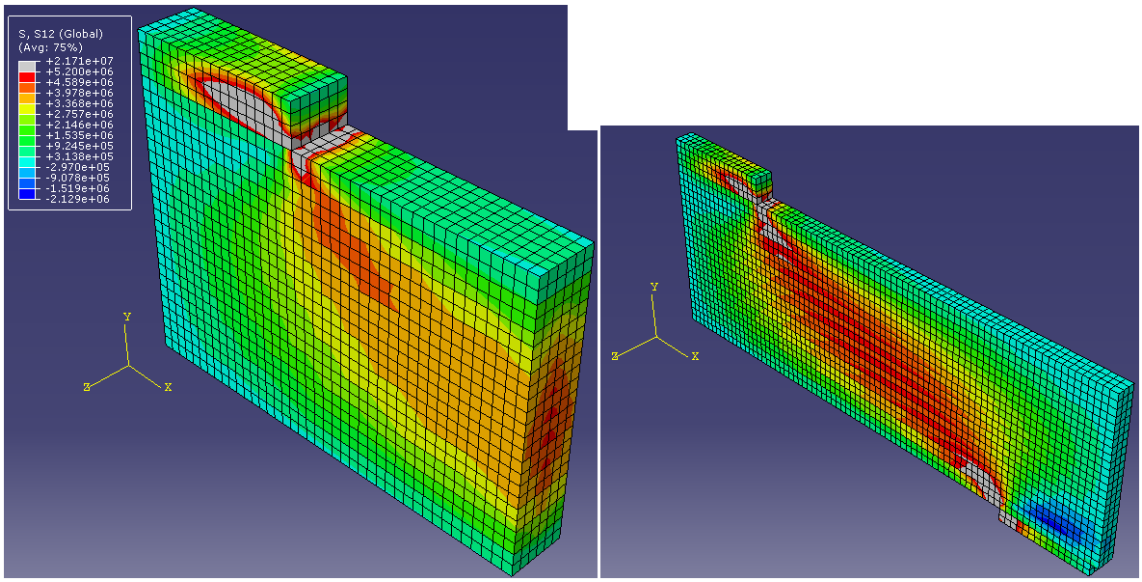

Figure 31. Shear stress τ_{xy}. The unit of the results is N/m^2.

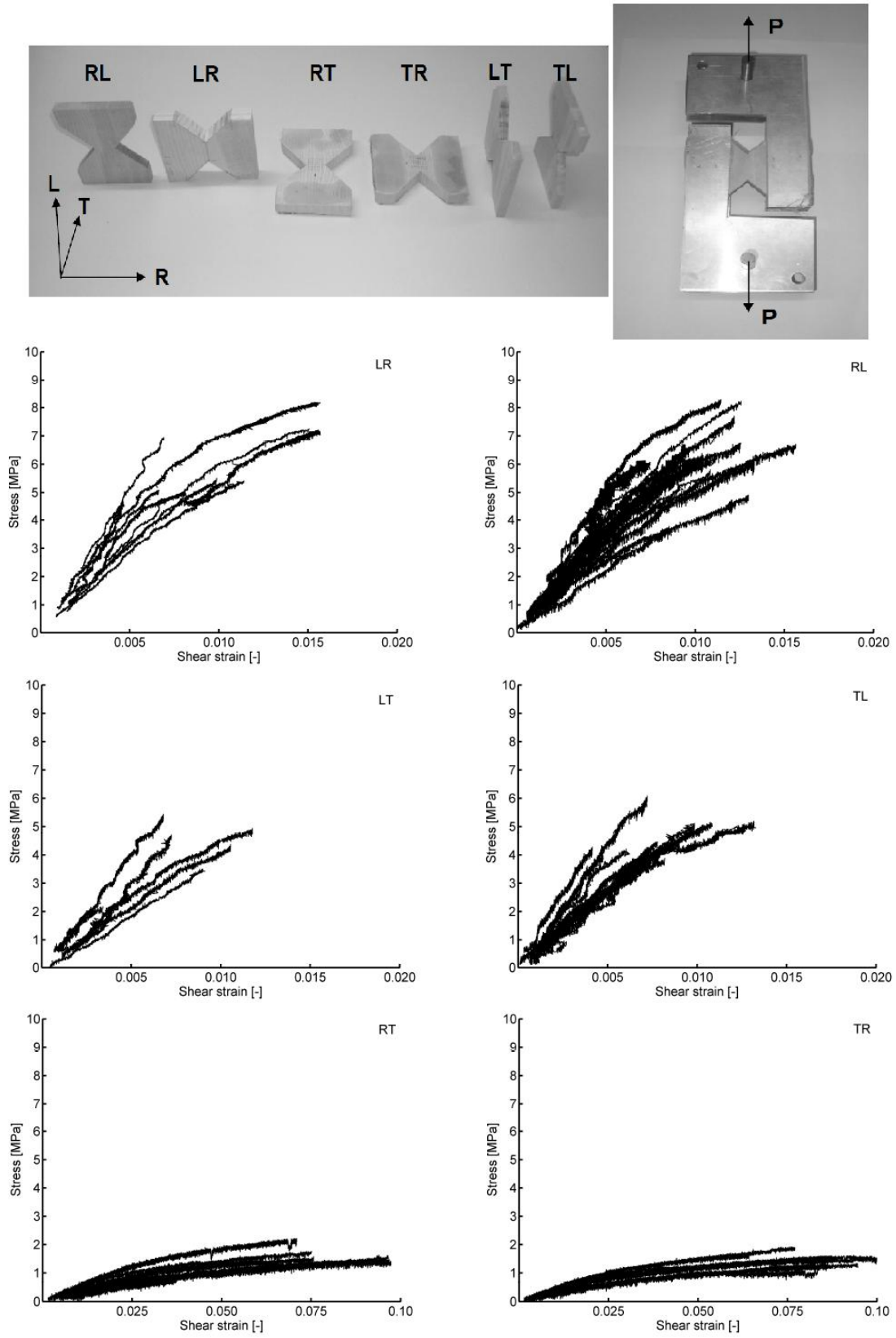

Figure 32. Shear strengths in different directions for clear wood specimens [15].

The distribution of shear stress τ_{xy} in global coordinate system is shown in Figure 31 in order to compare the manual and Abaqus calculations. Global coordinates in Abaqus can be seen from Figure 31. It is not the same to coordinate system used in the manual calculations with Euler-Bernoulli beam equation (Figure 15), but the absolute values of shear stress τ_{xy} obtained from the calculations can be compared. If local interference is ignored, the maximum value obtained for τ_{xy} is approximately 5,2 N/mm^2. The maximum value obtained from equation 19, when load is 350 kN, is approximately 4,23 N/mm^2. There is a significant difference in the values. Reasons for this difference should be studied in more detail. One possible reason could be that the glulam material is not homogeneous in a way that Euler-Bernoulli beam equation supposes.

One can notice from the directions of the principal stresses that the directions of the maximum shear stresses are close to the directions of global shear components τ_{xy} and τ_{yx} in the mid height of the beam. The values of shear stress τ_{xy} shown in Figure 31 are close to the maximum shear stresses in the mid height of the beam.

4.5.2 Strains and stresses from moisture content changes

Moisture induced strains and stresses were calculated with Abaqus together with two subroutines made by VTT. The subroutines are small algorithms written in FORTRAN language. The subroutines use ABAQUS state variables to calculate user's variables and to modify the ABAQUS state variables if necessary [11]. The two subroutines used were called UMAT and DFLUX. The UMAT calculates the stress increment and the Jacobian matrix for each time increment. The DFLUX calculates the flow of moisture between the air and the wood surface.

The model used in the moisture induced strain calculations was composed of a beam part of full height, half width and half of the length of the real beam. Mid length and mid width were used to decrease the amount of elements used in calculation. This kind of model could be applied because of symmetry planes in the middle of span and width. The beam was supported with hinged support that was approximately 0,5 m from the other end of the beam. Lamellas had rigid contact to each others. The modelled beam had no other loads than moisture load.

The local cylindrical coordinate systems of the lamellas were aligned similarly to the model of elastic calculation. The coordinate systems used in the calculation of moisture induced strains and stresses can be seen from Figure 33. Notation of the local coordinate system in Abaqus differs from the notation used previously in this study. The Abaqus notation shows in some pictures and may confuse the reader. The Abaqus notations correspond to the previous notations as follows: R-direction = r-direction, T-direction = t-direction and Z-direction = l-direction.

Material properties used in the calculation of moisture induced strains and stresses are shown in Table 4. Diffusion values used in the analysis are shown in Table 5. These values

were chosen because they have been noticed to correlate quite well in previous calculations and studies done to glulam at VTT.

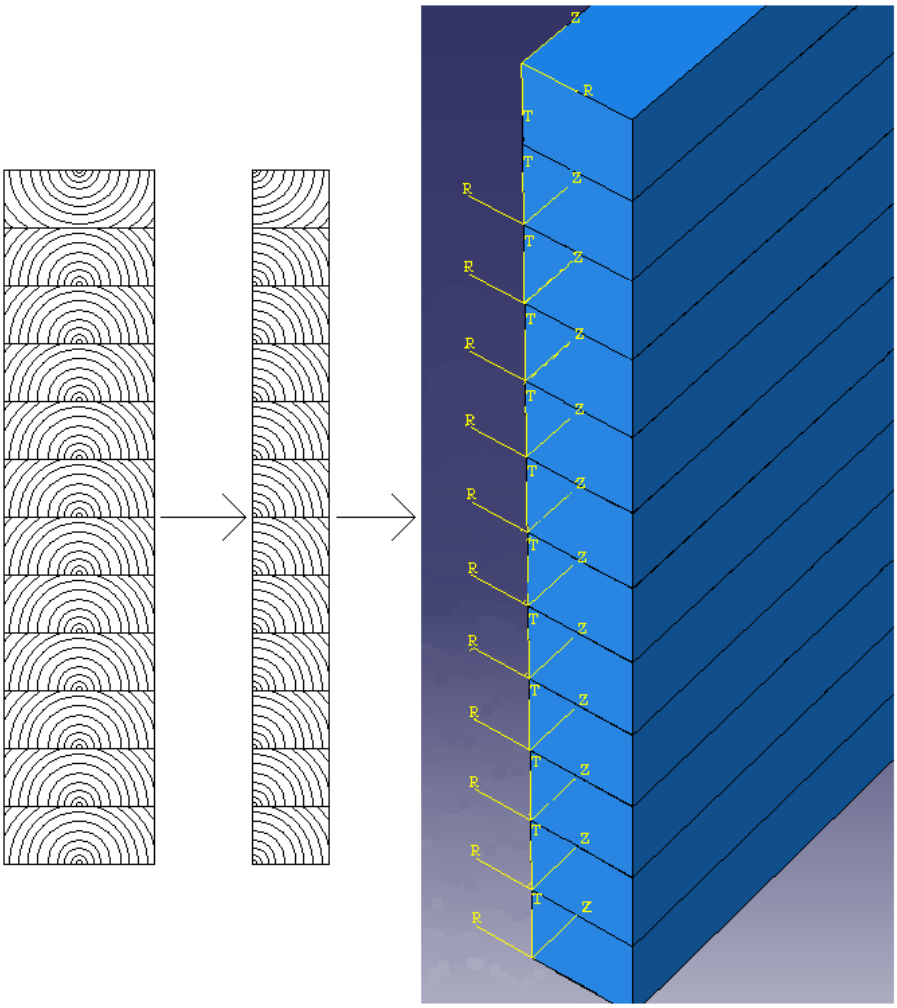

Figure 33. The coordinate systems used in calculation of moisture induced strains and stresses.

Table 4. Material properties used in the calculation of moisture induced strains and stresses.

Property number	Notation	Meaning	Value	Unit
1	E_r	Elastic moduli	817	MPa
2	E_t		420	MPa
3	E_l		11900	MPa
4	ν_{rt}	Poisson's ratios	0,555	-
5	ν_{rl}		0,038	-
6	ν_{tl}		0,014	-
7	G_{rt}	Shear moduli	42,5	MPa
8	G_{rl}		743	MPa
9	G_{tl}		624	MPa
10	$\alpha_{u,r}$	Coefficients of moisture expansion	0,13	-
11	$\alpha_{u,t}$		0,27	-
12	$\alpha_{u,l}$		0,005	-
13	ρ_0	Density at initial moisture content	450	kg/m^3
14	T_0	Initial temperature	20	°C
15	u_0	Initial moisture content	0,12	-
16	ρ_{ref}	Reference density	450	kg/m^3
17	T_{ref}	Reference temperature	20	°C
18	u_{ref}	Reference moisture content	0,2	-
19	a_1	Parameter related to the density	0,0003	m^3/kg
20	b_1	Parameter related to the temperature	-0,007	1/°C
21	c_1	Parameter related to the moisture content	-2,6	-
22	τ_1^{ve}	Retardation of the viscoelastic element number 1	2,4	h
23	J_1^{ve}	Viscoelastic compliance of element 1 given as a factor of the elastic compliance	0,085	-
24	τ_2^{ve}		24	h
25	J_2^{ve}		0,035	-
26	τ_3^{ve}		240	h
27	J_3^{ve}		0,07	-
28	τ_4^{ve}		2400	h
29	J_4^{ve}		0,2	-
30	τ_1^{ms}	Retardation of the mechanosorptive element number 1	0,01	-
31	$J_1^{ms,T}$	Compliance of the mechanosorptive element number 1 in tangential direction	0,003	1/MPa
32	$J_1^{ms,L}$	Mechanosorptive compliance of element 1 in longitudinal direction given as a factor of the elastic compliance at reference configuration	0,05	-
33	τ_2^{ms}		0,1	-
34	$J_2^{ms,T}$		0,003	1/MPa
35	$J_2^{ms,L}$		0,7	-
36	τ_3^{ms}		1	-
37	$J_3^{ms,T}$		0,07	1/MPa
38	$J_3^{ms,L}$		0,25	-
39	m_v	Parameter for the irrecoverable part of mechanosorptive creep	0,33	1/MPa

Table 5. Diffusion values used in the analysis.

Moisture content of wood [-]	Radial diffusion coefficient [m²/h]	Tangential diffusion coefficient [m²/h]	Longitudinal diffusion coefficient [m²/h]
0	0.0003888	0.0003888	0.0009
0.05	0.0004751	0.0004751	0.00504
0.055	0.0004841	0.0004841	0.00535
0.07	0.0005137	0.0005137	0.00567
0.085	0.0005461	0.0005461	0.00585
0.09	0.0005572	0.0005572	0.00567
0.135	0.0006690	0.0006690	0.00454
0.18	0.0008026	0.0008026	0.00307
0.23	0.0009690	0.0009690	0.00210
0.28	0.0012029	0.0012029	0.00135

The surface emissivity, S [m/s], used in the analysis was defined as equation 45.

$$S = 3 \cdot 10^{-9} \cdot e^{4u} \tag{45}$$

where u is the moisture content of the surface.

The value of surface emissivity was the only variable that was changed during the calculation process when attempting to make the calculated results correlate with the measured values.

Calculated moisture content distribution at different times can be seen from Figure 34. Moisture content was 12% at the beginning of the calculations. White lines in the beams show the location of the cross-section in question. The cross-sections shown in the Figure 34 are halves of the real cross-section. The left edge in the figure is the real outer surface and the right edge is in the mid width of the real cross-section. The height of every lamella is three elements in the figures presenting the results of moisture induced stresses.

The calculated moisture content distributions did not follow the measured average distribution exactly but the differences were not very high. Basically the moisture content changes were too fast in the model. The average moisture content of the cross-section was approximately one percentage point greater in the model compared to the measured average moisture content at the time of test phase S3. Similarly, the average moisture content of the cross-section was approximately two percentage points too dry when comparing to the measured values at the time of test phase S5. The calculated and measured values differed less that 0,5% from each other during test phases S2 and S4.

The parameters of the calculation could have been optimized to follow the measured values, but since the main concern was moisture induced stresses the differences in the

moisture contents were acceptable. Because of larger changes in the moisture content the obtained stresses are also larger than in reality. This makes the stresses to be on a safe side.

Figure 35 shows the deformed shapes of the cross-section in different phases of the tests.

Figure 36 shows the principal stresses at different test phases caused by the moisture content changes. For every test phase pictures on left and in the middle show all principal stresses. The middlemost pictures are taken perpendicular to the face of the beam. The pictures on right show only the positive principal stresses. Because wood has only a small tension strength perpendicular to grain, the positive principal stresses can cause cracks in the beam. The possible directions of the cracks can be analysed more easily for every test phase from the pictures on right in the Figure 36.

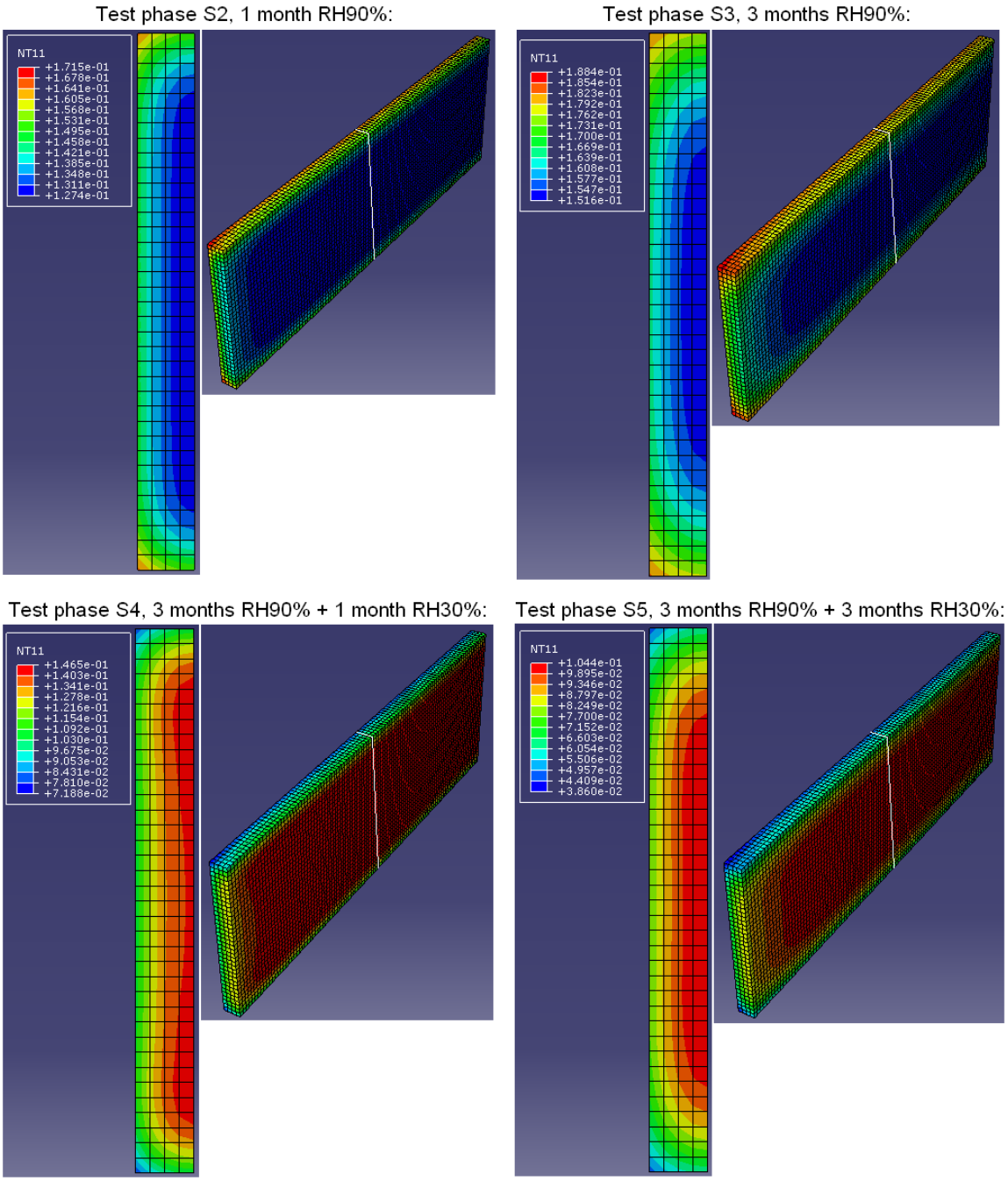

Figure 34. Moisture content distributions in different test phases. The moisture content values are expressed according to the following example: if the value in the figure is 1,715e-01 (= 0,1715) it means a moisture content of 17,15%.

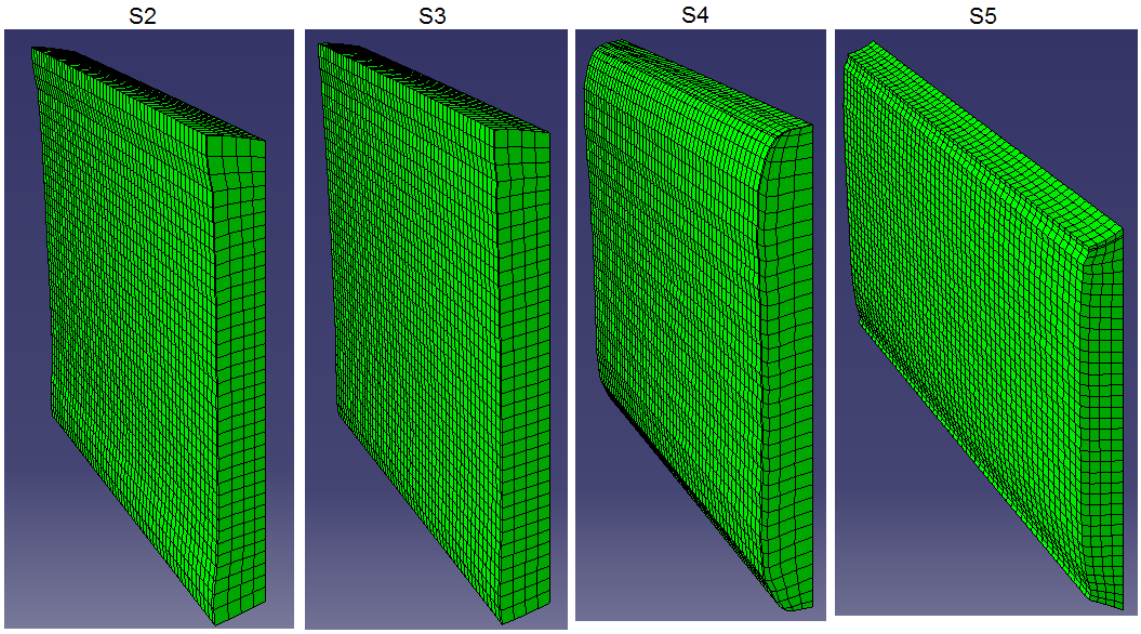

Figure 35. Deformed shapes of the cross-section of the beam in different test phases. The deformations are scaled to be approximately 40 times bigger than in reality.

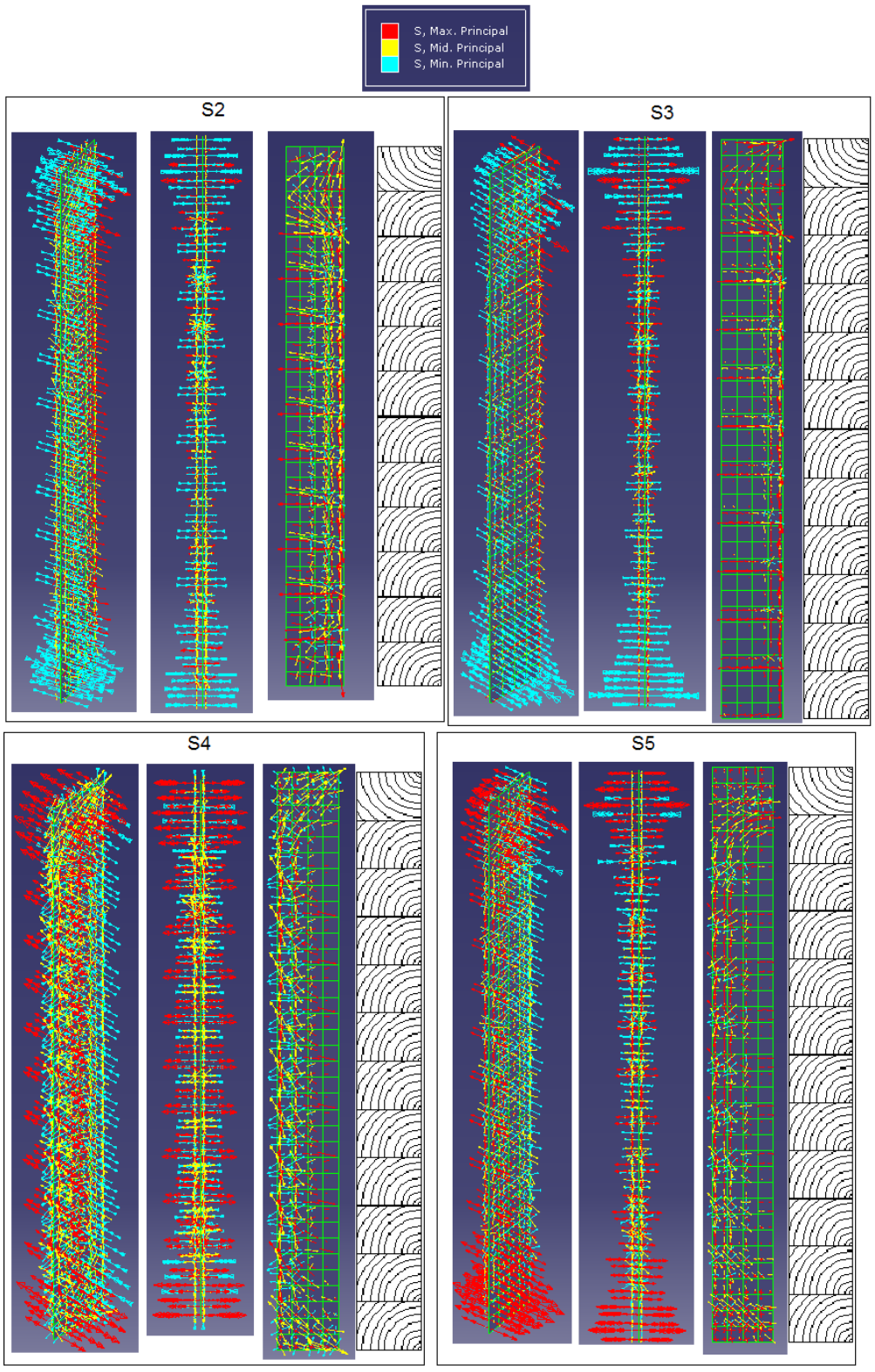

Figure 36. Moisture induced principal stresses in cross-section at different test phases. For every test phase picture on right shows only the positive principal stresses. The cross-section shown in the pictures is located one quarter away from the other end of the beam.

Moisture induced normal and shear stresses in different test phases are shown in Figures 37, 38, 39, 40, 41 and 42. In every case the presented cross-section is taken from a place where, if local interferences are ignored, the highest stresses align. The highest overall stresses were induced near the hinged support in every case.

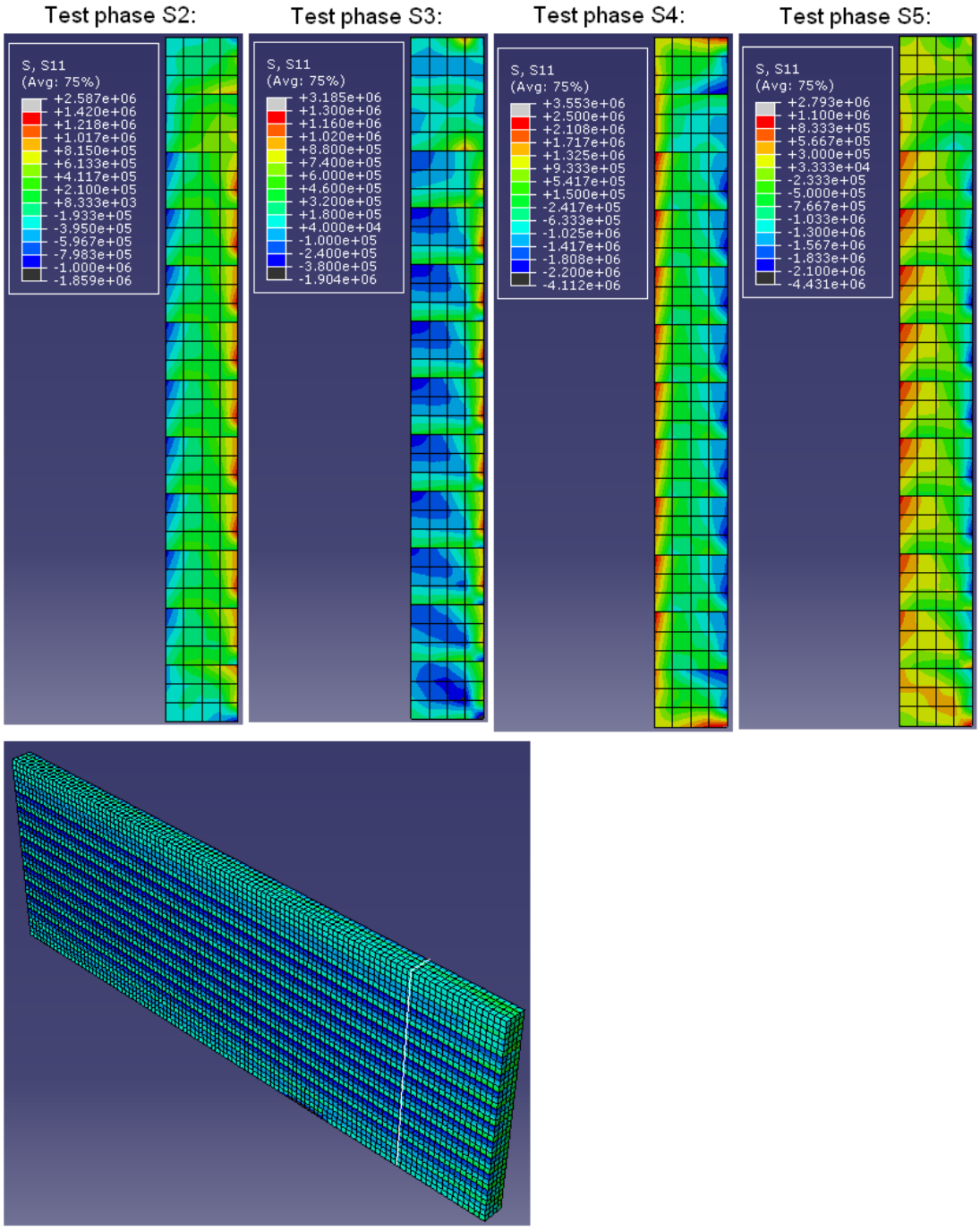

Figure 37. Normal stresses in r-direction at different test phases. The white line shows where the cross-sections in the figure are taken from. The unit of the results is N/m^2.

Normal stresses in radial and tangential directions are interesting because of their effect to the formation of cracks. The tension strengths in these directions are very small and therefore moisture induced stresses may easily cause visible cracks to the cross-section. Stresses obtain their highest values when moisture gradient is highest, that is to say in test phases S2 and S4.

Figure 37 shows stresses in radial direction caused by varying moisture content. When the moisture content of the beam increases starting from the surfaces, the surface part of beam swells, which causes radial tension stresses in the middle of the beam. A decreasing moisture content shrinks the surface part of the beam, which then causes radial compression stresses in the middle of the beam.

Figure 38 shows stresses in tangential direction caused by varying moisture content. The changes of the tangential stresses in function of moisture content are similar as in the radial direction. There are tangential tension stresses in the inner part of the beam due to the moisture induced swelling of the surface. On the sides of the beam, the tangential direction and the outer surface are almost parallel. When the swelling causes tensions in the inner part of the beam, the surface of the beam is compressed accordingly, because free deformations are not possible in the cross-section. Thus, there is compression also in the tangential direction. Vice versa, when the moisture content of the outer part decreases, the shrinking of the surface causes compression in the middle part of the beam and tension in the surface.

The characteristic tension strength perpendicular to grain of GL32c is only 0,45 MPa. It can be seen from Figures 37 and 38 that this strength is exceeded in some parts and directions of the beam. This can cause cracks in the cross-section.

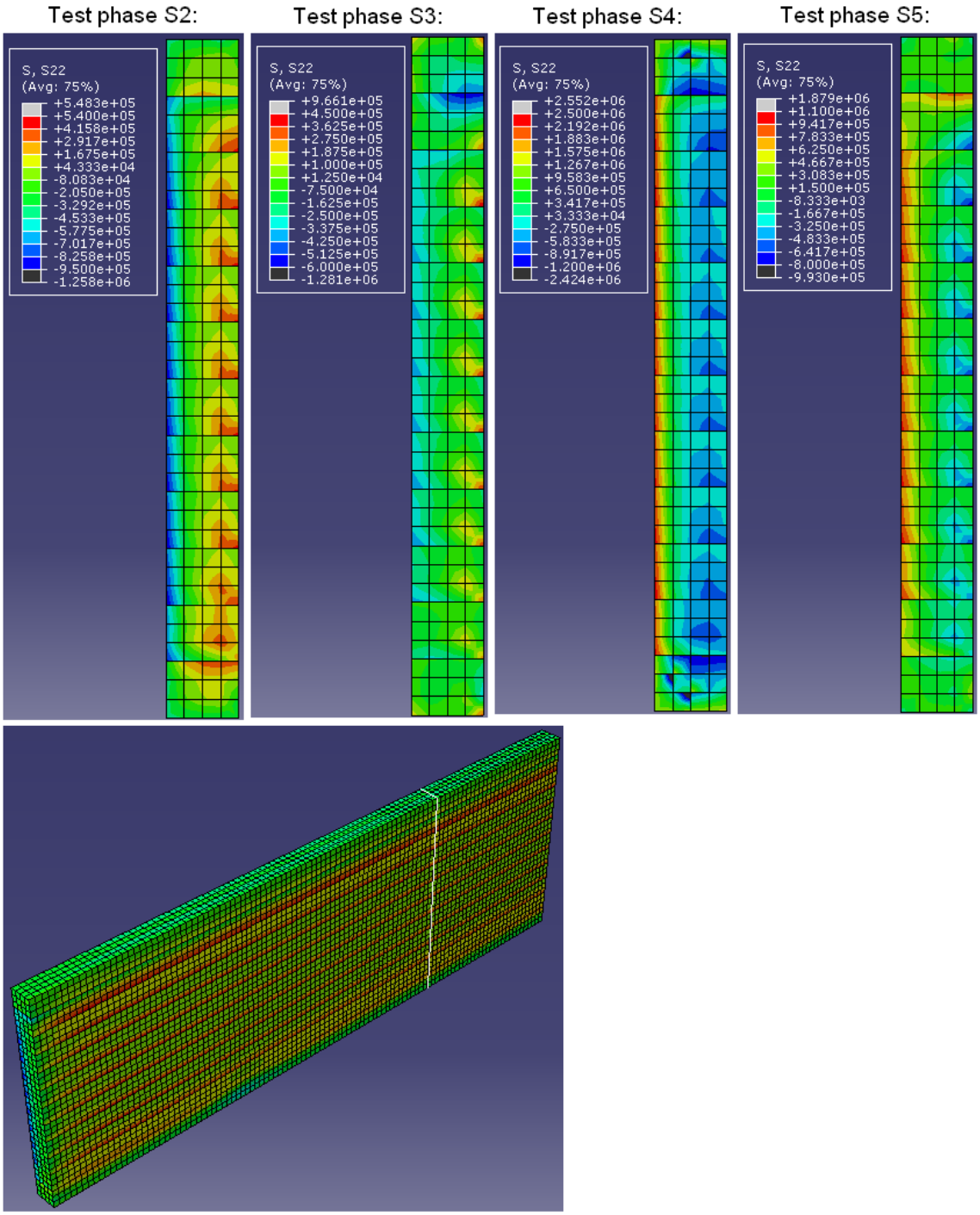

Figure 38. Normal stresses in t-direction at different test phases. The white line shows where the cross-sections in the figure are taken from. The unit of the results is N/m^2.

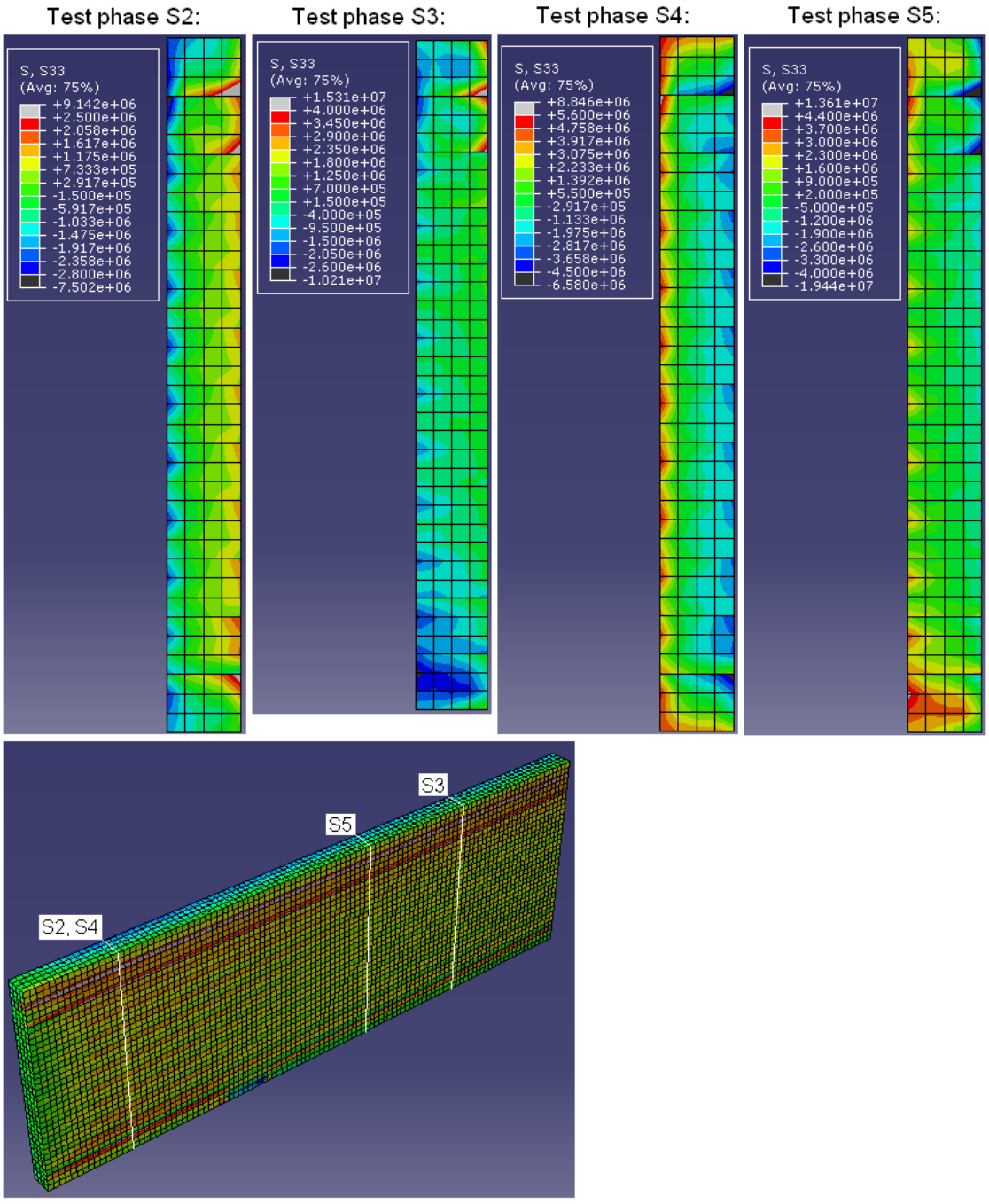

Figure 39. Normal stresses in l-direction at different test phases. The white line shows where the cross-sections in the figure are taken from. The unit of the results is N/m^2.

Figure 39 shows the normal stress in longitudinal direction. The middle parts of the cross-section can be seen to be in tension during the moistening period. Increase in the moisture content near the edges of the beam force the edge parts to expand which causes tension to inner parts. When the moisture content decreases during the drying period is phenomenon opposite and the inner parts are compressed.

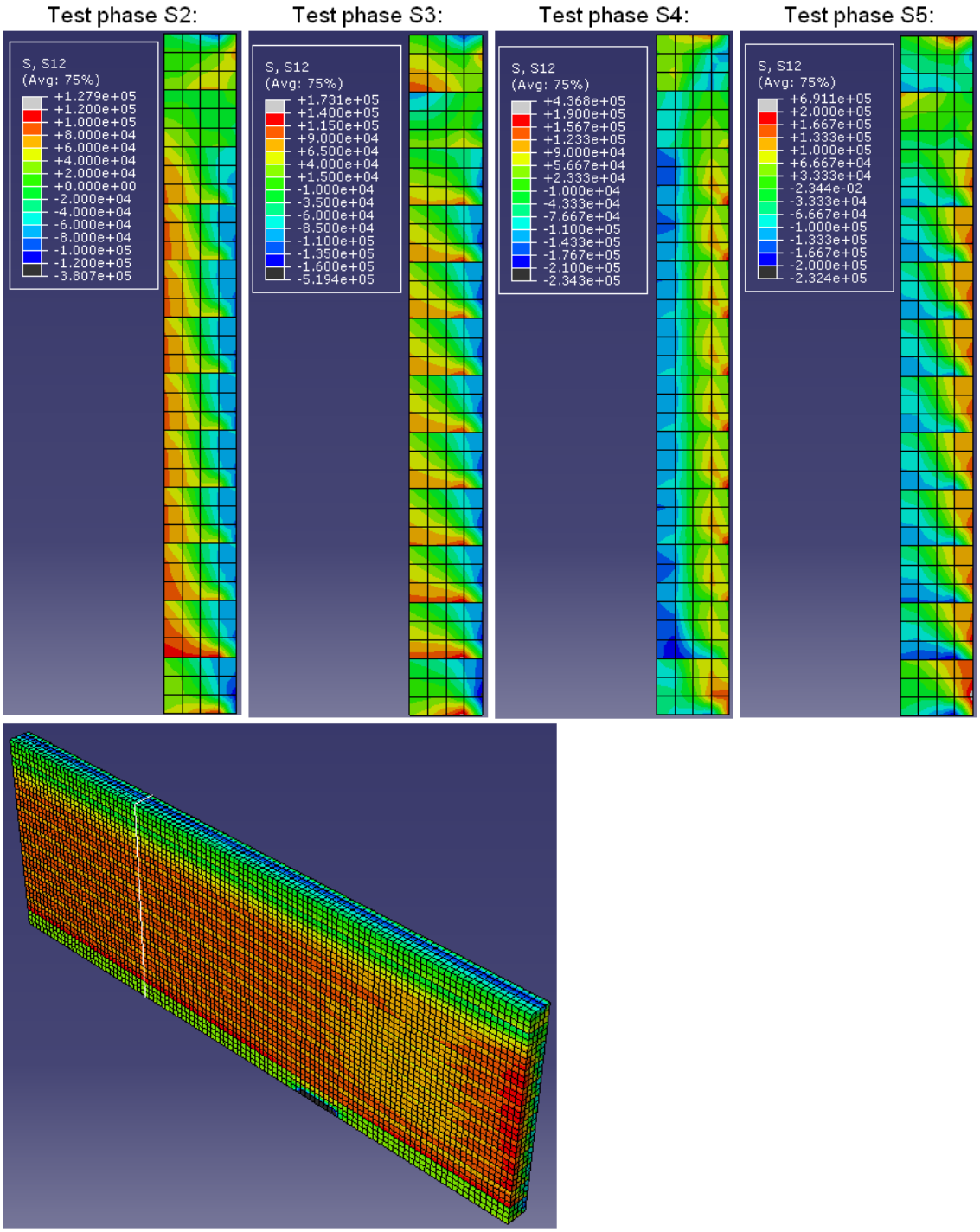

Figure 40. Shear stresses τ_{rt} at different test phases. The white line shows where the cross-sections in the figure are taken from. The unit of the results is N/m^2.

Shear stress τ_{rt} was the only local shear stress component that was calculated to have almost constant distribution in longitudinal direction. Calculated stresses were quite small, below ±0,21 N/mm^2 in every case if the interference of the support is ignored.

In elastic calculations the shear stresses in τ_{rt} directions are very small and therefore insignificant. Consequently, also the interaction of moisture induced shear stresses and elastic shear stresses in τ_{rt} direction is not significant.

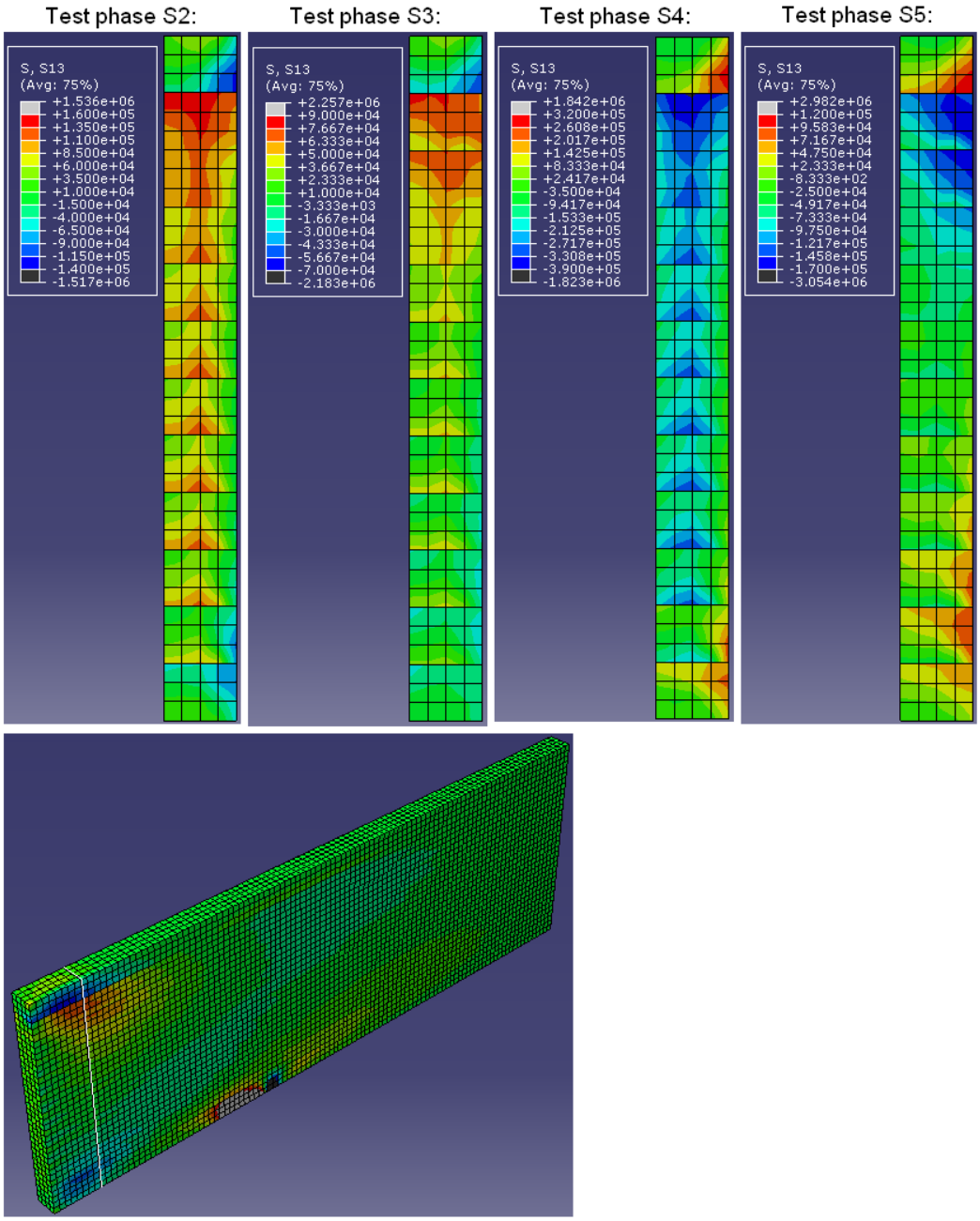

Figure 41. Shear stresses τ_{rl} at different test phases. The white line shows where the cross-sections in the figure are taken from. The unit of the results is N/m^2.

The effects of moisture changes to the shear stresses τrl and τtl were of special interest. The failure mechanism in most shear failures indicated that the shear strengths in these

directions were exceeded which caused the beams to fail. Also the elastic calculations showed that shear stresses in these directions were great in particular parts of a lamella. Moisture induced shear stresses τrl and τtl are shown in Figures 41 and 42.

The moisture induced stresses were however small in these directions. In every case their values were less than ±0,4 N/mm^2 when the local interference of the support is ignored. The stress distributions of τ_{rl} and τ_{tl} were also very local in longitudinal direction. No longitudinal stress fields were induced such as in case of the normal stresses in r-, t- and l-directions. It is understandable that in rl- and tl-directions there are no shear stresses when the moisture induced deformations are able to happen freely and the longitudinal deformations are uniform in the cross-section. Local effect in the end of the beam can be seen from the Figures 41 and 42. These local stress distributions are caused by different rates in the longitudinal shrinkage. Different rates are caused by the different ratios of surface area and volume between the edge and mid parts of the beam.

The distribution of moisture induced shear stress τ_{xy} in global coordinate system is shown in Figure 43. The end effect can be noticed also from the distribution of τ_{xy}. One can see that no shear stresses in the τ_{xy} direction are induced in that part of the beam which has great shear stresses in τ_{xy} direction in the elastic loading.

This result is in line with the test results that did not show any significant reduction in the shear resistance during the conditioning.

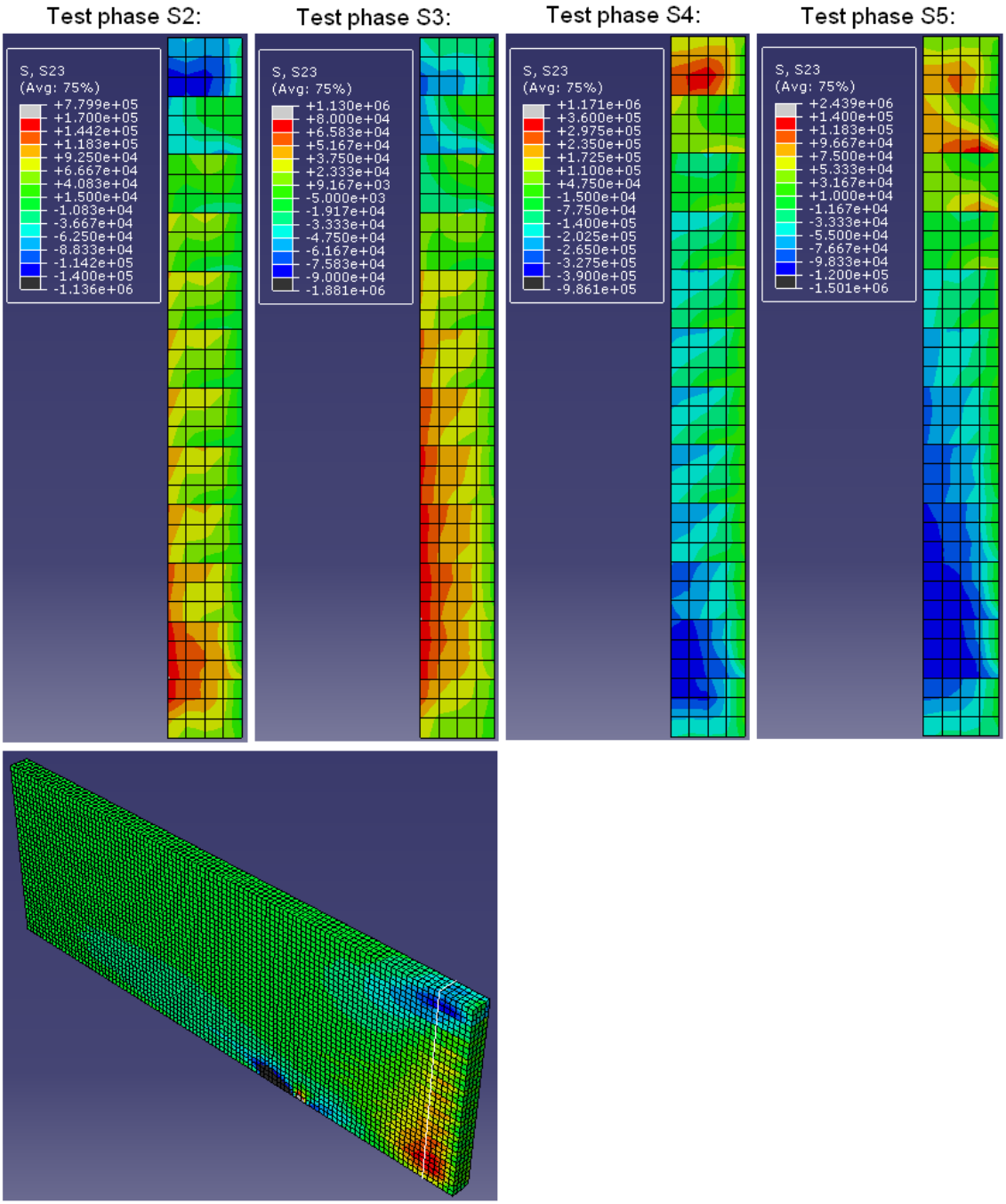

Figure 42. Shear stresses τ_{tl} at different test phases. The white line shows where the cross-sections in the figure are taken from. The unit of the results is N/m^2.

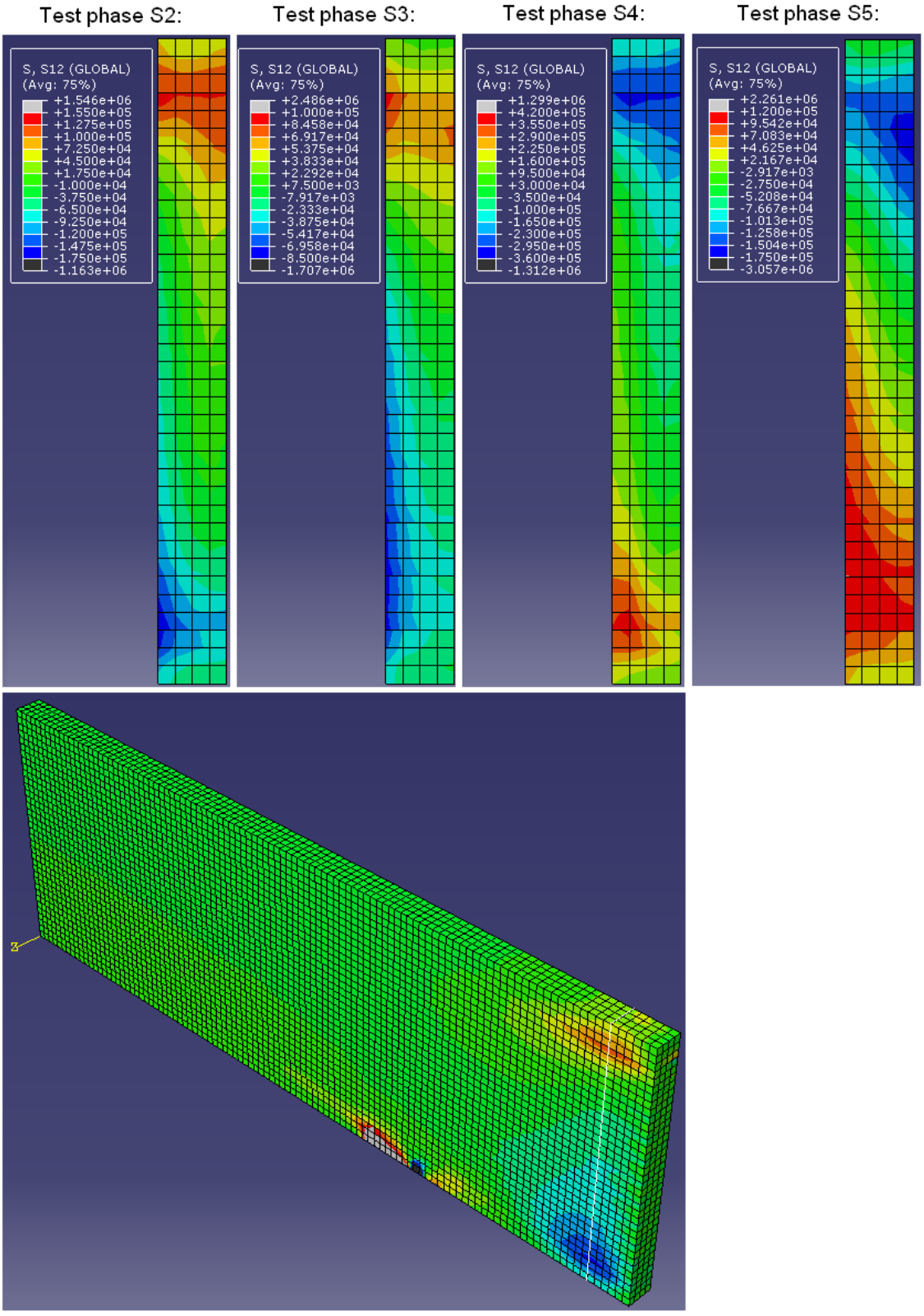

Figure 43. Shear stresses τ_{xy} at different test phases. The white line shows where the cross-sections in the figure are taken from. The unit of the results is N/m^2.

5. Results

A total of 103 tests out of 104 tests were successfully accomplished. The first test specimen was damaged because of an unsuccessful test setup so that a reliable shear resistance could not be determined for it. There were also few other minor difficulties during the tests but they did not disturb the determination on shear resistance.

There are two typical failure modes in this kind of test setup, shear and bending/tension failure. Typical shear failure is shown in Figure 44. A beam breaks into two halves usually from near the mid-point of the height. Two separate overlapping beams with total height similar to undamaged beam have only one quarter of the load bearing capacity of an undamaged beam. This usually means that bending/tension failure happens very quickly after shear failure if the load remains the same. Most of the beams that had shear failure were also damaged by bending after the shear failure. Fracture planes in shear failures followed mostly annual rings but in some cases fracture planes followed also a part of adhesive joints. Nevertheless, none of the fracture planes was sited clearly solely in adhesive joint.

Figure 44. A typical shear failure.

A typical bending/tension failure is shown in Figure 45. Typical bending failure starts from the tensioned lower edge of the beam. Failure happens in a part which is affected by a knot/knots or a finger joint. In most bending failure cases there were big knots, finger joints or both in the lower edge and near the mid span of the beam.

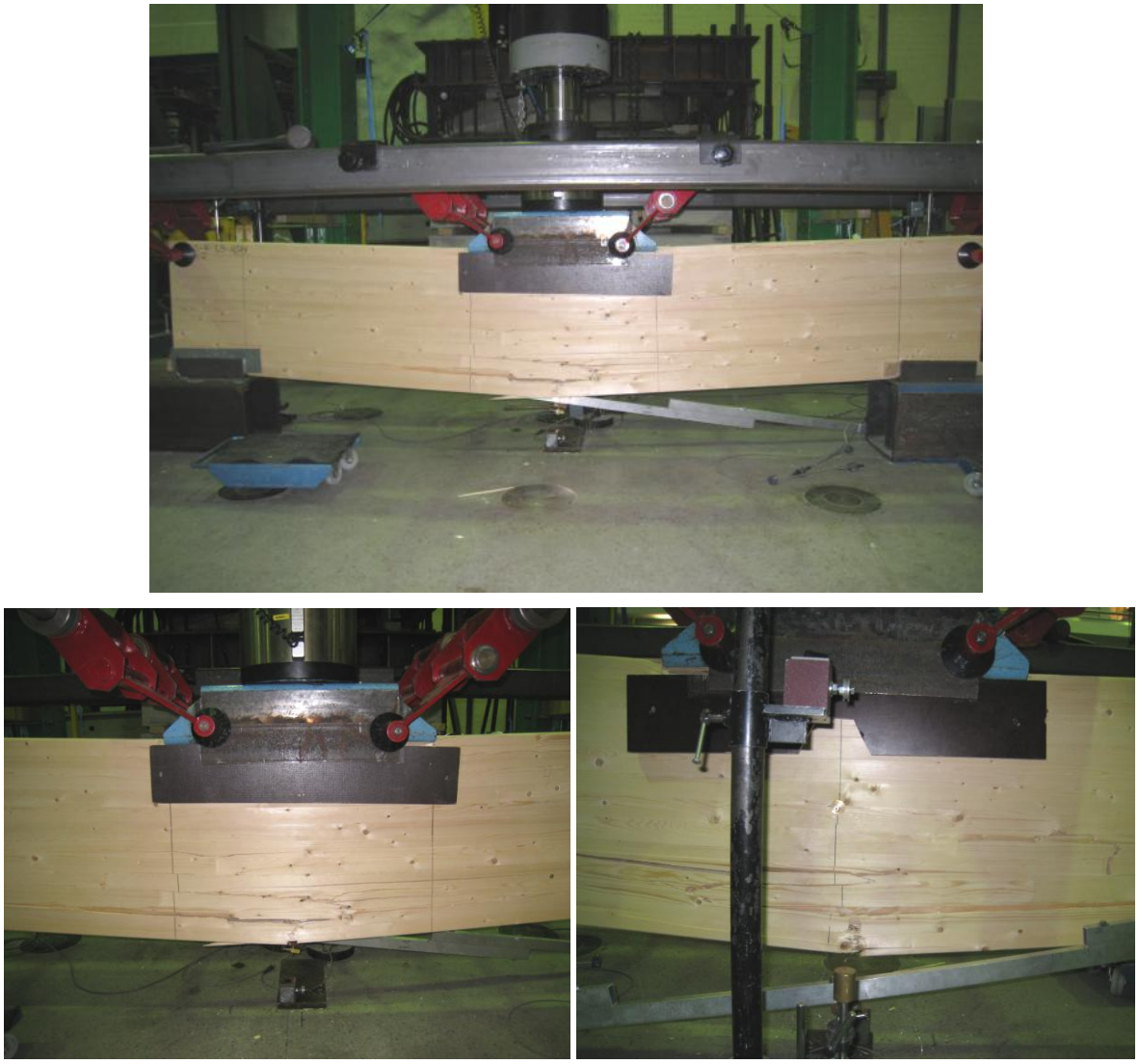

Figure 45. A typical bending failure.

Some of the failures were hard to divide strictly to shear or bending failures. In these cases the failure was usually brittle and the specific failure type could not be defined surely when observing the test. Beams were inspected after failure and sometimes there seemed to be evidence of both main failure types. Some kind of combination of bending and shear failures may have happened in the testing of these beams. Approximately 10 failures were hard to divide to be strictly a shear or a bending failure. The most probable failure type was chosen in these cases.

73 failures were classified to be shear type and 29 as bending type. 28 out of the 29 bending failures occurred with such high ultimate load that they were included to the consideration of the shear resistance. In bending failure cases, the shear resistance may be assumed to be at least the shear stress with the ultimate load.

The calculated mechanical results for the tests are shown in Tables 6, 7, 10, 13 and 16. Shear forces in the tables were calculated from the measured ultimate loads with equation 29. The shear stresses shown in the tables were calculated with the estimated dimensions of the beam by using equation 19. The estimated dimensions were calculated with equation 47 by using the following measured variables: cross-section dimensions, average moisture content of the cross-section and weights at different phases. Effective width (width times factor k_{cr}) has not been used in the calculations of shear stress values. The local and global elastic moduli were calculated from the manipulated expressions of deflection shown in equations 30 and 31 by using the characteristic dimensions and measured deflections. The calculated value of the local elastic modulus depends of the value of the shear modulus used in the calculation. The values of the local elastic moduli are calculated using the characteristic shear modulus of GL32c, 780 N/mm². The values for the shear modulus calculated from the measurements of the beams were approximately 15% smaller than the characteristic value. The values of local elastic moduli would have been approximately 3000 N/mm² greater if they had been calculated with these smaller measured values of shear moduli. The shear moduli were calculated from equation 44 by using the characteristic dimensions and measured deformations. Estimated densities were calculated from measured densities by taking into consideration the measured average moisture content and weight differences.

Monitored and calculated moisture content variables are shown in Tables 8, 9, 11, 12, 14, 15, 17 and 18. One variable was average moisture content in the cross-section. It was calculated from the measured moisture content values of test pieces 1–5 shown in Figure 14. Moisture content difference, or in other words the moisture gradient, in the cross-section was also calculated from the measured moisture content values. Moisture gradient causes moisture induced stresses in the cross-section and that is why it was monitored. Moisture gradient in the cross-section was monitored by comparing the moisture contents measured from the middle and from the edges of the cross-section. Comparison was done between moisture content in piece 3 (Figure 14) and average moisture contents measured from pieces 1 and 5. Comparison was done by subtracting moisture content of piece 3 from the average moisture content of pieces 1 and 5. Minus sign in moisture gradient indicates that midpoint of the cross-section is moister than edges.

Measured variables such as dimensions and ultimate loads for the specimens are shown in Appendix B. Measured moisture content values are shown in Appendix C.

5.1 Test series S1

Test series S1 was tested after about one month conditioning in RH 65%. The moisture content of test specimens should have been normalized to equilibrium moisture content in RH 65% before testing, so that the results can be considered comparable with previous results and the characteristic values. The equilibrium moisture content in RH 65% is ap-

proximately 12% for spruce. The conditioning was monitored by weighing. The mass of a specimen varies according to the moisture content. Constant mass means that the equilibrium moisture content is reached. The definition of constant mass was taken from EN408: "Constant mass is considered to be attained when the results of two successive weightings, carried out at an interval of 6 h, do not differ by more than 0,1% of the mass of the test piece." [7] Two specimens in test series S1 were observed and after noticing that they could be defined to have constant mass according to EN408, it was time to start the testing.

At first there were unexpected difficulties in the test setup and the test specimen S1-3/8, which was to be tested first, was damaged around supports and loading point so badly in the test that it could not be tested again with improved test setup. Because of adjustments in the test setup the second test specimen S1-4/8 was loaded two times around 300 kN and then released before applying the final loading which ended to shear failure. The rest of the test specimens were tested with the final test setup explained in chapter 4.

Approximated average density at 12% moisture content in specimens of test series S1 was 47 0kg/m³ and standard deviation was 7,1 kg/m³.

5.1.1 Strengths of test specimens

The results for series S1 are in Table 6.

Table 6. Test results of test series S1.

Beam	Coating	Failure type	Shear force with ultimate load [kN]	Shear stress τ_{max} with the ultimate load [N/mm²]	Local elastic modulus [N/mm²]	Global elastic modulus [N/mm²]	Shear modulus [N/mm²]	Estimated density MC 12% [kg/m³]
S1-1/8	Uncoated	Shear	180,9	4,35	15843	8718	663	478
S1-2/8	Uncoated	Shear	187,2	4,49	15111	8492	662	468
S1-3/8*	Uncoated	-	136,6	3,33	10584	6847	627	467
S1-4/8**	Uncoated	Shear	184,7	4,49	9916	6560	682	476
S1-5/8	Uncoated	Bending	150,3	3,66	11934	7387	664	457
S1-6/8	Uncoated	Bending	187,7	4,56	13770	8051	711	477
S1-7/8	Uncoated	Bending	168,4	4,08	14260	8217	648	471
S1-8/8	Uncoated	Bending	177,8	4,31	13770	8052	649	464

*Test result of the beam is ignored in the study due to bad test setup. Shear or bending rupture was not achieved, beam was damaged unusable near loading point and supports because of bad test setup.

**The beam was tested three times while improving the test setup between the tests. Load in the first two tests was near 300 kN. The ultimate load was achieved in the third test which was done with the proper test setup shown in Figure 13.

Figure 46 shows deflection in the midpoint of the centre line of the beam in function of the load for test series S1. Deflection of the centre line is measured with the gauge 2 in Figure 13.

The curve of the beam S1-3/8 is also shown in Figure 46. One can see that it differs from the other curves quite a lot and that is why it should be ignored when analysing the shear resistance. Stiffness of S1-4/8 differs from the other specimens, probably because it was loaded twice to about 80% of its ultimate resistance before the third and final loading time.

The beam S1-5/8 had a bending failure with low ultimate load and it is justified to remove it from the total consideration when studying shear resistance. The stiffness of S1-5/8 was also minor compared to other specimens. When ignoring S1-3/8 and S1-5/8 the average maximum shear stress in the beams with the ultimate loads was 4,38 N/mm^2 sample standard deviation being 0,18 N/mm^2. When ignoring only S1-3/8 from the beams in Table 6 the average maximum bending stress with failure loads was 38,9 N/mm^2 and standard deviation was 2,8 N/mm^2. Average maximum shear stress was about 36,9% higher than characteristic shear strength of glulam GL32c, 3,2 N/mm^2, while average maximum bending strength was about 21,6% higher than the characteristic bending strength, 32 N/mm^2.

The measured deformation in the midpoints of the centre line of the test specimens showed that S1-1/8 was the stiffest specimen and the S1-5/8 was the most flexible if S1-3/8 and S1-4/8 are ignored. The average local elastic modulus for test series S1 was 14110 N/mm^2 without the anomalous S1-3/8 and S1-4/8 and standard deviation was 1340 N/mm^2. The average global elastic modulus was about 8150 N/mm^2 and standard deviation was 457 N/mm^2. Average global elastic modulus is clearly minor compared to characteristic value of the elastic modulus, 13700 N/mm^2. Reason for this is that the test setup emphasizes the effect of shear force induced deformations. However, the average local elastic modulus is more significant than the characteristic value, as it should be, because the characteristic value is obtained from calculations of global elastic modulus in tests that are done according to EN408:2003.

The values for shear modulus were obtained from equation 44 by using the measured data of gauges 3 and 4. Shear modulus was calculated from the deformation that happened on loads between $0,1F_{max}$ and $0,4F_{max}$. Shear force distribution in the beam S1-3/8 was the same as in other specimens, and therefore all specimens in test series S1 can be observed when studying shear modulus. The average shear modulus in test series S1 was 663 N/mm^2 and standard deviation was 25 N/mm^2. The average shear modulus was 15% smaller than the characteristic shear modulus G_{mean}, 780 N/mm^2.

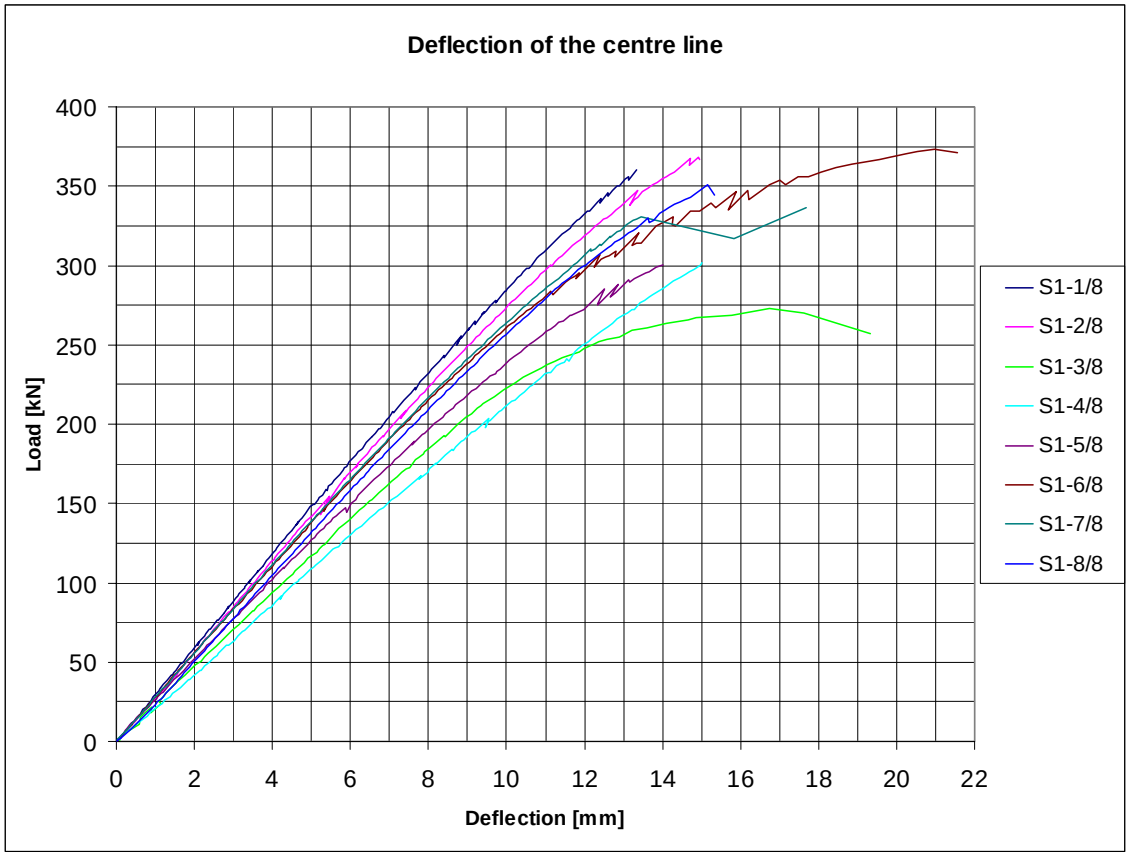

Figure 46. Deflection in the centre line of the beam in function of load for the specimens in test series S1.

5.1.2 Failure modes

Test series S1 had 7 successful failures. The first test specimen was damaged because an unsuccessful test setup, and could not be tested again to achieve shear or bending failure with a reliable result. Three out of seven failures were shear failures, four being bending failures. Three out of four bending failures occurred with fairly great load and shear resistance can be said to be at least the shear stress with ultimate load.

5.1.3 Moisture properties of test specimens

Measured average moisture content in the specimens of test series S1 just after testing was 12,4% while sample standard deviation was 1,5%. Two of the specimens, namely S1-5/8 and S1-6/8, were clearly moister than the other specimens. Their average moisture contents were 15% and 14,8%. If those specimens were ignored, the average moisture content was 11,5% while sample standard deviation was 0,4%. Measured moisture contents for the specimens are shown in Appendix C.

In every beam the moisture content in the outermost measured pieces 1 and 5 (shown in Figure 14), which are next to faces of beam, seemed to be either lower or higher than the moisture content in the middle area of the beam. This indicates that the beams were not completely in equilibrium. A completely conditioned specimen would have had constant moisture content in its every part. However, the differences were not substantial, that is, in most specimens below 0,5 percentage point. In the two anomalously moist specimens S1-5/8 and S1-6/8 this difference was greater, ca. one percentage points.

Afterwards it can be said that S1-5/8 and S1-6/8 were too moist in the test situation which affected their results. Their conditioning would have taken much more time than the one month for which they were conditioned. This error happened because not every specimen in test series S1 was observed to have constant mass before the testing. Only two specimens were observed and they did not happen to be S1-5/8 nor S1-6/8. Elastic modulus can roughly be assumed to be about 5% lower for a specimen moisture content of which is around 15% compared to a specimen with moisture content is about 12%.

5.2 Test series S2

Test series S2 was tested after conditioning specimens in RH 90% for one month. Test series S2 was completed without any substantial problems.

One problem occurred when testing S2-13/24, when the hydraulic press did not follow its program to the end of the loading. The press suddenly took the load off and returned to its initial position and after that pressed the beam straight to failure. The load was about 379 kN when the malfunction in the press occurred and this was chosen to be the maximum load for the specimen. The specimen would have probably borne a little more but the data gathered after the malfunction cannot be considered reliable.

Approximated average density at 12% moisture content in specimens of test series S2 was 472 kg/m³ and standard deviation was 9,9 kg/m³.

5.2.1 Strengths of test specimens

The results for test series S2 are in Table 7. Figure 47 shows deflection in the midpoint of the centre line of the beam as a function of the load for test series S2.

Table 7. Test results of test series S2.

Beam	Coating	Failure type	Shear force with ultimate load [kN]	Shear stress τ_{max} with the ultimate load [N/mm²]	Local elastic modulus [N/mm²]	Global elastic modulus [N/mm²]	Shear modulus [N/mm²]	Estimated density MC 12% [kg/m³]
S2-1/24	A2	Shear	132,39	3,16	15450	8598	688	481
S2-2/24	A2	Shear	201,46	4,81	16833	9010	703	487
S2-3/24	A2	Shear	142,30	3,40	15958	8753	672	483
S2-4/24	A1	Shear	146,23	3,49	14359	8249	649	463
S2-5/24	A1	Shear	174,54	4,16	16211	8829	713	484
S2-6/24	A1	Shear	148,81	3,55	14429	8272	727	470
S2-7/24	A2	Shear	184,77	4,47	13810	8065	672	462
S2-8/24	A2	Shear	186,80	4,51	14972	8448	643	472
S2-9/24	A2	Bending	182,82	4,41	13416	7929	625	461
S2-10/24	A1	Shear	183,94	4,43	13144	7833	589	471
S2-11/24	A1	Shear	174,36	4,20	13136	7830	642	456
S2-12/24	A1	Shear	168,03	4,06	13503	7959	676	461
S2-13/24	L	Shear	189,86	4,59	13106	7820	647	481
S2-14/24	L	Bending	185,61	4,50	11733	7309	691	483
S2-15/24	L	Bending	200,81	4,86	12384	7557	640	476
S2-16/24	Uncoated	Shear	171,58	4,12	12659	7659	657	488
S2-17/24	Uncoated	Bending	197,94	4,77	13479	7951	629	477
S2-18/24	Uncoated	Bending	187,70	4,53	14145	8178	699	473
S2-19/24	L	Bending	175,06	4,20	13323	7897	688	463
S2-20/24	L	Bending	188,71	4,55	13383	7918	633	455
S2-21/24	L	Bending	176,62	4,25	12785	7704	645	466
S2-22/24	Uncoated	Shear	177,68	4,28	14975	8449	656	470
S2-23/24	Uncoated	Shear	164,90	3,96	13132	7829	759	464
S2-24/24	Uncoated	Shear	211,98	5,11	14743	8375	644	478

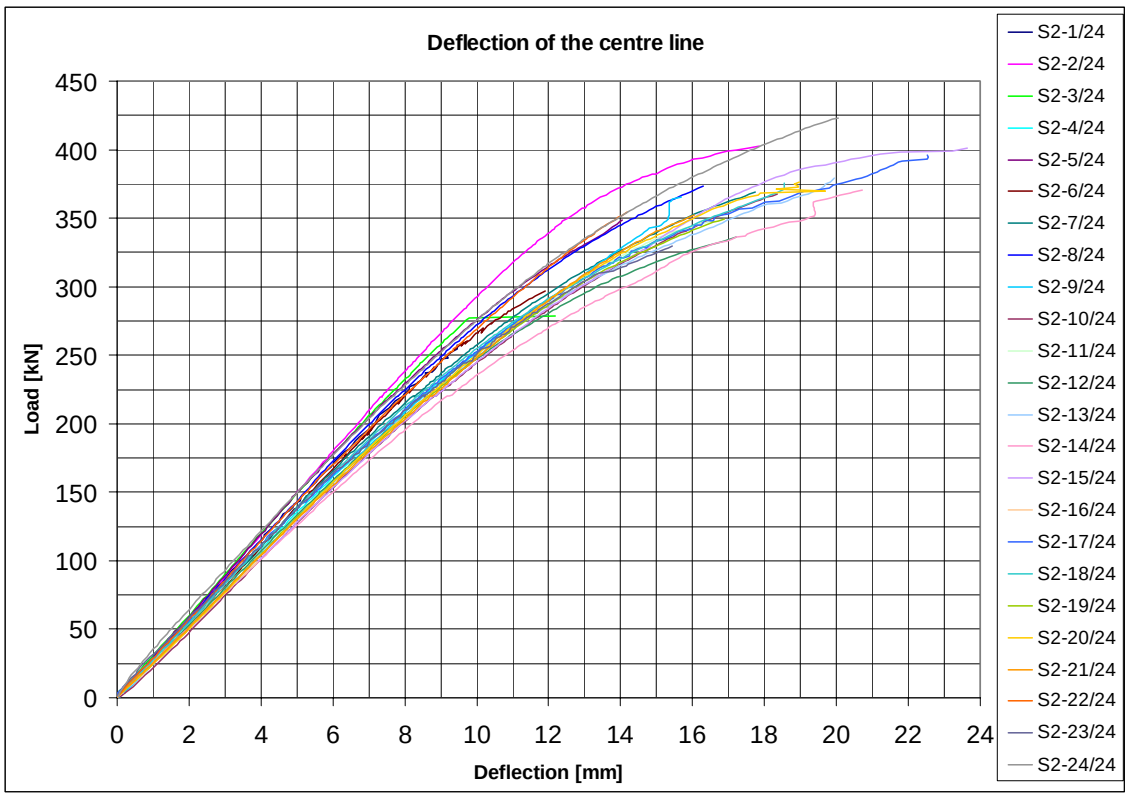

Figure 47. Deflection in the centre line of the beam as a function of load for the specimens in test series S2.

None of the bending failures in S2 happened with low ultimate load and it is justified to incorporate them in the study when considering shear resistance. The average maximum shear stress in all the beams of test series S2 with the ultimate loads was 4,27 N/mm^2, while the sample standard deviation was 0,48 N/mm^2. The average maximum bending stress with failure loads was 38,7 N/mm^2 and standard deviation was 4,4 N/mm^2. Average maximum shear stress was about 33,4% higher than characteristic shear strength of glulam GL32c, while average maximum bending strength was about 20,7% higher than characteristic bending strength.

The measured deformations in the midpoints of the centre lines of the test specimens indicated that S2-2/24 was the stiffest specimen and S2-14/24 was the most flexible one. The average local elastic modulus for test series S2 was 13960 N/mm² and standard deviation was 1280 N/mm². The average global elastic modulus was about 8100 N/mm^2 and standard deviation was 423 N/mm^2.

The average shear modulus in test series S2 was 666 N/mm² and standard deviation was 37 N/mm^2. The average shear modulus was 14,6% smaller than the characteristic shear modulus G_{mean}.

5.2.2 Failure modes

As can be seen from Table 7, 16 out of the 24 specimens had shear failure while 8 had bending failure. All bending failures occurred with quite high load, so they can be taken into account when calculating shear resistance.

5.2.3 Moisture properties of test specimens

Measured average moisture content in cross-sections of the specimens in test series S2 just after testing can be seen from Table 8. Actual measured moisture contents for the specimens are shown in Appendix C.

Table 8. Moisture content of test specimens in test series S2.

Specimen	Average MC after testing [%]	Sample standard deviation [%]
All	13,27	1,34
All but 13–18	12,62	0,77
13–18	15,21	0,56
Coating A2	12,51	0,45
Coating A1	12,61	0,76
Coating L	13,64	1,61
No coating	14,30	1,30
Coating L 13–15	15,11	0,54
Coating L 19–21	12,17	0,68
No coating 16–18	15,31	0,57
No coating 22–24	13,29	0,98

There were six clearly more moist specimens in test series S2. These were S2-13/24, S2-14/24, S2-15/24, S2-16/24, S2-17/24 and S2-18/24, which were from the same shipment as the two moist specimens in test series S1. Three of these moist specimens were coated with Linogard Underhållsolja and the other three were uncoated. The 6 moist specimens alter the average value of moisture content and increase the sample standard deviation when studying all specimens. Table 8 shows the average values and standard deviations with and without the moist specimens in the different groups. Their effect to the average and standard deviation values is so significant that they should be investigated separately.

Table 9 shows the moisture gradient in the test series S2. Minus sign in moisture gradient indicates that midpoint of the cross-section is moister than edges. As can be seen from Table 9 the variance in the gradient is great also between different coatings. No clear conclusions can be made from the values in Table 9. The moist specimens S2-13/24−S2-18/24 affect average and standard deviation values and therefore they are studied also separately.

Table 9. Moisture gradient in the cross-section, test series S2.

Specimen	Moisture gradient [%]	Sample standard deviation [%]
All	0,50	0,59
All but 13–18	0,68	0,51
13–18	-0,05	0,47
Coating A2	0,56	0,38
Coating A1	0,97	0,60
Coating L	0,00	0,48
No coating	0,48	0,53
Coating L 13–15	-0,37	0,24
Coating L 19–21	0,37	0,33
No coating 16–18	0,28	0,43
No coating 22–24	0,68	0,62

5.3 Test series S3

Test series S3 was tested after conditioning specimens in RH90% for three months. Also the test series S3 was completed without any great problems.

One problem occurred in the testing of S3-17/24, when movement limit of the hydraulic press was achieved before a bending or a shear failure in beam. There were severe deformations in the supports and the loading area in the beam. The load was about 384 kN when the movement limit was achieved and it was chosen to be the maximum load for the specimen. The specimen would have probably borne a little more, but it was not loaded again because of the severe deformations in the supports and the loading area.

Gauge 2, which measured the deflection of the mid span in the centre line of the beam malfunctioned during the testing of three specimens. Malfunction happened during testing of S3-2/24, S3-6/24 and S3-16/24 after there was a load of 140–200 kN. Nevertheless, elastic modulus could be determined also for these specimens because the load was great enough when the malfunctions happened.

A problem occurred also when testing S3-1/24. The control system of the hydraulic press had wrong settings and the loading was not steady. There was small cyclic variation in the load through the loading. The variation was however so small that it probably did not affect to the result at all.

Approximated average density at 12% moisture content in specimens of test series S3 was 475 kg/m³ and standard deviation was 10,7 kg/m³.

5.3.1 Strengths of test specimens

The results for test series S3 are in Table 10. Figure 48 shows deflection in the midpoint of the centre line of the beams as a function of the load for test series S3.

Table 10. Test results of test series S3.

Beam	Coating	Failure type	Shear force with ultimate load [kN]	Shear stress τ_{max} with the ultimate load [N/mm²]	Local elastic modulus [N/mm²]	Global elastic modulus [N/mm²]	Shear modulus [N/mm²]	Estimated density MC 12% [kg/m³]
S3-1/24	A2	Shear	169,83	4,04	16387	8881	749	486
S3-2/24	A2	Shear	176,80	4,21	16250	8840	746	483
S3-3/24	A2	Shear	153,91	3,65	16155	8812	686	481
S3-4/24	A1	Shear	169,89	4,04	16951	9044	684	488
S3-5/24	A1	Shear	153,37	3,65	14456	8281	660	474
S3-6/24	A1	Shear	156,78	3,72	13420	7931	596	476
S3-7/24	A2	Shear	170,97	4,09	13859	8082	574	473
S3-8/24	A2	Shear	172,74	4,14	13463	7945	616	467
S3-9/24	A2	Shear	175,59	4,21	13717	8033	598	474
S3-10/24	A1	Shear	197,69	4,75	15285	8547	598	479
S3-11/24	A1	Shear	153,38	3,67	13105	7819	548	437
S3-12/24	A1	Bending	183,22	4,38	13610	7997	561	473
S3-13/24	L	Bending	187,54	4,53	12330	7537	639	473
S3-14/24	L	Bending	195,94	4,72	12057	7434	571	479
S3-15/24	L	Bending	175,46	4,21	12340	7541	548	487
S3-16/24	Uncoated	Bending	193,37	4,64	13894	8094	636	483
S3-17/24*	Uncoated	-	191,90	4,61	13593	7991	645	482
S3-18/24	Uncoated	Bending	170,76	4,11	13744	8042	597	466
S3-19/24	L	Shear	151,72	3,64	13045	7798	605	480
S3-20/24	L	Bending	172,02	4,12	13683	8022	643	476
S3-21/24	L	Shear	161,24	3,86	12540	7615	595	476
S3-22/24	Uncoated	Shear	153,66	3,67	12064	7436	602	472
S3-23/24	Uncoated	Shear	188,52	4,53	14192	8194	681	470
S3-24/24	Uncoated	Bending	182,28	4,38	13079	7810	657	457

* Movement limit of hydraulic actuator was achieved before actual failure, severe deformations on supports and on loading area.

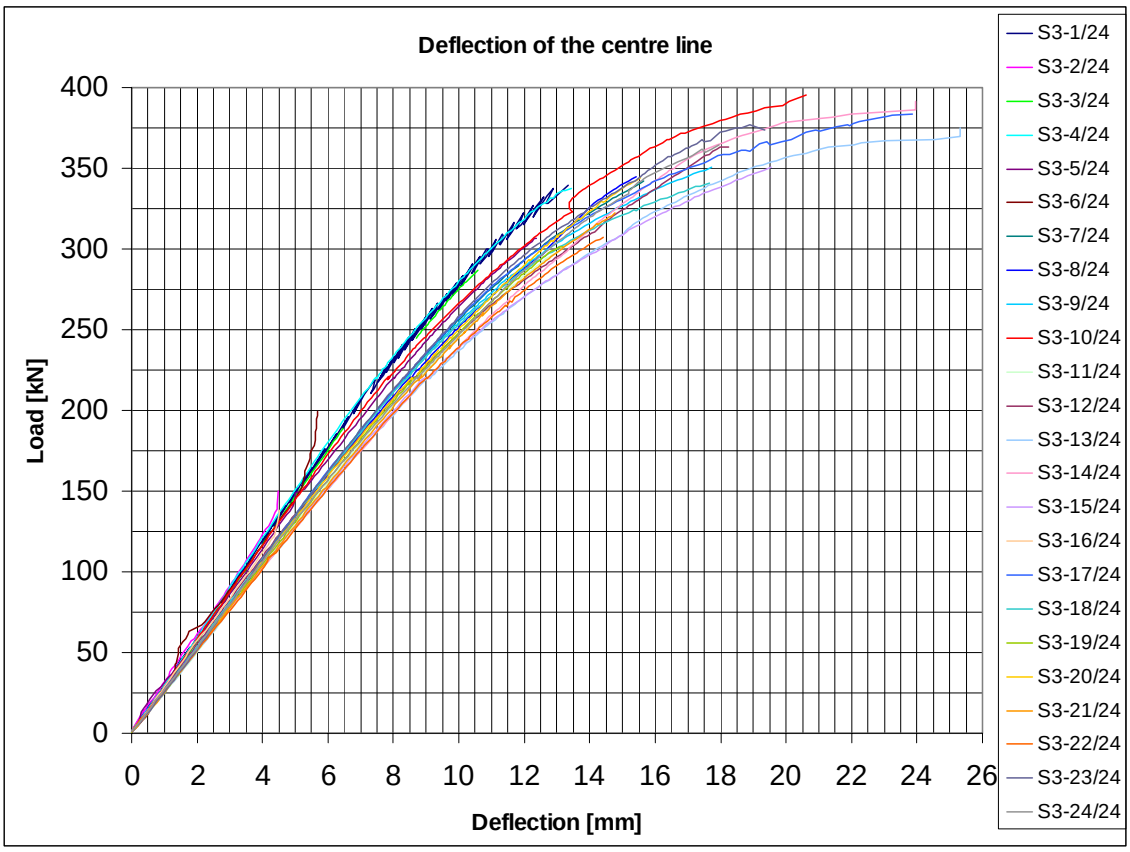

Figure 48. Deflection in the centre line of the beam as a function of load for the specimens in test series S3.

None of the bending failures in S3 happened with low ultimate load and it is justified to incorporate them in the study of shear resistance. The average maximum shear stress in all beams of test series S3 with the ultimate loads was 4,15 N/mm^2, while the sample standard deviation was 0,36 N/mm^2. Average maximum bending stress with failure loads was 37,5 N/mm^2 and standard deviation was 3,3 N/mm^2. Average maximum shear stress was about 29,7% higher than characteristic shear strength of glulam GL32c, while average maximum bending strength was about 17,2% higher than characteristic bending strength.

The measured deformation in the midpoint of the centre line of the test specimens indicated that S3-4/24 was the stiffest specimen and the most flexible one was the S3-14/24. The average local elastic modulus for test series S3 was 13880 N/mm² and standard deviation was 1390 N/mm². The average global elastic modulus was about 8070 N/mm^2 and standard deviation was 460 N/mm^2.

The average shear modulus in test series S3 was 626 N/mm² and standard deviation was 55 N/mm^2. The average shear modulus was 19,7% smaller than the characteristic shear modulus G_{mean}.

5.3.2 Failure modes

As can be seen from Table 10, 15 out of the 24 specimens had shear failure while 8 had bending failure and one specimen did have neither bending nor shear failure. All bending failures occurred with quite a high load, so they can be taken into account when calculating shear resistance.

5.3.3 Moisture properties of test specimens

Measured average moisture content in cross-sections of the specimens in test series S3 just after testing can be seen from Table 11.

Table 11. Moisture content of the test specimens.

Specimen	Average MC after testing [%]	Sample standard deviation [%]
All	13,82	1,19
All but 13–18	13,30	0,84
13–18	15,37	0,57
Coating A2	13,14	0,78
Coating A1	13,72	0,85
Coating L	14,33	0,94
No coating	14,08	1,66
Coating L 13–15	15,08	0,65
Coating L 19–21	13,58	0,49
No coating 16–18	15,66	0,29
No coating 22–24	12,50	0,53

There were six clearly moister specimens also in test series S3, namely S3-13/24, S3-14/24, S3-15/24, S3-16/24, S3-17/24 and S3-18/24, which were from the same shipment as the moist specimens in test series S1 and S2. Three of these moist specimens were coated with Linogard Underhållsolja and the other three were uncoated. These 6 moist specimens alter the average value of moisture content and increase the sample standard deviation when investigating all specimens. Table 11 shows the average values and standard deviations with and without the moist specimens in the different groups. Their effect to the average and standard deviation values is so significant that they should be studied separately.

Table 12 shows the moisture gradient in the test series S3. Minus sign in moisture gradient indicates that the midpoint of the cross-section is moister than the edges. As can be seen from Table 12 variance in the gradient is substantial also between different coatings. No clear conclusions can be drawn from values of Table 12. The moist specimens S3-13/24−S3-18/24 effect average and standard deviation values also when studying this

property. That is why they are studied separately as well. It is exceptional that the moist specimens were moister in the middle even though they had been in the moist conditions for three months. The fact that air in the test hall during the tests was dry, relative humidity was about 30%, may have effected to the moisture content near the surfaces. Beams were in the test hall for about 8 hours at the most and because the change in moisture content is very slow it should not have affected appreciably to the results.

Table 12. Moisture gradient in the cross-section, test series S3.

Specimen	Moisture gradient [%]	Sample standard deviation [%]
All	0,31	0,60
All but 13–18	0,59	0,38
13–18	-0,53	0,13
Coating A2	0,74	0,16
Coating A1	0,59	0,44
Coating L	0,09	0,79
No coating	-0,17	0,38
Coating L 13–15	-0,63	0,10
Coating L 19–21	0,80	0,23
No coating 16–18	-0,44	0,08
No coating 22–24	0,10	0,36

5.4 Test series S4

Test series S4 was tested after conditioning specimens in RH 90% for three months and between 5 to 6 weeks in drier air. Relative humidity varied from about 40% to 50% in the first two weeks of the drying period. At first, the ventilation unit of the conditioning room was not able to drop the relative humidity to 30%. Two additional air dehumidifiers were installed in the conditioning room and then the targeted RH 30% was reached. The testing of test series S4 was completed without further problems.

Approximated average density at 12% moisture content in specimens of test series S4 was 470 kg/m³ with a standard deviation of 9,1 kg/m³.

5.4.1 Strength of test specimens

The results for test series S4 are presented in Table 13. Figure 49 shows the deflection in the midpoint of the centre line of the beams as a function of the load for test series S4.

Table 13. Test results of test series S4.

Beam	Coating	Failure type	Shear force with ultimate load [kN]	Shear stress τ_{max} with the ultimate load [N/mm²]	Local elastic modulus [N/mm²]	Global elastic modulus [N/mm²]	Shear modulus [N/mm²]	Estimated density MC 12% [kg/m³]
S4-1/24	A2	Shear	173,89	4,15	16804	9002	628	470
S4-2/24	A2	Shear	159,36	3,80	15366	8572	651	464
S4-3/24	A2	Shear	185,64	4,43	15333	8562	621	466
S4-4/24	A1	Shear	167,12	4,01	16889	9026	684	476
S4-5/24	A1	Shear	199,02	4,75	16445	8898	677	454
S4-6/24	A1	Shear	187,52	4,50	16947	9043	705	478
S4-7/24	A2	Shear	182,31	4,41	15002	8458	606	463
S4-8/24	A2	Shear	173,13	4,18	14462	8283	586	468
S4-9/24	A2	Bending	174,78	4,22	14558	8315	594	459
S4-10/24	A1	Bending	194,43	4,73	14689	8357	628	480
S4-11/24	A1	Shear	179,12	4,35	14375	8255	575	457
S4-12/24	A1	Shear	176,37	4,28	14178	8189	559	460
S4-13/24	L	Shear	209,21	5,11	15058	8475	698	486
S4-14/24	L	Shear	171,04	4,19	15033	8468	637	486
S4-15/24	L	Bending	189,59	4,65	13904	8097	692	473
S4-16/24	Uncoated	Shear	179,84	4,40	13826	8071	580	469
S4-17/24	Uncoated	Shear	202,15	4,95	14443	8277	661	469
S4-18/24	Uncoated	Shear	186,13	4,55	13480	7951	609	461
S4-19/24	L	Shear	179,10	4,35	14585	8323	633	466
S4-20/24	L	Shear	175,93	4,28	14919	8431	665	467
S4-21/24	L	Bending	186,07	4,53	14855	8411	701	476
S4-22/24	Uncoated	Bending	182,57	4,44	14343	8244	681	466
S4-23/24	Uncoated	Shear	202,20	4,92	16860	9018	661	471
S4-24/24	Uncoated	Shear	194,95	4,74	15772	8697	689	488

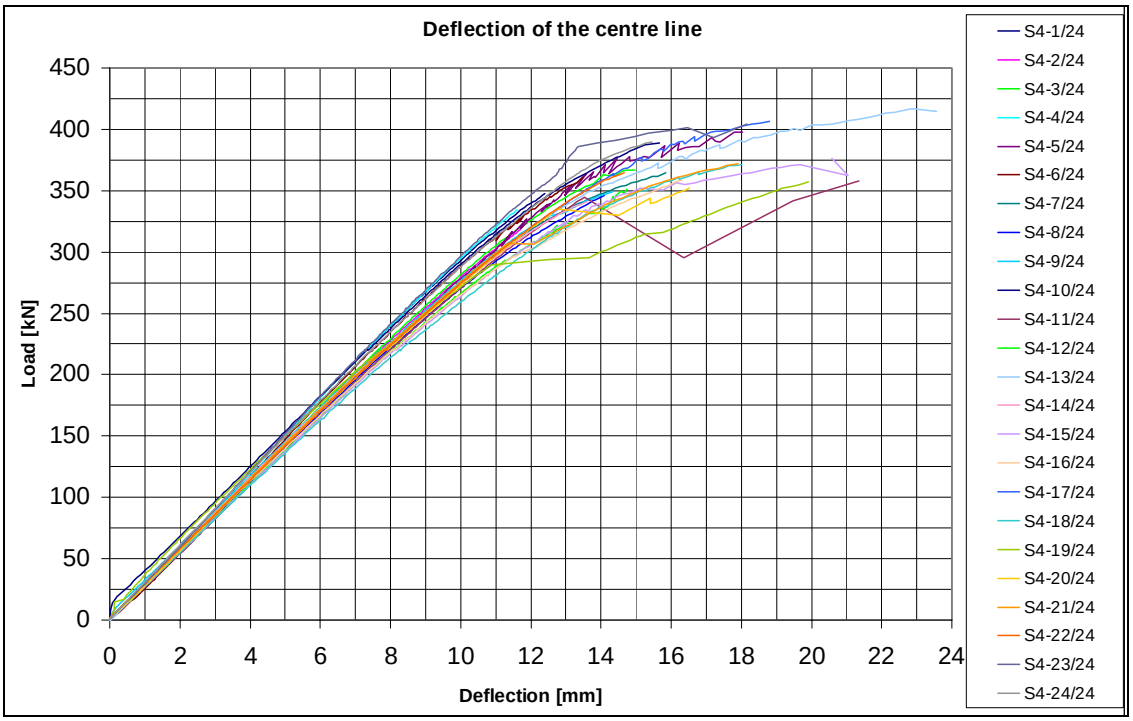

Figure 49. Deflection in the centre line of the beam as a function of load for the specimens in test series S4.

None of the bending failures in S4 occurred with low ultimate loads and it is justified to combine them in the study when considering shear resistance. The average maximum shear stress in all beams of test series S4 with the ultimate loads was 4,46 N/mm^2, while the sample standard deviation was 0,31 N/mm^2. The average maximum bending stress at failure was 40,5 N/mm^2 and standard deviation was 2,9 N/mm^2. The average maximum shear stress was about 39,4% higher than the characteristic shear strength of glulam GL32c, while the average maximum bending strength was about 26,6% higher than the characteristic bending strength.

The average local elastic modulus for test series S4 was 15090 N/mm² and the standard deviation was 1030 N/mm². The average global elastic modulus was about 8480 N/mm^2 and standard deviation was 320 N/mm^2.

The average shear modulus in test series S4 was 642 N/mm² and standard deviation was 44 N/mm^2. The average shear modulus was 17,7% smaller than the characteristic shear modulus G_{mean}.

5.4.2 Failure modes

As can be seen from Table 13, 19 out of the 24 specimens had a shear failure. All five bending failures occurred with quite a high load, so these were combined to the calculation

of shear resistance. Four beams, S4-6/24, S4-11/24, S4-13/24 and S4-19/24, that eventually had shear failure, had severe cracks in the lowest lamella before shear failure. In all of those beams the load dropped for a moment when the cracks developed to the lower edge but after the load raised again and the primary failure was of a shear type. It is hard to estimate how much the cracks in the lower edge of the beams affected the ultimate loads. The efficient heights of the beams were of course decreased because of the cracks, but in most beams the cracks appeared only near the mid length of the beams.

5.4.3 Moisture properties of test specimens

The measured average moisture contents in cross-sections of the specimens in test series S4 just after testing is given in Table 14.

Table 14. Moisture content of the test specimens.

Specimen	Average MC after testing [%]	Sample standard deviation [%]
All	12,39	1,27
All but 13–18	12,04	1,01
13–18	13,46	1,37
Coating A2	12,30	0,74
Coating A1	12,22	1,06
Coating L	12,43	1,66
No coating	12,61	1,45
Coating L 13–15	13,59	1,36
Coating L 19–21	11,28	1,00
No coating 16–18	13,34	1,42
No coating 22–24	11,88	1,08

There were six clearly more moist specimens also in test series S4. These were S4-13/24−18/24, which were from the same shipment as the moist specimens in test series S1, S2 and S3. Three moist specimens were coated with Linogard Underhållsolja and the other three were uncoated. Those 6 moist specimens alter the average value of moisture content and increase the sample standard deviation when grouping all specimens. Table 14 shows the average values and standard deviations with and without the moist specimens in the different groups.

Table 15 shows the moisture gradient in the test series S4. Minus sign in the moisture gradient indicates that midpoint of the cross-section was more moist than the edges, as was the case in all specimens here. The moist specimens S4-13/24−18/24 differ clearly from other specimens and of course affect the average and standard deviation values so they are studied also separately.

Table 15. Moisture gradient in the cross-section, test series S4.

Specimen	Moisture gradient [%]	Sample standard deviation [%]
All	-2,16	0,60
All but 13–18	-1,88	0,37
13–18	-3,01	0,15
Coating A2	-1,43	0,15
Coating A1	-2,02	0,17
Coating L	-2,50	0,51
No coating	-2,69	0,42
Coating L 13–15	-2,95	0,18
Coating L 19–21	-2,06	0,12
No coating 16–18	-3,06	0,12
No coating 22–24	-2,32	0,14

5.5 Test series S5

Series S5 was tested after conditioning the specimens in RH 90% for three months and another three months in dry air. In first two weeks of the drying period relative humidity varied from about 40% to 50%. The ventilation unit of the conditioning room was not able to drop the relative humidity to 30% at first. Two additional air dehumidifiers were brought into the conditioning room and after some time the RH 30% was reached. The relative humidity dropped below 30% after about 1,5 months. In the final 1,5 months the relative humidity was about 25%. The testing of test series S5 was completed without any substantial problems.

Approximated average density at 12% moisture content in specimens of test series S5 was 468 kg/m³ and standard deviation was 14 kg/m³.

5.5.1 Strength of test specimens

The results for the test series S5 are presented in Table 16. Figure 50 shows deflection in the midpoint of the centre line of the beams as a function of the load in test series S5.

Table 16. Test results of the test series S5.

Beam	Coating	Failure type	Shear force with ultimate load [kN]	Shear stress τ_{max} with the ultimate load [N/mm²]	Local elastic modulus [N/mm²]	Global elastic modulus [N/mm²]	Shear modulus [N/mm²]	Estimated density MC 12% [kg/m³]
S5-1/24	A2	Shear	192,48	4,63	18208	9390	686	463,63
S5-2/24	A2	Shear	171,49	4,13	16282	8850	667	454,74
S5-3/24	A2	Shear	194,70	4,70	17607	9227	718	477,36
S5-4/24	A1	Shear	164,03	3,96	15489	8610	646	462,06
S5-5/24	A1	Shear	197,20	4,75	16352	8870	681	473,92
S5-6/24	A1	Shear	191,18	4,62	18201	9388	711	478,75
S5-7/24	A2	Shear	184,92	4,49	15215	8525	615	468,13
S5-8/24	A2	Shear	193,99	4,71	14917	8430	596	443,81
S5-9/24	A2	Bending	164,57	4,00	15099	8488	589	465,91
S5-10/24	A1	Shear	173,89	4,26	14414	8267	567	448,46
S5-11/24	A1	Shear	177,40	4,33	15211	8523	609	468,38
S5-12/24	A1	Shear	179,58	4,39	13425	7932	572	446,17
S5-13/24	L	Shear	208,24	5,15	14604	8330	655	479,94
S5-14/24	L	Shear	187,89	4,63	12773	7700	613	462,74
S5-15/24	L	Bending	166,66	4,11	12448	7581	681	449,72
S5-16/24	Uncoated	Shear	195,50	4,83	14799	8393	686	480,28
S5-17/24	Uncoated	Shear	196,74	4,87	14741	8374	668	474,79
S5-18/24	Uncoated	Bending	199,35	4,91	14800	8393	763	467,35
S5-19/24	L	Shear	162,53	3,97	15990	8763	698	490,32
S5-20/24	L	Shear	164,60	4,02	13001	7782	647	465,91
S5-21/24	L	Shear	162,68	3,97	16397	8884	692	495,32
S5-22/24	Uncoated	Shear	206,85	5,05	16223	8832	643	470,81
S5-23/24	Uncoated	Shear	197,35	4,82	16885	9025	703	491,04
S5-24/24	Uncoated	Bending	170,67	4,18	14154	8181	718	456,80

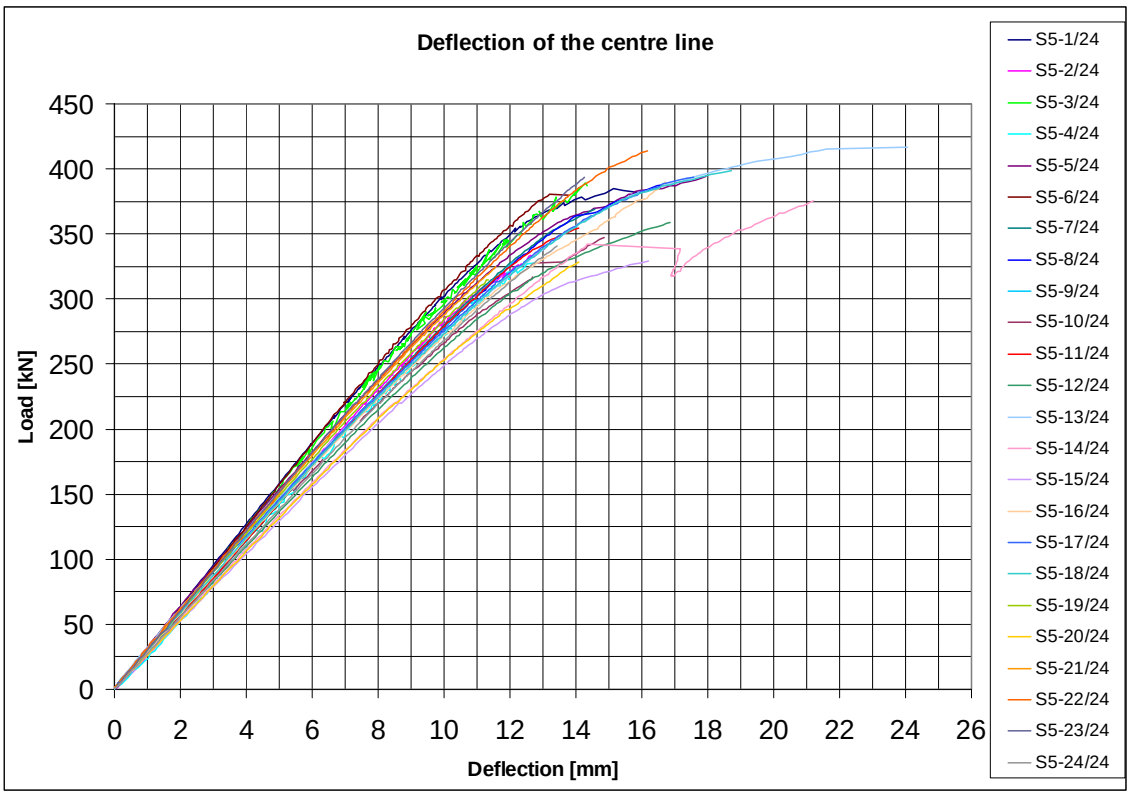

Figure 50. Deflection in the centre line of the beam as a function of load for the specimens in test series S5.

None of the bending failures in S5 occurred at low ultimate loads and it is justified to include them to the study of shear resistance. The average maximum shear stress in all beams of test series S5 with the ultimate loads was 4,48 N/mm^2, while the sample standard deviation was 0,37 N/mm^2. Average maximum bending stress with failure loads was 40,8 N/mm^2 and standard deviation was 3,5 N/mm^2. Average maximum shear stress was about 40% higher than characteristic shear strength of glulam GL32c, while average maximum bending strength was about 27,5% higher than characteristic bending strength.

The average local elastic modulus for the test series S5 was 15300 N/mm² and standard deviation was 1560 N/mm². The average global elastic modulus was about 8530 N/mm^2 and standard deviation was 490 N/mm^2.

The average shear modulus in the test series S5 was 659 N/mm² and standard deviation was 51 N/mm^2. The average shear modulus was 15,5% smaller than the characteristic shear modulus G_{mean}.

5.5.2 Failure modes

As can be seen from Table 16, 20 out of the 24 specimens had shear failure. All four bending failures occurred with quite a high load, so these were included to the calculation of

shear resistance. Two beams, 5 and 14, that eventually had a shear failure, had cracks in the lowest lamella before the shear failure. In testing of the beam S5-14/24 the load dropped for a moment after the cracks developed to the lower edge but then the load rose again and the primary failure was of a shear type.

5.5.3 Moisture properties of test specimens

The measured average moisture content in the cross-section of the specimens in test series S5 just after testing can be seen from Table 17.

Table 17. Moisture content of the test specimens.

Specimen	Average MC after testing [%]	Sample standard deviation [%]
All	11,03	1,06
All but 13–18	10,79	0,89
13–18	11,74	1,19
Coating A2	10,90	0,80
Coating A1	10,87	1,00
Coating L	11,09	1,14
No coating	11,25	1,24
Coating L 13–15	11,64	1,14
Coating L 19–21	10,53	0,84
No coating 16–18	11,83	1,28
No coating 22–24	10,67	0,90

Also in test series S5 there were six clearly more moist specimens. The moist specimens were S5-13/24−18/24, which were again from the same shipment as the moist specimens in the test series S1, S2, S3 and S4. Three moist specimens were coated with Linogard Underhållsolja and the rest three were uncoated. These 6 moist specimens change the average value of moisture content and increase the sample standard deviation when investigating all specimens. Table 17 shows the average values and standard deviations with and without the moist specimens in the different groups.

Table 18 shows the moisture gradients in test series S5. A minus sign for the moisture gradient indicates that the centre of the cross-section is more moist than the edges as was the case in all specimens. The moist specimens S5-13/24−18/24 differ clearly from the other specimens and of course affect the average and standard deviation values. That is why they are studied also separately.

Table 18. Moisture gradient in the cross-section, test series S5.

Specimen	Moisture gradient [%]	Sample standard deviation [%]
All	-1,94	0,45
All but 13–18	-1,71	0,19
13–18	-2,63	0,23
Coating A2	-1,51	0,15
Coating A1	-1,78	0,08
Coating L	-2,17	0,41
No coating	-2,32	0,50
Coating L 13–15	-2,53	0,08
Coating L 19–21	-1,80	0,11
No coating 16–18	-2,73	0,32
No coating 22–24	-1,91	0,11

5.6 Results for the shrinkage in height direction

The shrinkage in the height direction of the beam was studied from the test results of series S5. The main dimensions and weight of the beams in this study were measured in the pre-test phase. With the exception of test series S5, only the changes in weight were observed before the testing. The height of 18 beams in S5 was also measured just before the testing. The shrinkage percentage of the beams in the height direction was studied by comparing the change in height and moisture content. The moisture content at a pre-test phase was derived from the measured moisture content after testing by observing the change in weight between pre-test and test phase. The average dry mass of the whole beam was calculated with equation 46 derived from the definition of moisture content:

$$m_{dry} = \frac{m_{wet}}{\frac{MC}{100\%} + 1} \tag{46}$$

The estimated average moisture content in pre-test phase was calculated from the measured wet mass in the pre-test phase and the dry mass calculated from equation 46. The changes in the average moisture content and height are plotted in Figure 51.

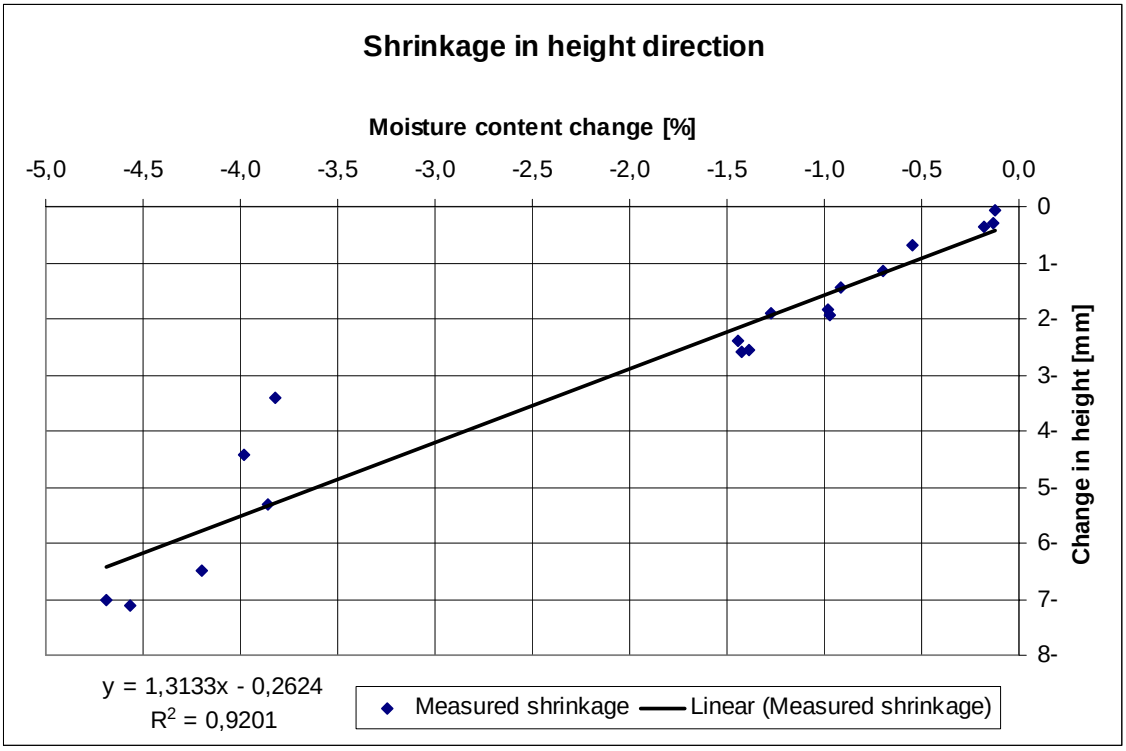

Figure 51. Shrinkage in height direction.

As can be seen from the equation of the trend line in Figure 51, the measured change in height was approximately 1,3 mm per 1% change in moisture content. Shrinkage percentage can be derived from equation 6 as follows:

$$S = \frac{\Delta x}{x} \cdot \frac{fsp}{\Delta MC}, S_{height} = \frac{1{,}3mm}{540mm} \cdot \frac{30\%}{1\%} \approx 7{,}2\% \qquad (47)$$

where Δx is the measured change of length in the considered direction as a result of a one percent change in the moisture content, in other words the slope of the trend line in Figure 51, mm.

The calculated shrinkage percentage in height direction seems to be close to the commonly known value of shrinkage in tangential direction for spruce, 7,8%. The calculated value seems to be realistic considering the orientation of the lamellas in the cross-section. On both sides of the beam the tangential direction of wood is parallel to height direction of the beam. In the middle of the beam the radial direction is parallel to the height of the beam. When considering the vertical direction, this means that a larger part of the beam is nearly in the tangential direction and a smaller part is in the radial direction. Keeping this in mind and remembering also that the moisture induced deformations are greater in the tangential direction, the deformations in tangential direction are emphasized in the overall shrinkage of the cross-section.

Shear stresses in this study are calculated with estimated dimensions of the cross-section. The estimated dimensions are calculated from the measured dimensions measured in the pre-test phase by examining the changes in the average moisture contents between the pre-test and the test phases. Shrinkage percentage calculated above is used in the calculations in height and also in width direction.

5.7 Results of the X-ray examination for all test series

The X-ray examination was carried out to all beams in the pre-test phase. The main dimensions and the weight of the examined beam were measured just before the X-ray examination. The average density of the beams was thereby known in the examining situation.

Figure 52 shows the relationship between the defined Mean Grey Value and the average wet density. The relationship seems to be linear. One specimen clearly stands out compared to the others. Some measurement has probably failed and that specimen should be ignored when considering the relationship.

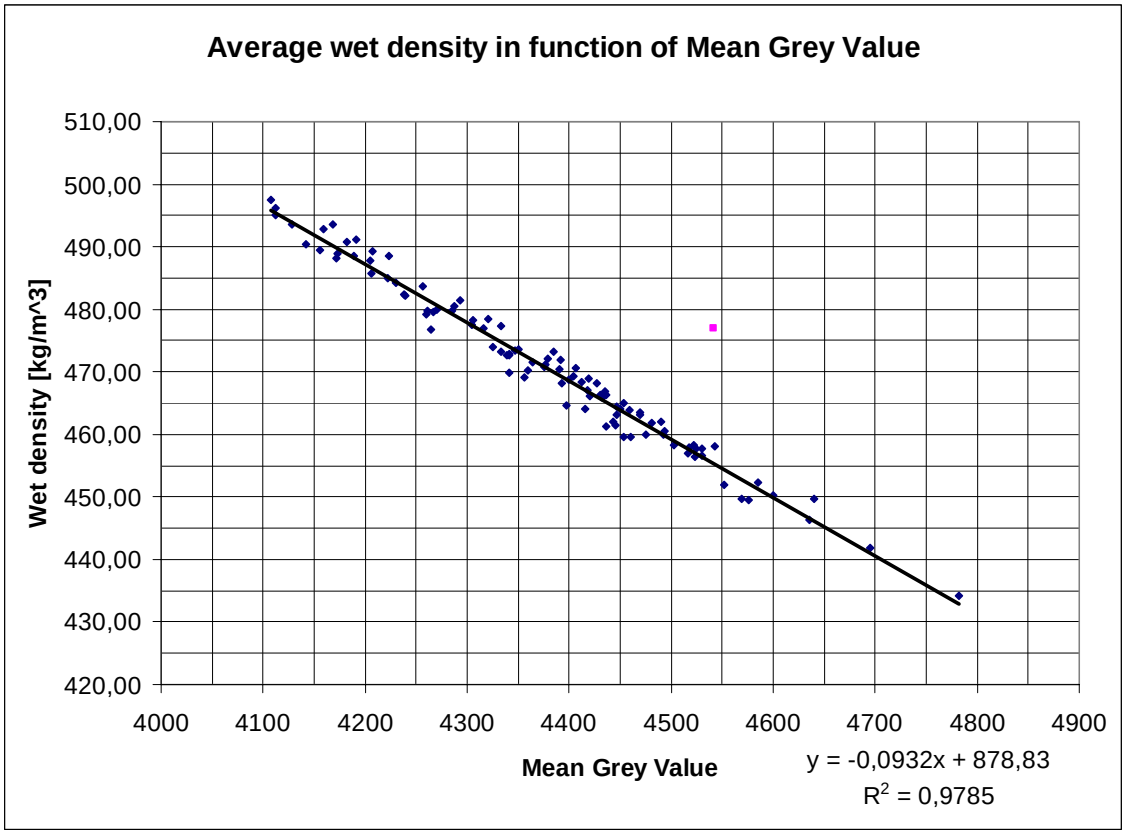

Figure 52. Measured wet density as a function of defined Mean Grey Value for all specimens.

The trend line shown in the Figure 52 is matched to the data without the one anomalous point. The relationship between average wet density and Mean Grey Value (MGV) can be written as follows:

$$\rho_{ave,w}(MGV) = -0{,}0932\frac{kg}{m^3}\cdot MGV + 878{,}83\frac{kg}{m^3} \quad (48)$$

Equation 48 can be used to determine wet densities of particular areas from the X-ray pictures. For example density of a particular lamella can be defined and the proportion of knots in different lamellas can be monitored. It is hard to say how accurately equation 48 describes the relationship of MGV and wet density with timber density of which is not in the range of 430 kg/m³ to 500 kg/m³. Equation 48 is used in the analysis of lamellas in those beams that had unusual failure even though the local densities and Mean Grey Values were not always in the range shown in Figure 52.

Points in the edges of the observation range differ very little from the trend line. This fact encourages using equation 48 also in wider density and Mean Grey Value range. It seems that extrapolation of equation 48 should lead to quite a small error at least when using reasonable values for density and Mean Grey Value. However, further investigations should be done to confirm the relationship. The range of MGV in the knot analysis was between 3 690 and 5 330.

6. Analysis of the results

6.1 Comparison of results of test series

6.1.1 Average moisture content

The measured average moisture contents for the beams with different coatings in the specific conditioning phases are shown in Figure 53. The values of the pre-test phase are estimated from the weight differences between the pre-test phase and the test phase.

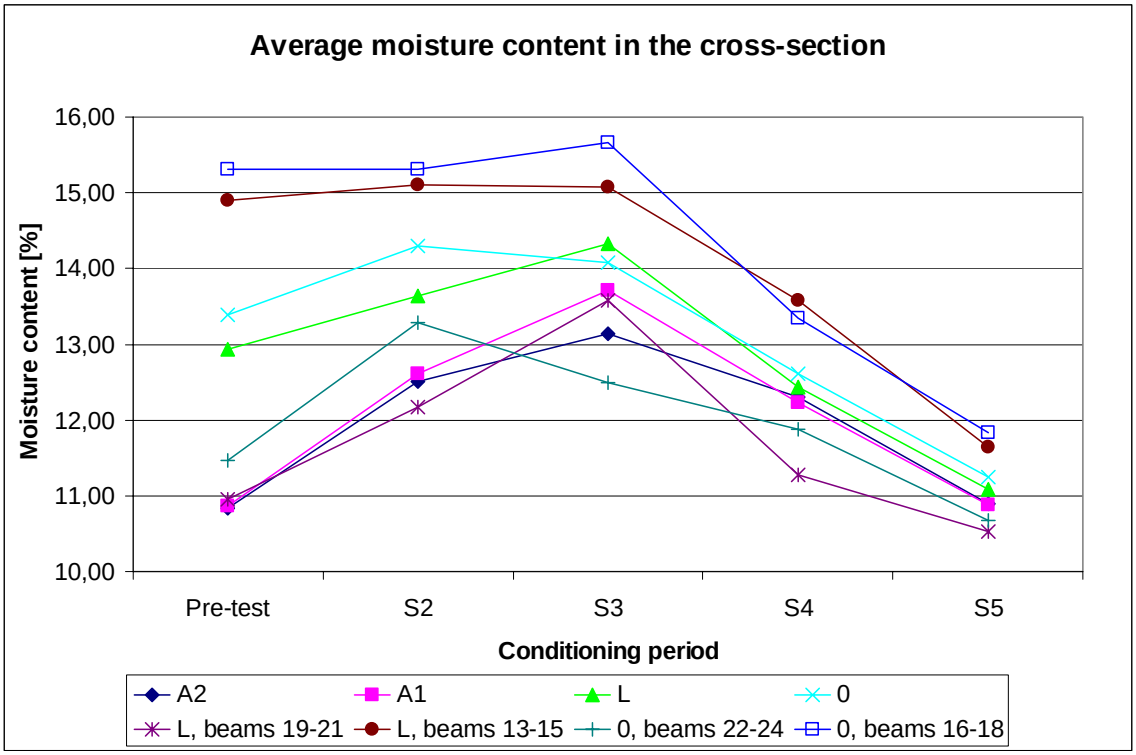

Figure 53. Average moisture contents of the beams at different phases of the test.

The actual values and sample standard deviations are shown in Table 19.

The beams 13–18 in every test sample S2-S5 are from the manufacturer that delivered the more moist beams. These beams increase the statistical divergence very much when studying moisture content so they are studied also separately.

The moisture content of the moist specimens increased only a little during the RH 90% conditioning. Even though the rate of change is slower when moisture content approaches equilibrium moisture content, the result was surprising. Equilibrium moisture content for spruce in RH 90% is approximately 20%.

The moisture content evolution of uncoated beams 22–24 was illogical when considering the moisture content after test series S3. The beams had been conditioned in RH 90% for three months and moisture content should have been highest at that phase. The beams of test series S4 and S5 were weighed after conditioning them in RH 90% for three months. The average moisture contents after RH 90% conditioning estimated from the weight differences and measured moisture contents after tests of S4 and S5 suggest that average moisture content of the uncoated beams 22–24 should have been higher than the measured values after the S3 tests. It is possible that there is a test or measurement error involved here. Table 20 shows the values of calculated average moisture contents after RH 90% conditioning for different coatings calculated from the weight differences and the measured moisture contents after tests of S4 and S5.

Table 19. Average moisture contents and sample standard deviations at different phases of the test.

Test series	Beam number	Coating	Number of specimens	Average MC [%]	STD of average MC [%]
S1	1–4, 7, 8	Uncoated	6	11,5	0,39
	5,6	Uncoated	2	14,9	0,17
	1–8	Uncoated	8	12,4	1,58
S2	1–3, 7–9	A2	6	12,5	0,27
	4–6, 10–12	A1	6	12,6	0,45
	13–15, 19–21	L	6	13,6	1,64
	13–15	L	3	15,1	0,33
	19–21	L	3	12,2	0,40
	16–18, 22–24	Uncoated	6	14,3	1,20
	16–18	Uncoated	3	15,3	0,62
	22–24	Uncoated	3	13,3	0,37
S3	1–3, 7–9	A2	6	13,1	0,75
	4–6, 10–12	A1	6	13,7	0,73
	13–15, 19–21	L	6	14,3	0,88
	13–15	L	3	15,1	0,51
	19–21	L	3	13,6	0,06
	16–18, 22–24	Uncoated	6	14,1	1,76
	16–18	Uncoated	3	15,7	0,16
	22–24	Uncoated	3	12,5	0,40
S4	1–3, 7–9	A2	6	12,3	0,39
	4–6, 10–12	A1	6	12,2	0,55
	13–15, 19–21	L	6	12,4	1,30
	13–15	L	3	13,6	0,29
	19–21	L	3	11,3	0,36
	16–18, 22–24	Uncoated	6	12,6	0,81
	16–18	Uncoated	3	13,3	0,12
	22–24	Uncoated	3	11,9	0,08
S5	1–3, 7–9	A2	6	10,9	0,45
	4–6, 10–12	A1	6	10,9	0,66
	13–15, 19–21	L	6	11,1	0,63
	13–15	L	3	11,6	0,04
	19–21	L	3	10,5	0,25
	16–18, 22–24	Uncoated	6	11,3	0,65
	16–18	Uncoated	3	11,8	0,21
	22–24	Uncoated	3	10,7	0,04

Table 20. Calculated average moisture contents for beams with different coatings after RH 90% conditioning.

Beam number	Coating	Number of specimens	Calculated average MC [%]	STD of estimated average MC [%]
1–3, 7–9	A2	12	14,0	0,47
4–6, 10–12	A1	12	14,5	0,74
13–15, 19–21	L	12	15,7	1,64
13–15	L	6	17,2	0,20
19–21	L	6	14,1	0,22
16–18, 22–24	Uncoated	12	16,0	1,22
16–18	Uncoated	6	17,1	0,15
22–24	Uncoated	6	14,8	0,34

There are differences in the moisture contents of Table 20 and 19. The estimated moisture contents seem to be approximately 0,5–2% higher than the corresponding measured moisture contents.

Average moisture content distribution was calculated from the Abaqus calculations in two different ways. First, the average value was calculated by assuming that the moisture content distribution would be similar to the distribution at mid height in every part of the beam. Then the average value for the moisture content was approximated directly from the calculated distribution. Approximately an error of 0,5% in the moisture content was noticed between these different ways of calculating the average moisture content of the cross-section.

This error explains quite well the differences between the measured average moisture contents of the test series S3 and the estimated average moisture contents of the test series S4 and S5 after the RH 90% conditioning.

The difference in the average moisture content of the uncoated beams 22–24 in the Tables 20 and 19 is however high and this suggests that an error has occurred in the determination of moisture contents.

6.1.2 Moisture content gradient

The change in moisture content gradient during the conditioning is shown in Figure 54.

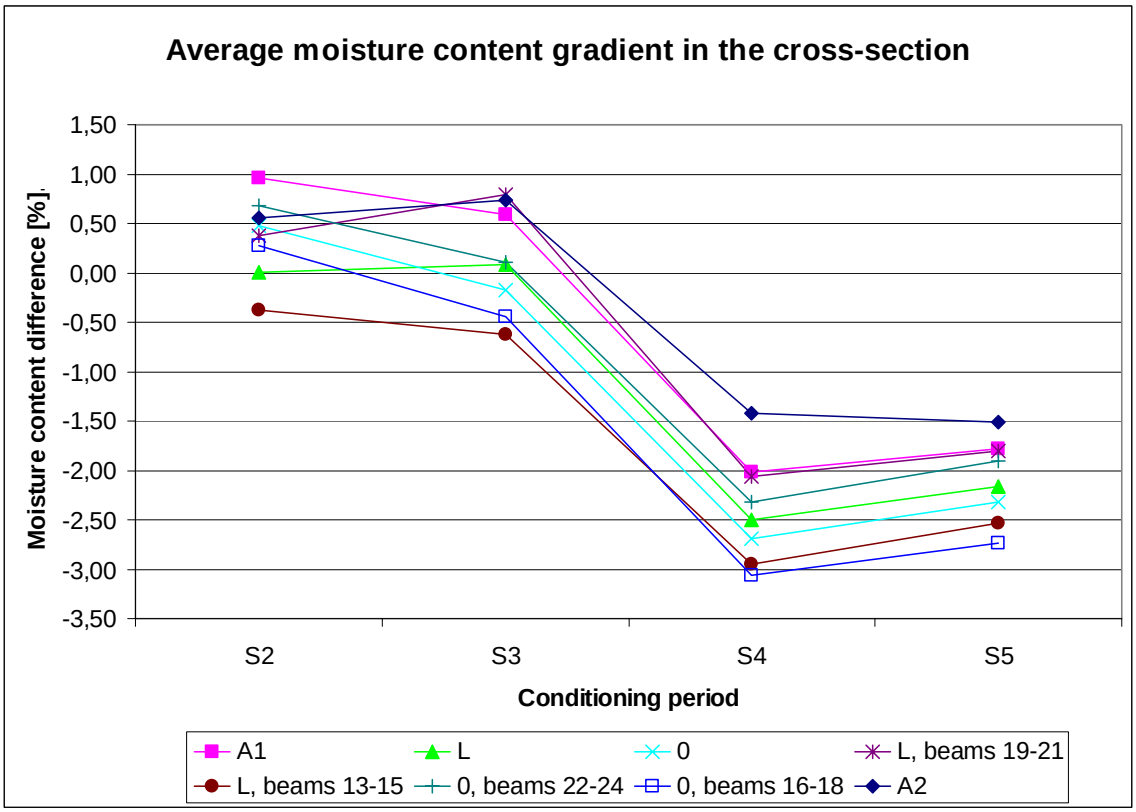

Figure 54. Average moisture content gradients of the beams at different phases of the test.

The actual values and sample standard deviations of moisture content gradients are shown in Table 21.

Table 21. Average moisture content gradients and sample standard deviations at different phases of the test.

Test series	Beam number	Coating	Number of specimens	MC gradient [%]	STD of MC gradient [%]
S1	1–4, 7, 8	Uncoated	6	-0,1	0,28
	5,6	Uncoated	2	-1,2	0,37
	1–8	Uncoated	8	-0,4	0,55
S2	1–3, 7–9	A2	6	0,6	0,38
	4–6, 10–12	A1	6	1,0	0,60
	13–15, 19–21	L	6	0,0	0,48
	13–15	L	3	-0,4	0,24
	19–21	L	3	0,4	0,33
	16–18, 22–24	Uncoated	6	0,5	0,53
	16–18	Uncoated	3	0,3	0,43
	22–24	Uncoated	3	0,7	0,62
S3	1–3, 7–9	A2	6	0,7	0,16
	4–6, 10–12	A1	6	0,6	0,44
	13–15, 19–21	L	6	0,1	0,79
	13–15	L	3	-0,6	0,10
	19–21	L	3	0,8	0,23
	16–18, 22–24	Uncoated	6	-0,2	0,38
	16–18	Uncoated	3	-0,4	0,08
	22–24	Uncoated	3	0,1	0,36
S4	1–3, 7–9	A2	6	–1,4	0,15
	4-6, 10-12	A1	6	-2,0	0,17
	13–15, 19–21	L	6	-2,5	0,51
	13–15	L	3	-3,0	0,18
	19–21	L	3	-2,1	0,12
	16–18, 22–24	Uncoated	6	-2,7	0,42
	16–18	Uncoated	3	-3,1	0,12
	22–24	Uncoated	3	-2,3	0,14
S5	1–3, 7–9	A2	6	-1,5	0,15
	4–6, 10–12	A1	6	-1,8	0,08
	13–15, 19–21	L	6	-2,2	0,41
	13–15	L	3	-2,5	0,08
	19–21	L	3	-1,8	0,11
	16–18, 22–24	Uncoated	6	-2,3	0,50
	16–18	Uncoated	3	-2,7	0,32
	22–24	Uncoated	3	-1,9	0,11

The observed moisture content gradients followed quite well the expected evolution of the gradient. In this study the gradient is defined so that if a beam is moister from the cross section centre than from the edge its gradient is negative. In the opposite case the gradient is positive. Gradients were expected to have their greatest positive value at the time of test phase S2 and greatest negative value at the time of test phase S4.

The measured values of the moisture content gradient in the test series S2 were little lower than expected. The absolute values of the gradients in the test phases S2 and S4 were predicted to be closer to each other even though the alteration in storage conditions was bigger for the test phase S4 (RH 90% to RH 30%) than for the test phase S2 (RH 65% to RH 90%).

6.1.3 Shear resistance

The calculated average shear resistances for beams with different coatings during the different conditioning phases are shown in Figure 55. The calculated characteristic values of shear resistance for beams with different coatings during the different conditioning phases are shown in Figure 56. The actual average values, sample standard deviations and calculated characteristic values are shown in Table 23. The calculation of characteristic values was done according to European Standard EN 14358.

EN 14358 determines the calculation of characteristic 5-percentile values for a sample. Mean value $\bar{y}$ and standard deviation s_y are determined from equations 49 and 50.

$$\bar{y} = \frac{1}{n}\sum_{i=1}^{n} \ln m_i \tag{49}$$

$$s_y = \sqrt{\frac{1}{n-1}\sum_{i=1}^{n} (\ln m_i - \bar{y})^2} \tag{50}$$

where m_i is the considered test value.

The characteristic value is determined as

$$m_k = \exp(\bar{y} - k_s s_y) \tag{51}$$

where k_s is taken from Table 22.

Table 22. The values of factor k_s.

Number of test specimens	Factor
n	k_s
3	3,15
5	2,46
10	2,10
15	1,99
20	1,93
30	1,87
50	1,81
100	1,76
500	1,71
∞	1,65

The moist specimens did not differ clearly from the other beams when examining the shear resistance so these were not studied separately.

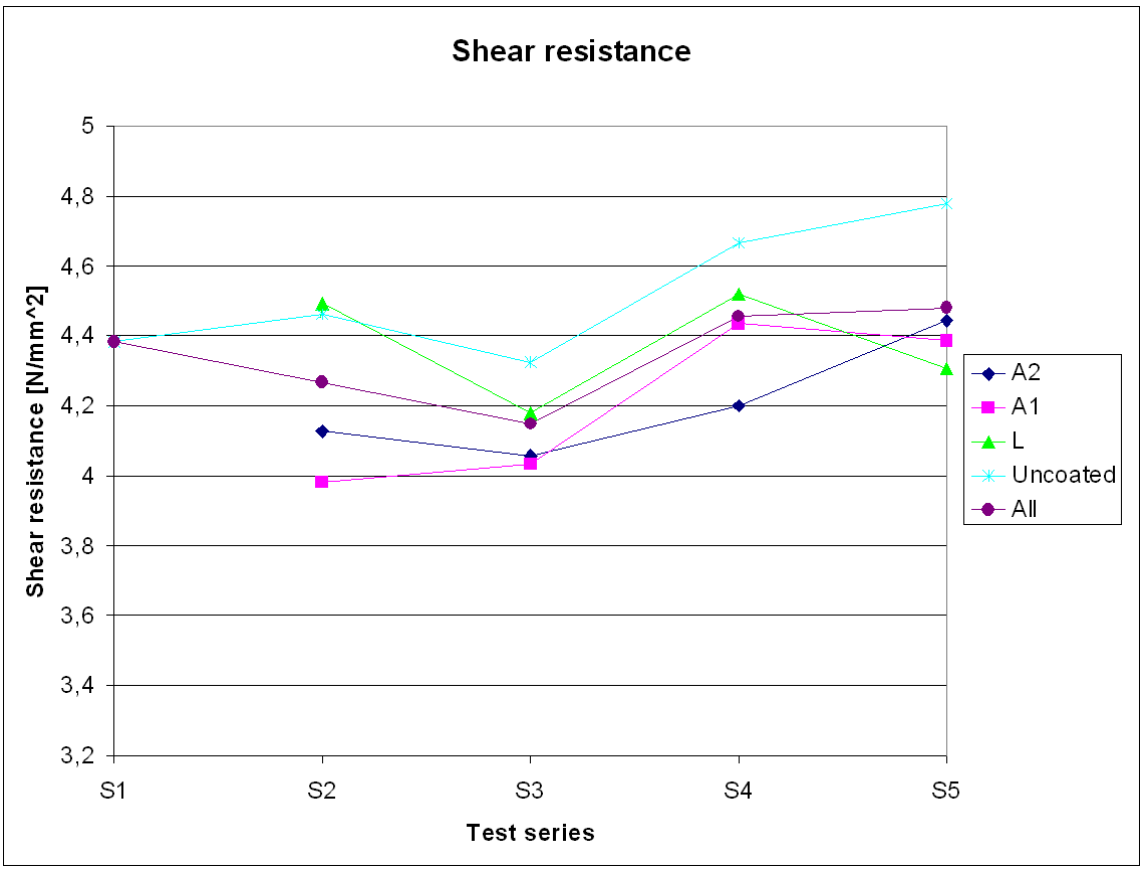

Figure 55. Shear resistance in different conditioning phases.

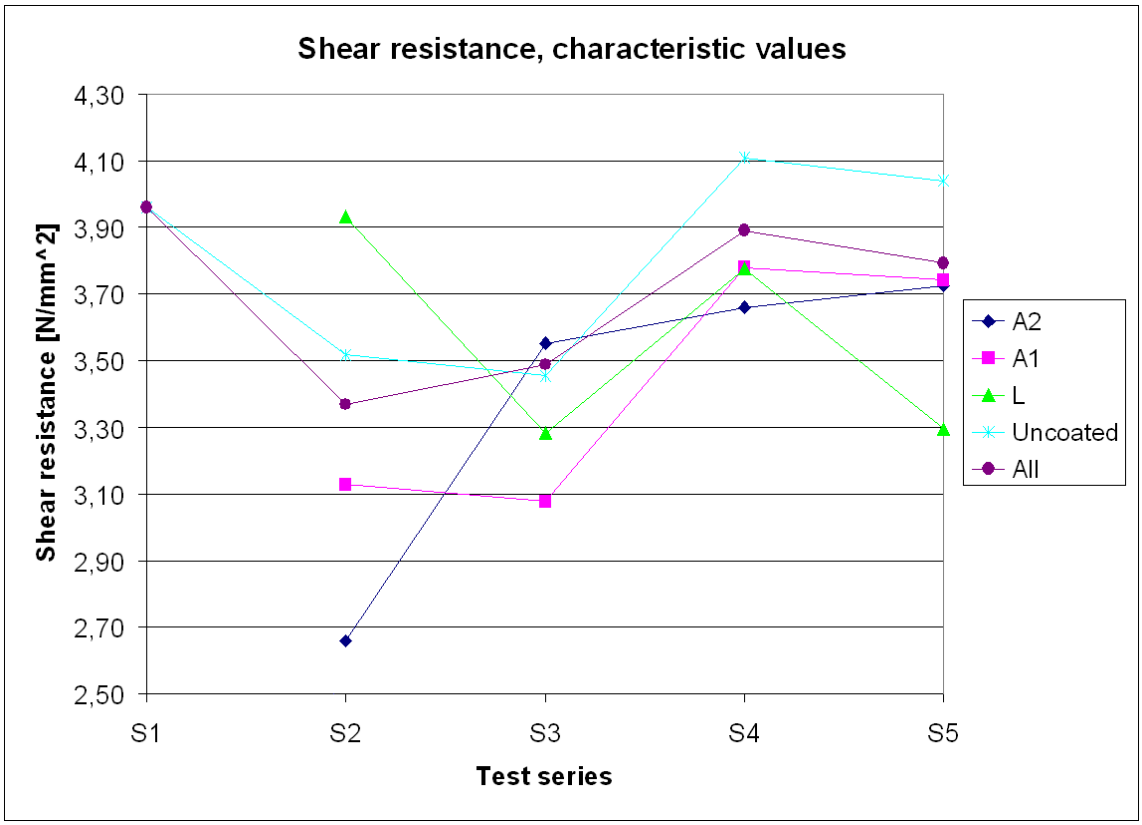

Figure 56. Characteristic values of shear strength in different conditioning phases.

Table 23. Average shear resistances and sample standard deviations at different phases of the test.

Test series	Coating	Number of qualified specimens	Average shear resistance [N/mm²]	Sample standard deviation [N/mm²]	Characteristic value of shear resistance [N/mm^2]
S1	Uncoated	6	4,38	0,18	3,96
	All	6	4,38	0,18	3,96
S2	A2	6	4,13	0,68	2,66
	A1	6	3,98	0,38	3,13
	L	6	4,49	0,24	3,93
	Uncoated	6	4,46	0,43	3,52
	All	24	4,27	0,48	3,37
S3	A2	6	4,06	0,21	3,55
	A1	6	4,03	0,45	3,08
	L	6	4,18	0,40	3,28
	Uncoated	6	4,33	0,37	3,45
	All	24	4,15	0,36	3,49
S4	A2	6	4,20	0,23	3,66
	A1	6	4,44	0,28	3,78
	L	6	4,52	0,33	3,78
	Uncoated	6	4,67	0,24	4,11
	All	24	4,46	0,31	3,89
S5	A2	6	4,44	0,31	3,73
	A1	6	4,39	0,28	3,74
	L	6	4,31	0,48	3,29
	Uncoated	6	4,78	0,31	4,04
	All	24	4,48	0,38	3,79

6.2 Effect of moisture induced stresses to the shear resistance

Moisture induced stresses did not have any clear effect on the shear resistance in this study. Some decrease in the shear resistance can be seen in the results of the test series S2 and S3 when comparing to the reference test series S1. The average shear resistances of the test series S4 and S5 were however higher than the resistance of the reference test series. This may be due to that the small decrease of shear resistance in the test series S2 and S3 was induced by the higher moisture content rather than the moisture induced stresses.

According to Abaqus calculations moisture induced stresses are highest when the moisture content gradient is highest. This means that if moisture induced stresses would affect the shear resistance of glulam beams there should have been decreases at least in the shear resistances of the test series S2 and S4. However, such decreases were not detected in these

tests. The moisture induced stresses obtained from Abaqus calculations affected the beams primarily in different directions than the stresses caused by the load. Therefore it is apparent that the moisture induced stresses do not affect the shear resistance of the beams at least in these loading cases.

Moisture induces stresses cause cracks to the cross-section. Figure 57 shows the crack generation in the end of a beam during the conditioning. The end in the pre-test phase is pictured on the left. The same end is pictured again on the right after being conditioned three months in relative humidity of 90% and one month in relative humidity of 30%. Old cracks have expanded and some new cracks have appeared during the conditioning. Some of the cracks are in radial direction and some in tangential direction. Nevertheless, the cracks do not seem to affect the shear resistance. Apparently these cracks are only local and do not extend horizontally very deep in to the beam. Especially cracks in tangential direction seem to be hazardous when considering shear resistance, but they did not decrease the shear resistance in the tests.

Figure 57. Crack generation in the end of a beam during conditioning.

The relationship of average moisture content and shear resistance is shown in Figure 58. It can be seen than there is no noticeable correlation in the graph.

The relationship of moisture content gradient and shear resistance is shown in Figure 59. One can see that no clear correlation between moisture content gradient and shear resistance could be found.

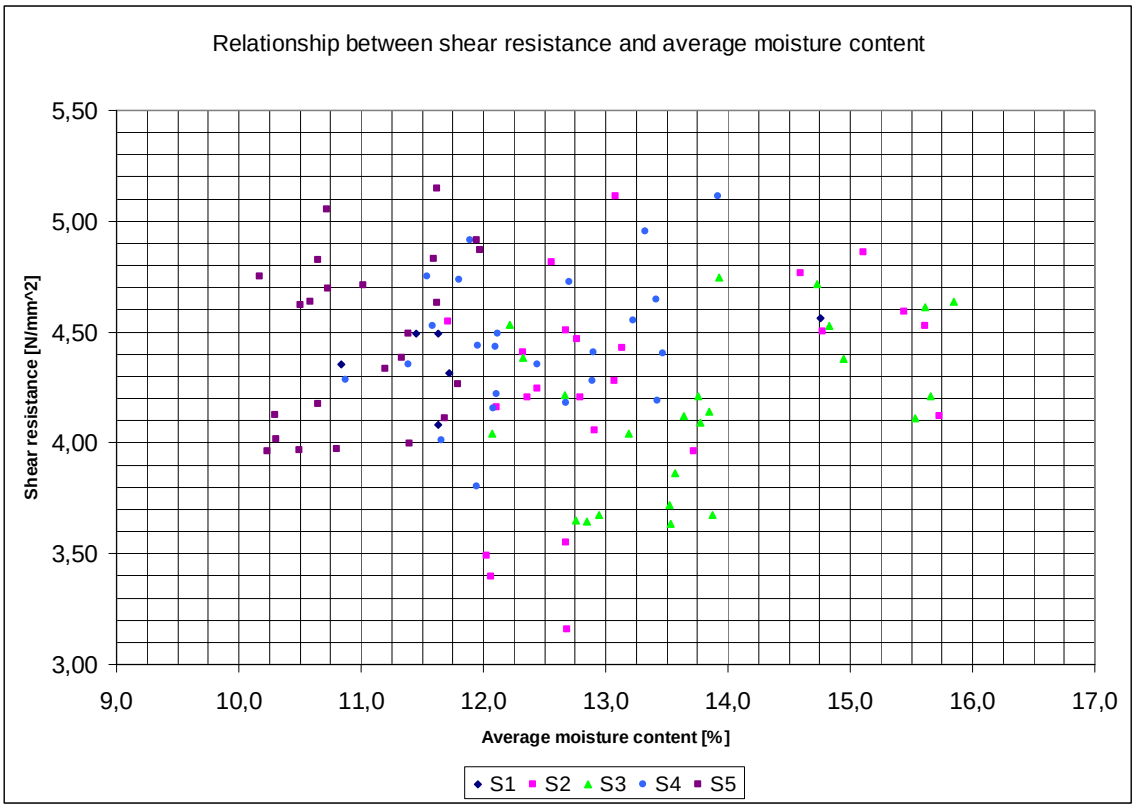

Figure 58. The relationship between average moisture content and shear resistance.

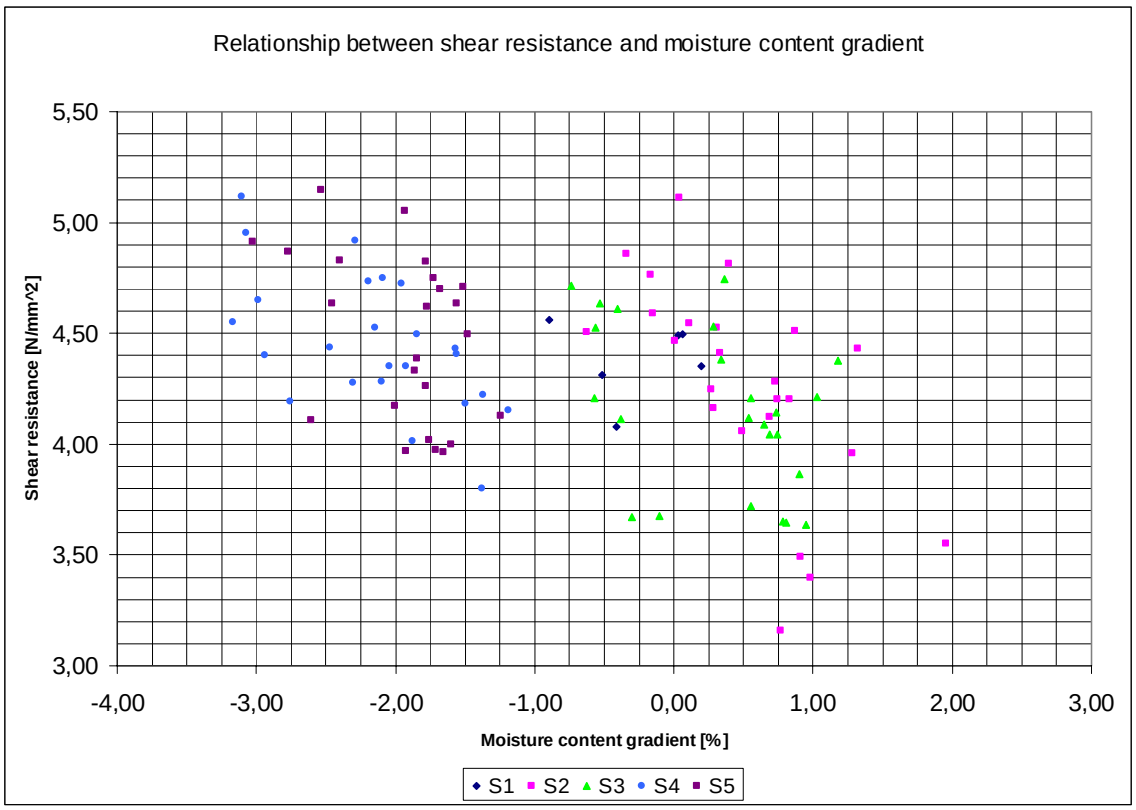

Figure 59. The relationship of moisture content gradient and shear resistance.

6.3 Effect of coatings

In this study, no major differences in shear resistance of the beams with different coatings were observed. Different coatings were assumed to increase the shear resistance during the conditioning but the results were different. The uncoated beams had highest shear resistance in almost all the test series. Only in the test series S2 the average shear resistance of beams with Linotech coating was higher than the average shear resistance of uncoated beams. However, also in that case the difference between the resistances was small.

The evolutions of average moisture content and moisture content gradient had noticeable but small differences between the different coatings. The differences were not always as was assumed. The high initial moisture scatter between the material coming from one of the four producers disturbed the interpretation of moisture results. Also other deviations in the measured moisture contents was high that it is impossible to draw reliable conclusions from these values.

6.4 Relationship between elastic modulus and failure type

When analyzing the measured data from the testing some correlation was found between elastic moduli and failure types. The value of local/global elastic modulus calculated from the elastic deflections of the beam had a clear connection to the failure type. Local elastic modulus was calculated from the equation of deformation of Timoshenko beam theory by using measured deflection of the centre line of the beam. Characteristic value of shear modulus, 780 N/mm^2, was used in the calculation for all beams. Local elastic modulus was calculated from the part of the load-deflection curve where load was between $0{,}1F_{max}$ to $0{,}4F_{max}$. Beams that finally had a failure in bending had lower elastic modulus. The average local elastic modulus for shear failures, bending failures and all comparable specimens is shown in Table 24. Specimens S1-3/8 and S1-4/8 were excluded from the total consideration because their different test-setup. There is also one more specimen in the final consideration compared to the sum of shear and bending failure cases because there was one specimen, namely S3-17/24, which had not an identifiable failure type.

Table 24. Average local elastic modulus for different failure types.

Test series	Failure type	Number of specimens	Average local elastic modulus E_{local} [N/mm²]	Sample standard deviation E_{local} [N/mm²]
S1	Shear failure	2	15477	518
	Bending failure	4	13434	1026
	All failures	6	14115	1341
S2	Shear failure	16	14401	1269
	Bending failure	8	13081	751
	All failures	24	13961	1275
S3	Shear failure	15	14326	1529
	Bending failure	8	13148	718
	All failures	23	13897	1423
S4	Shear failure	19	15251	1089
	Bending failure	5	14470	368
	All failures	24	15089	1028
S5	Shear failure	20	15537	1546
	Bending failure	4	14125	1186
	All failures	24	15301	1564
All specimens	Shear failure	72	14955	1423
	Bending failure	29	13516	941
	All failures	101	14542	1454

It can be seen from Table 24 that there is a clear difference in the local elastic moduli in beams with different failure types. However, the standard deviation is significant in all cases. Some conclusions can nevertheless be drawn from the different mean values. Stiffer beams seemed to get a shear failure more easily.

The relationship between measured shear modulus and failure type was also examined but no correlation was found.

6.5 Effect of defects in beams

6.5.1 Defects in tension side of beams

When studying shear resistance, the failure type should be a typical shear failure in as many test specimens as possible. Otherwise the true shear resistance is not attained. Difficulties relating to bending failure were noticed when planning the test setup but still there were 29 out of 104 beams which had a bending failure. Different defects in the tensioned lower half of the beam were always the starting point of the bending failure.

In most bending failure cases the initiating point of the failure was near the mid span where the tension stress is highest. Sometimes a big knot or a finger joint was the starting point of the failure even though it was near the support where the tension stress is not as intensive as in the mid span.

Figure 60 shows two untypical bending failures. Both had their initiating failure point either completely or partially in a finger joint.

Figure 60. Two untypical bending failures.

6.5.2 Knots in the shear zone of beams

The effect of knots in the shear zone of the beams was examined by comparing the test results and the X-ray pictures. A typical shear failure in these tests has a fracture plane following the year rings, like in Figure 44. Knots that are aligned in radial direction can be assumed to effect to the failure in a plane that follows a year ring by acting as a reinforcement against the slip. The effect of knots was studied by comparing the amount of knots in certain areas of the beams that had notable differences in failure type. Examined failure types were: shear failures with low ultimate load, shear failures with high ultimate load and bending failures with high ultimate load which also means high shear stress in the middlemost lamellas. The amount of knots was analyzed from X-ray pictures using ImageJ software.

The beams with three different failure types were compared in order to study if there is a relationship between the amount of knots and the shear resistance. 12 beams that had a shear failure with ultimate load of about 320 kN or less were examined. Also 7 beams that had a shear failure with ultimate load of about 370 kN or more were examined. One com-

parison group consisted of 11 beams that had a bending failure with ultimate load of 370 kN or more. Overall examination of the average proportion of knots was done for 6 randomly chosen beams.

In shear failure cases the proportion of knots in the lamella, where the failure plane was situated, was examined in each beam. The examined length of the lamella was about one third of the whole length of the beam. Only one third was examined because the failure plane did not usually align in the same lamella for its whole length. Then, the examined area was usually quite small compared to area examined in bending failure cases. The MGV of clear wood was measured from about 5 places in every lamella and the average value was used in the calculations.

In bending failure cases, the proportion of knots in two middlemost lamellas, where the shear stress could be assumed to be highest before the bending failure occurred, was examined. The examined area contained the whole length of the two middlemost lamellas and it was about six times larger than the examined area in shear failure cases. The MGV of clear wood was measured from about 5 parts in a lamella which makes about 10 measurements for the examined area. The average value of the measurements was used in the calculations.

The reference value for the average proportion of knots in a lamella was studied by examining the whole area of 6 beams. The MGV value used for clear wood in each beam was the average value calculated from 60 different measurements. There were 5 measurement areas distributed evenly along the length of each lamella.

Table 25 shows the obtained MGV values, densities and the proportions of knots in the examined beams.

Table 25. Knot proportions in beams with different failure types.

	Beam	Mean Grey Value with knots	Mean Grey Value of clear wood	Density with knots [kg/m³]	Density of clear wood [kg/m³]	Knot proportion [%]	Ultimate load [kN]	Failure type
Shear failures with low ultimate load	S2-1/24	4356	4423	472,9	466,6	7,4	265	Shear
	S2-3/24	4213	4294	486,2	478,6	10,4	285	Shear
	S2-4/24	4419	4530	467,0	456,6	10,9	292	Shear
	S2-6/24	3971	4043	508,7	502,1	13,4	298	Shear
	S3-3/24	4083	4169	498,3	490,3	13,1	308	Shear
	S3-5/24	4546	4679	455,1	442,8	11,4	307	Shear
	S3-6/24	4429	4494	466,0	460,0	6,6	314	Shear
	S3-11/24	5177	5330	396,4	382,0	8,4	307	Shear
	S3-19/24	5103	5167	403,2	397,3	3,8	303	Shear
	S3-21/24	4296	4417	478,4	467,2	13,3	322	Shear
	S3-22/24	3988	4020	507,1	504,2	6,2	307	Shear
	S4-2/24	4824	4919	429,2	420,4	6,8	319	Shear
					Average	9,3		
					Sample standard deviation	3,2		
Bending failures with high ultimate load	S1-6/8	4113	4311	495,5	477,0	24,8	375	Bending
	S2-14/24	4215	4403	486,0	468,4	21,1	371	Bending
	S2-15/24	4489	4637	460,5	446,7	13,1	402	Bending
	S2-17/24	4600	4751	450,1	436,1	12,2	396	Bending
	S2-18/24	4600	4737	450,1	437,3	11,2	375	Bending
	S2-20/24	4703	4874	440,5	424,5	12,6	377	Bending
	S3-13/24	4076	4218	499,0	485,7	20,1	375	Bending
	S3-14/24	4382	4547	470,5	455,1	15,9	392	Bending
	S3-16/24	4394	4549	469,3	454,9	14,9	387	Bending
	S4-10/24	4254	4384	482,4	470,2	14,9	389	Bending
	S4-15/24	4295	4406	478,5	468,2	12,4	379	Bending
	S5-18/24	4148	4274	492,3	480,5	16,6	399	Bending
					Average	15,8		
					Sample standard deviation	4,2		
Shear failures with high ultimate load	S2-8/24	4301	4424	477,9	466,5	13,4	374	Shear
	S2-24/24	4209	4297	486,5	478,4	11,2	424	Shear
	S3-23/24	4644	4861	446,0	425,8	16,1	377	Shear
	S4-3/24	4601	4733	450,0	437,7	10,8	371	Shear
	S4-5/24	4694	4809	441,3	430,7	8,8	398	Shear
	S4-6/24	4906	5011	421,6	411,8	7,0	375	Shear
	S4-23/24	4554	4605	454,4	449,7	4,7	404	Shear
					Average	10,3		
					Sample standard deviation	3,9		
Bending failures with low ultimate load	S1-5/8	4401	4594	468,7	450,7	17,8	301	Bending
	S3-18/24	3906	4043	514,7	502,0	25,7	342	Bending
	S3-20/24	3690	3776	534,9	526,9	32,5	344	Bending
	S4-9/24	4380	4514	470,6	458,2	13,3	350	Bending
	S5-9/24	4138	4215	493,2	486,0	10,9	329	Bending
	S5-15/24	4757	4918	435,5	420,5	11,4	333	Bending
	S5-24/24	4682	4858	442,4	426,0	13,1	341	Bending
					Average	17,8		
					Sample standard deviation	8,3		
Overall proportion of knots in randomly chosen beams	S1-5/8	4341	4481	474,3	461,2	14,4	301	Bending
	S2-11/24	4460	4627	463,2	447,6	15,0	349	Shear
	S3-23/24	4586	4712	451,4	439,6	10,6	377	Shear
	S4-2/24	4260	4405	481,8	468,3	16,2	319	Shear
	S4-23/24	4444	4563	464,6	453,5	11,3	404	Shear
	S5-18/24	4378	4505	470,8	459,0	12,8	399	Bending
					Average	13,4		
					Sample standard deviation	2,2		

It can be seen from Table 25 that the deviation in the chosen groups is notable, but the average values seem to support the statement that knots in the middlemost lamellas increase the shear capacity. Beams that had more knots in the middlemost lamellas were not sheared before bending failure occurred with a fairly high load. Shear capacity of the middlemost lamellas was not obtained although the shear stresses were high with the high loads. Shear capacities of lamellas with more than average amount of knots were higher than the average shear capacity. As well, beams that were sheared with low ultimate loads had less than average amount of knots in the lamellas where the failure plane aligned. Beams that were sheared with high ultimate load had more knots in lamellas where the failure plane aligned compared to the case of shear failure with low ultimate load. The average proportion of knots in sheared lamellas in both shear failure cases was however smaller than the average proportion of knots in a lamella.

This result could encourage further studies whether the middlemost lamellas in glulam beams could have even more knots than used nowadays. Shear capacity would be increased and, in addition, the low grade timber could be utilised.

7. Conclusions

The aim of the experiments was to find out if the variation of humidity affects the shear strength of large size glulam members. It is known that moisture gradients are induced in dynamic humidity variations, and these produce internal stress distributions perpendicular to the grain [11]. The target here was to find out if these stress gradients have an effect on the shear strength of the beam.

The coatings applied had minor effects on the induced moisture gradients. The high initial moisture scatter between the material coming from one producer (out of four) did disturb the interpretation of test results especially when considering moisture content effects. The beams with high initial moisture had only small moisture gain during the wetting period so also the moisture induced stresses were minor compared to other beams in that phase. The deviation in the moisture content measurements was significant even when the moisture scatter from one producer was not taken into account. This matter complicated the analysis of the effects of moisture content changes to the shear resistance.

The differences in shear strengths between manufacturers had also an effect to the results. The effects of moisture induced stresses could have been easier to observe if the material had been more homogenous.

Finite element calculations supported the obtained results from the tests. The calculated moisture induced stresses were small in those directions that had biggest stresses in the actual loading. The visual examination of failure planes together with finite element calculations referred that shear failure occurred because shear strengths τ_{rl} and τ_{tl} were exceeded in the loading. Moisture induced shear stresses in those directions were however small and local.

To the knowledge of the authors, shear strength experiments on real size glulam beams have not been conducted previously in such a large scale as the tests of this study. Currently there is no test standard for determining shear strength of real size glulam beams. The tests conducted in this study implicate that the used test setup could be a starting point for developing such standard, since the majority of the failures in this study were shear failures. A good alternative for the standard test setup could be the symmetric five-point loading, which has also been suggested in previous references, but due to the height of real

size beams, their length would probably be impractical and laborious for test purposes. The test setup would also be more complicated in a symmetric five-point loading.

According to the tests of this study, the characteristic value of shear strength at present is at a reasonable level – only one beam had a slightly lower shear strength. Since the environmental load in this study was quite extreme, the service class can be determined to be number two. Keeping this in mind, the results of this study suggest that the characteristic shear strength could possibly be slightly increased.

The test results show that moisture gradients have only small or no effect on the shear strength. Nevertheless, it should be studied in more detail how the varying humidity conditions affect the shear strength of glulam beams that are under a permanent or long-term mechanical load. In these further studies one could first conduct computer calculations and after that mechanical tests.

The MGV value defined from the X-ray pictures was found to correlate with density very well. This could be utilized in manufacturing of glulam in order to arrange lamellas more functionally. This way the manufacturers could avoid placing finger joints and large groups of knots into the middle of the span and the lower edge of the beam. Based on the knot analysis from the X-ray pictures and test results, manufacturers could choose timber with more knots to the mid-lamellas of beams than they currently do. However, this should first be studied in more detail. It would probably be possible to find a linear correlation between MGV value and density for lamellas of different widths. It would be interesting to study the benefits in both bending and shear resistance obtained from more functional placing of lamellas.

In respect of the shear resistance of glulam, it might be useful to study different possibilities in positioning lamellas. Also the use of different composite reinforcements could be studied.

Currently the shear modulus is defined indirectly from the elastic moduli. The shear modulus can be determined directly from strain measures, as was done in this study. A shear modulus determined this way is more reliable. In this study the measured values of shear modulus were somewhat smaller than current characteristic values of GL32c. Thus, it would be interesting to study and compare the shear modulus values obtained from both strain measurements and elastic modulus methods. The values should, of course, be obtained from the same specimen.

In conclusion it can be stated that the test results give no evidence to the recommended crack factor ($k_{cr} = 0,67$) recently added to EN1995-1-1 design procedures for the reduction of shear resistance.

Acknowledgements

The authors gratefully acknowledge the financial support of Woodwisdom-Net (www.woodwisdom.net) and the wood industry partnership Building with Wood for funding the research work within the project “Improved moisture”. This work forms part of that project.

References

1. Tekes - Finnish Funding Agency for Technology and Innovation, home page of WoodWisdom-Net project, contact person Ilmari Absetz [Referred 1 July 2009]. http://www.woodwisdom.net/.

2. Improved Moisture Project Consortium, Project of the Month: Improved Moisture [Web article] 2009. [Referred 1 July 2009]. http://www.nexdo.com/view.do?w=579&page=Main+page.

3. Ranta-Maunus, A. & Gowda, S. Curved and cambered glulam beams. Part 2. Long term load tests under cyclically varying humidity. Espoo 1994, Technical Research Centre of Finland, VTT Publications 171. 36 p. + app. 18 p.

4. Ormarsson, S. Numerical Analysis of Moisture-Related Distortions in Sawn Timber. Göteborg 1999, Chalmers University of Technology, Department of Structural Mechanics. 214 p. ISSN 0347-9226.

5. Kanko, T. Kuusen kosteusominaisuudet. Espoo 1990, Valtion teknillinen tutkimuskeskus, VTT Tutkimuksia 682. 35 p. ISBN 951-38-3703-3. (In Finnish)

6. Imakoma, H., Okazaki, M. & Toei, R. Mathematical Model for Drying of Adsorptive Porous Materials. Helsinki 1985, Acta Polytechnica Scandinavia. 32 p. ISBN 951-666-208-0.

7. Technical Committee CEN/TC 124. EN 408:2003 (E) Timber structures – Structural timber and glued laminated timber – Determination of some physical and mechanical properties. European Committee for Standardization.

8. Yoshihara, H. & Furushima, T. Shear strengths of wood measured by various short beam shear test methods. Matsue 2001, Shimane University. Wood Sci Technol 37. 7 p.

9. Rammer, D. Shear strength of glued-laminated timber beams and panels. Madison 1996, Forest Products Laboratory, USDA Forest Service. 9 p.

10. Frühwald, E., Serrano, E., Toratti, T., Emilsson, A. & Thelandersson, S. Design of safe timber structures – How can we learn from structural failures in concrete, steel and timber? Lund, Espoo and Falun 2007, Division of Structural Engineering, Lund University. 222 p.

11. Mirianon, F., Fortino, S. & Toratti, T. A method to model wood by using ABAQUS finite element software, Part 1. Constitutive model and computational details. Espoo 2008, VTT Publications 687. 51 p. http://www.vtt.fi/inf/pdf/publications/2008/P687.pdf.

12. Odên, J. & Anderson, D. Träs skjuvhållfasthet och limträbalkars tvärkraftskapacitet – provningar och beräkningar. Lund 2009, Division of Structural Mechanics, Lund University. 97 p. (In Swedish)

13. Dahl, K. Mechanical properties of clear wood from Norway spruce. 2009, Department of Structural Engineering, Norwegian University of Science and Technology. 235 p. ISBN 978-82-471-1911-2.

14. Fonselius, M. Effect of size on the bending strength of laminated veneer lumber. Wood Science and Technology 31. Springer-Verlag 1997.

15. Dahl, K. Mechanical properties of clear wood from Norway spruce. 2009, Department of Structural Engineering, Norwegian University of Science and Technology. 235 p. ISBN 978-82-471-1911-2.

Appendix A: Product information of used coatings

TEKNOS www.teknos.com

DATA SHEET 1040
6 17.02.2009

AQUATOP 2600
Varnish

VARNISH TYPE

AQUATOP 2600 varnish is a water-borne varnish based on acrylic that dries quickly and is weather-resistant.

USAGE

Wooden windows and outer doors. Before using the product, the manufacturer should be contacted to check the suitability of the product for the object in question.

TECHNICAL DATA

Solids	35 ±2% by volume
Total mass of solids	AQUATOP 2600-24 and AQUATOP 2600-03: abt. 400 g/l AQUATOP 2600-74: abt. 330 g/l
Volatile organic compound (VOC)	abt. 50 g/l
Theoretical spreading rate	5.0 m²/l (wet film 225 µm, dry film 81 µm)
Drying time, +23°C, relative humidity 50% (glass plate 120 µm)	
- dust free	after 20 min
- touch dry	after 30 min
	The drying times given are indicative because the product is intended for use on wooden substrates.
Overvarnishable	after 1 - 2 h
Thinner, clean up	Water
Finish	AQUATOP 2600-03: semi-matt AQUATOP 2600-24: semigloss AQUATOP 2600-74: semigloss
Colours	Clear

PTO

Appendix A: Product information of used coatings

DIRECTION FOR USE

Surface preparation	The surface must be clean and dry. The moisture content of the wood is to be below 20%. It is recommended that the wood is treated with an efficient wood preservative that protects it against rot, blue stain fungi and mildew.
Application conditions	The temperature of the air, the surface and the varnish shall be above +15°C and the relative humidity of the air below 80% during the time of application and drying. The best result is achieved when the temperature of the air is +23 - +38°C, the relative humidity of the air 50 - 70% and the ventilation is good.
Varnishing	Stir the varnish thoroughly before use. Apply by spray, also electrostatic spray can be used. AQUA PRIMER 2900-02 can be used as a primer. It is recommended that tinted AQUA PRIMER 2900-02 that has been used as primer is added into the top coating varnish in an amount of 3 - 5%.
STORAGE	Must not freeze. The best storage temperature is between +10 - +25°C.

Linogard underhållsolja – Natural wood protection!

PRODUCT INFORMATION

Composition: Extra pure Swedish cold-pressed linseed oil.

Uses: Water-proofing impregneting oil for wood outdoors and indoors; priming of wood before painting; treatment of wood surfaces.

Quantity needed: 1 L. covers approx. 6-10 m2.

Drying period: approx. 24 hours at room temperature.

General remarks on linseed oil: Rags, waste wool, sponges and the like that are used with linseed oil or with linseed-oil paints should be kept well moistened in airtight plastic bags, burnt, or kept in non-inflammable containers, preferably equipped with lids. Risk of selfignition!

Our impregnating oil contains a highly refined and particularly pure linseed oil which makes it able to penetrate more deeply into the wood. It is used on wood in particularly exposed environments. It can also be used indoors. The product contains no solvents or heavy metals.

Employment of impregnating oil: Impregnating oil can be used for many different purposes: for oiling of dried-out wood; for water-proofing of deckings, clading, garden furniture, trellises, landing-stages and boats and for treating unpainted wooden carpentry. The impregneting oil can also be used before painting as a priming oil, which prolongs paint life.

Work Procedure.

Use a paintbrush with natural bristle for application of impregnating oil. Apply the oil liberally without pouring it on. In places where the oil sinks in you may apply more. After about 30 minutes wipe the surface dry.

In order to obtain an especially fine surface, polish with fine sandpaper (abrasive index 220-240) while the oil is still wet, before wiping. The result will be a velvet-smooth surface.

Linogard impregnated wood: Use the impregnating oil for impregnating cuting edges and ends when working with decking or clading. Can also be used for maintaining the surface after cleaning.

Facades and windows: Before impregnating with oil, surfaces must be stripped and all old paint removed. Any glueing work should also be carried out before starting the treatment. Larger cracks in facades can be mended using linseed-oil cement of the same kind as window putty, which is then smoothed out with a rag dipped in linseed-oil varnish. Apply the impregnating oil liberally with a paintbrush, leave to dry for about 20-30 minutes and then wipe away the excess thoroughly with a rag. If the impregnated surface is to be painted, leave it to dry for at least 24 hours before applying the base-coat.

LINOTECH AB, Gamla Mejeriet Salavägen, 740 21 JÄRLÅSA, Sweden

Tel: +46 18 39 16 33, Fax +46 18 39 16 22, E-mail info@linotech.se

Appendix A: Product information of used coatings

Wood outdoors: Outdoor furniture, trellises and other wood located outdoors can be treated with impregnating oil once or several times depending on how exposed they are to wind and weather. Always make sure that the surface to be treated is clean and dry. Apply the oil liberally with a paintbrush, leave to dry about 20-30 minutes and then wipe away the excess thoroughly with a rag. The treatment may afterwards be repeated whenever necessary.

Wood by water: Landing-stages and boats can also be treated with impregnating oil. Make sure that all surfaces are clean and dry before starting work. Parts that are particularly exposed to water can be placed with the end of the wood in warm impregnating oil - this might mainly apply to fresh construction of landing-stages or foot-bridges near water. Apply the oil liberally with a paintbrush. At the end of each application wait about 20-30 minutes and then wipe away the excess with a rag. It is important here to repeat the treatment two or three times in order to saturate the wood.

Wood indoors: Untreated wooden furniture is perfectly suited to treatment with impregnating oil. It is however extremely important to make sure that all traces of paint stripper are gone, if paint was removed with lye or by any other chemical paint stripping method, as the slightest residue may spoil the work. Residues can be neutralised with vinegar essence diluted with water. It is always a good idea to sandpaper while the oil is still wet to get an especially fine surface.

Rustpreventive treatment: Priming with impregnating oil lends good basic protection against rust to iron fittings. Clean the surface thoroughly with e.g. a steel brush, to remove all loose material. Apply a thin coat of warm impregnating oil.

Linotech AB is a member of the Swedish Woodprotection Society.

Linotech AB is a company working in the cleantech-sector

LINOTECH AB, Gamla Mejeriet Salavägen, 740 21 JÄRLÅSA, Sweden

Tel: +46 18 39 16 33, Fax +46 18 39 16 22, E-mail info@linotech.se

Appendix B: Measured variables of the specimens in the pre-test phase and the ultimate loads

Beam	Coating	Ultimate load [kN]	Average height [mm]	Average width [mm]	Length [mm]	Mass [kg]
S1-1/8	Uncoated	361,7	539	115	3202	93,9
S1-2/8	Uncoated	374,4	539	115	3201	91,9
S1-3/8*	Uncoated	273,2	539	114	3202	92,7
S1-4/8**	Uncoated	369,4	539	114	3204	94
S1-5/8	Uncoated	300,5	539	115	3202	93,55
S1-6/8	Uncoated	375,3	539	115	3202	97,25
S1-7/8	Uncoated	336,8	539	115	3200	92,5
S1-8/8	Uncoated	355,6	538	115	3201	91,2

*Test result of the beam is ignored in the study due to bad test setup. Shear or bending rupture was not achieved, beam was damaged unusable near loading point and supports because of bad test setup.

**The beam was tested three times while improving the test setup between the tests. Load in the first two tests was near 300kN. The ultimate load was achieved in the third test which was done with the proper test setup shown in Figure 13.

Appendix B: Measured variables of the specimens in the pre-test phase and the ultimate loads

Beam	Coating	Ultimate load [kN]	Average height [mm]	Average width [mm]	Length [mm]	Mass [kg]
S2-1/24	A2	264,78	541	115	3199	95
S2-2/24	A2	402,91	540	115	3196	95,95
S2-3/24	A2	284,59	541	115	3201	95,45
S2-4/24	A1	292,45	540	115	3200	90,7
S2-5/24	A1	349,08	540	115	3199	95,25
S2-6/24	A1	297,61	540	115	3199	92,05
S2-7/24	A2	369,54	540	114	3201	90,95
S2-8/24	A2	373,6	540	114	3200	92,6
S2-9/24	A2	365,64	540	114	3202	90,6
S2-10/24	A1	367,88	540	114	3201	91,95
S2-11/24	A1	348,71	540	114	3202	89,2
S2-12/24	A1	336,05	539	114	3202	90,3
S2-13/24	L	379,71	539	115	3202	96,8
S2-14/24	L	371,21	539	115	3203	97,55
S2-15/24	L	401,62	539	115	3201	95,95
S2-16/24	Uncoated	343,15	540	115	3203	98,6
S2-17/24	Uncoated	395,88	540	115	3202	96,7
S2-18/24	Uncoated	375,4	540	115	3203	95,9
S2-19/24	L	350,11	539	115	3201	90,7
S2-20/24	L	377,42	538	115	3200	88,8
S2-21/24	L	353,23	539	115	3200	90,9
S2-22/24	Uncoated	355,35	539	115	3201	92,75
S2-23/24	Uncoated	329,8	539	115	3202	91,4
S2-24/24	Uncoated	423,95	539	115	3202	94,45

Beam	Coating	Ultimate load [kN]	Average height [mm]	Average width [mm]	Length [mm]	Mass [kg]
S3-1/24	A2	339,66	541	115	3202	95,65
S3-2/24	A2	353,59	541	115	3200	95,1
S3-3/24	A2	307,81	541	115	3200	94,25
S3-4/24	A1	339,77	540	115	3200	95,6
S3-5/24	A1	306,73	540	115	3197	92,7
S3-6/24	A1	313,55	540	115	3199	93,05
S3-7/24	A2	341,93	540	114	3205	92,85
S3-8/24	A2	345,47	540	114	3203	91,65
S3-9/24	A2	351,17	540	114	3203	93
S3-10/24	A1	395,37	539	114	3205	94,2
S3-11/24	A1	306,76	539	114	3206	85,75
S3-12/24	A1	366,43	539	114	3203	92
S3-13/24	L	375,07	539	115	3202	95
S3-14/24	L	391,88	539	115	3202	95,8
S3-15/24	L	350,92	539	115	3202	96,9
S3-16/24	Uncoated	386,73	540	115	3202	97,6
S3-17/24*	Uncoated	383,8	540	115	3202	97,15
S3-18/24	Uncoated	341,52	539	115	3202	94,1
S3-19/24	L	303,43	539	115	3201	94,4
S3-20/24	L	344,03	538	115	3201	93,4
S3-21/24	L	322,48	538	115	3203	92,95
S3-22/24	Uncoated	307,32	539	115	3201	91,85
S3-23/24	Uncoated	377,03	538	115	3201	91,75
S3-24/24	Uncoated	364,56	539	115	3201	89,35

* Movement limit of hydraulic actuator was achieved before actual failure, severe deformations on supports and on loading area.

Appendix B: Measured variables of the specimens in the pre-test phase and the ultimate loads

Beam	Coating	Ultimate load [kN]	Average height [mm]	Average width [mm]	Length [mm]	Mass [kg]
S4-1/24	A2	347,77	541	115	3200	93,05
S4-2/24	A2	318,72	541	115	3199	91,8
S4-3/24	A2	371,27	541	115	3201	92,15
S4-4/24	A1	334,23	540	115	3199	93,8
S4-5/24	A1	398,04	540	116	3199	89,95
S4-6/24	A1	375,03	540	115	3199	94,25
S4-7/24	A2	364,61	540	114	3201	91,35
S4-8/24	A2	346,26	540	114	3202	92,15
S4-9/24	A2	349,55	540	114	3201	90,55
S4-10/24	A1	388,85	539	114	3201	94,75
S4-11/24	A1	358,24	539	114	3200	90,2
S4-12/24	A1	352,73	540	114	3205	90,85
S4-13/24	L	418,41	539	115	3202	98,35
S4-14/24	L	342,08	539	115	3202	98,5
S4-15/24	L	379,17	539	115	3202	96,1
S4-16/24	Uncoated	359,68	540	115	3202	95,3
S4-17/24	Uncoated	404,3	539	115	3202	95,1
S4-18/24	Uncoated	372,26	539	115	3201	93,1
S4-19/24	L	358,2	538	115	3200	91,35
S4-20/24	L	351,86	538	115	3200	91,75
S4-21/24	L	372,13	538	115	3201	93,45
S4-22/24	Uncoated	365,13	538	115	3202	92,15
S4-23/24	Uncoated	404,39	539	115	3201	93,4
S4-24/24	Uncoated	389,89	539	115	3201	96,5

Beam	Coating	Ultimate load [kN]	Average height [mm]	Average width [mm]	Length [mm]	Mass [kg]
S5-1/24	A2	384,96	540	115	3198	91,2
S5-2/24	A2	342,97	540	115	3200	89,55
S5-3/24	A2	389,4	540	115	3199	94
S5-4/24	A1	328,06	540	115	3199	90,6
S5-5/24	A1	394,4	540	115	3200	93,55
S5-6/24	A1	382,35	540	115	3199	94,1
S5-7/24	A2	369,84	540	114	3201	92,2
S5-8/24	A2	387,98	540	114	3202	87,45
S5-9/24	A2	329,13	540	114	3202	91,75
S5-10/24	A1	347,78	540	114	3199	88,7
S5-11/24	A1	354,8	539	114	3201	92,25
S5-12/24	A1	359,16	539	114	3201	88,05
S5-13/24	L	416,48	539	115	3201	97,2
S5-14/24	L	375,77	539	115	3201	93,75
S5-15/24	L	333,32	539	115	3202	91,2
S5-16/24	Uncoated	391	540	115	3201	98,05
S5-17/24	Uncoated	393,47	540	115	3201	96,85
S5-18/24	Uncoated	398,7	540	115	3202	95,3
S5-19/24	L	325,05	538	115	3200	96,5
S5-20/24	L	329,2	538	115	3197	91,6
S5-21/24	L	325,35	538	115	3196	97,35
S5-22/24	Uncoated	413,69	539	115	3200	93,15
S5-23/24	Uncoated	394,7	539	115	3202	97,2
S5-24/24	Uncoated	341,34	539	115	3201	90,3

Appendix C: Measured values of moisture content for all specimens

		Moisture content of the test piece [%]				
Number of the beam in the test series	Test piece number	S1	S2	S3	S4	S5
1	1	10,90	13,00	12,77	11,53	9,86
	2	10,75	12,39	12,02	12,51	11,07
	3	10,78	12,28	11,76	12,61	11,33
	4	10,69	12,66	11,66	12,45	11,01
	5	11,04	13,08	12,13	11,32	9,68
2	1	11,44	12,78	13,11	11,30	9,46
	2	11,56	12,46	12,65	12,37	10,74
	3	11,36	12,35	12,04	12,62	10,80
	4	11,48	12,50	12,49	12,27	10,82
	5	11,42	12,71	13,03	11,18	9,65
3	1	11,61	12,24	13,27	11,48	9,73
	2	12,17	11,67	12,43	12,67	11,21
	3	12,03	11,61	12,40	12,84	11,54
	4	12,03	11,83	12,58	12,42	11,15
	5	12,06	12,95	13,08	11,06	9,99
4	1	11,49	13,42	13,45	10,94	9,37
	2	11,62	12,08	13,21	12,43	10,76
	3	11,59	11,57	12,74	12,53	11,01
	4	11,68	11,49	13,00	12,03	10,70
	5	11,75	11,55	13,52	10,35	9,34
5	1	14,51	11,47	13,21	10,48	9,31
	2	15,71	11,77	12,53	12,31	10,67
	3	15,63	11,96	12,45	12,49	10,98
	4	15,24	12,33	12,72	12,13	10,70
	5	13,91	13,02	13,31	10,32	9,20
6	1	14,14	13,60	13,47	11,04	9,65
	2	15,15	11,87	13,24	12,88	10,99
	3	15,12	11,81	13,25	12,87	11,34
	4	15,08	12,18	13,55	12,75	11,07
	5	14,30	13,93	14,13	11,02	9,48
7	1	11,43	12,76	13,93	12,11	10,85
	2	11,76	12,87	13,69	13,35	12,03
	3	11,81	12,72	13,40	13,66	12,09
	4	11,77	12,79	13,69	13,32	11,58
	5	11,37	12,69	14,18	12,08	10,37
8	1	11,49	13,32	14,05	11,90	10,06
	2	11,91	12,75	13,56	13,21	11,37
	3	11,95	12,21	13,46	13,33	11,71
	4	11,85	12,25	13,86	13,15	11,60
	5	11,39	12,84	14,34	11,78	10,34

Appendix C: Measured values of moisture content for all specimens

Number of the beam in the test series	Test piece number	Moisture content of the test piece [%]				
		S1	S2	S3	S4	S5
9	1	-	11,75	13,78	11,45	10,44
	2	-	12,06	13,52	12,58	11,90
	3	-	12,14	13,47	12,75	12,15
	4	-	12,47	13,73	12,44	11,85
	5	-	13,19	14,27	11,32	10,66
10	1	-	14,33	15,42	11,53	10,85
	2	-	12,97	14,50	13,26	12,39
	3	-	12,49	13,71	13,58	12,64
	4	-	12,61	13,30	13,41	12,24
	5	-	13,30	12,72	11,71	10,86
11	1	-	13,39	13,34	11,37	10,33
	2	-	12,78	13,58	13,16	11,84
	3	-	12,38	13,88	13,57	12,09
	4	-	12,40	14,37	12,43	11,62
	5	-	13,03	14,21	11,67	10,11
12	1	-	13,30	15,28	11,55	10,36
	2	-	12,92	14,72	13,52	11,93
	3	-	12,77	14,27	13,95	12,19
	4	-	12,32	14,84	13,69	11,88
	5	-	13,22	15,63	11,74	10,32
13	1	-	16,38	14,88	12,41	10,23
	2	-	15,93	15,10	14,72	12,32
	3	-	15,50	15,09	15,39	12,84
	4	-	15,08	14,92	14,94	12,31
	5	-	14,32	14,17	12,15	10,39
14	1	-	14,40	13,49	12,04	10,34
	2	-	14,94	14,61	14,45	12,27
	3	-	15,10	15,06	14,70	12,74
	4	-	14,89	15,35	14,06	12,52
	5	-	14,56	15,15	11,86	10,24
15	1	-	14,75	15,20	12,15	10,32
	2	-	15,23	15,90	14,43	12,40
	3	-	15,23	15,89	14,85	12,94
	4	-	15,30	15,89	14,07	12,45
	5	-	15,02	15,43	11,58	10,33
16	1	-	15,93	15,76	12,15	10,46
	2	-	15,46	16,20	14,62	12,49
	3	-	15,33	16,08	14,87	12,68
	4	-	15,84	15,87	14,03	12,23
	5	-	16,10	15,32	11,70	10,09
17	1	-	14,60	15,46	11,79	10,44
	2	-	14,86	15,78	14,40	12,76
	3	-	14,60	15,76	14,74	13,26
	4	-	14,65	15,84	14,16	12,85
	5	-	14,28	15,23	11,54	10,54

Number of the beam in the test series	Test piece number	Moisture content of the test piece [%]				
		S1	S2	S3	S4	S5
18	1	-	15,79	15,42	11,82	10,48
	2	-	15,71	15,74	14,45	12,97
	3	-	15,38	15,74	14,69	13,35
	4	-	15,59	15,45	13,98	12,76
	5	-	15,58	15,29	11,20	10,15
19	1	-	12,71	13,76	10,28	9,45
	2	-	12,07	13,43	12,02	11,01
	3	-	12,02	12,94	12,26	11,42
	4	-	12,19	13,52	11,98	11,04
	5	-	12,82	14,01	10,38	9,55
20	1	-	12,48	14,11	10,08	9,39
	2	-	11,88	13,62	11,66	10,81
	3	-	11,70	13,33	11,87	11,18
	4	-	11,36	13,54	11,30	10,70
	5	-	11,13	13,62	9,47	9,45
21	1	-	11,52	13,27	10,08	9,87
	2	-	12,18	13,07	11,99	11,46
	3	-	12,46	13,19	12,61	11,56
	4	-	12,11	13,39	12,38	11,28
	5	-	13,94	14,90	10,85	9,84
22	1	-	13,33	13,02	10,96	9,74
	2	-	12,90	12,93	12,82	11,34
	3	-	12,71	13,26	13,12	11,60
	4	-	12,89	12,65	12,54	11,35
	5	-	13,54	12,89	10,33	9,59
23	1	-	13,18	11,42	10,57	9,43
	2	-	12,37	11,88	12,72	11,11
	3	-	12,40	12,05	12,88	11,45
	4	-	16,44	12,51	12,67	11,36
	5	-	14,19	13,23	10,62	9,90
24	1	-	12,86	12,42	10,67	9,89
	2	-	12,85	12,04	12,42	11,46
	3	-	13,06	12,20	12,82	11,58
	4	-	13,30	12,30	12,48	11,03
	5	-	13,33	12,66	10,59	9,27

VTT Working Papers

141 Juha Forström, Esa Pursiheimo, Veikko Kekkonen & Juha Honkatukia. Ydinvoimahankkeiden periaatepäätökseen liittyvät energia- ja kansantaloudelliset selvitykset. 2010. 82 s. + liitt. 29 s.

142 Ulf Lindqvist, Maiju Aikala, Maija Federley, Liisa Hakola, Aino Mensonen, Pertti Moilanen, Anna Viljakainen & Mikko Laukkanen. Hybrid Media in Packaging. Printelligence. 2010. 52 p. + app. 7 p.

143 Olavi Lehtoranta. Knowledge flows from incumbent firms to newcomers. The growth performance of innovative SMEs and services start-ups. 2010. 36 p. + app. 2 p.

144 Katri Grenman. The future of printed school books. 2010. 42 p.

145 Anders Stenberg & Hannele Holttinen. Tuulivoiman tuotantotilastot. Vuosiraportti 2009. 2010. 47 s. + liitt. 5 s.

146 Antti Nurmi, Tuula Hakkarainen & Ari Kevarinmäki. Palosuojattujen puurakenteiden pitkäaikaistoimivuus. 2010. 39 s. + liitt. 6 s.

147 Juhan Viitaniemi, Susanna Aromaa, Simo-Pekka Leino, Sauli Kiviranta & Kaj Helin. Integration of User-Centred Design and Product Development Process within a Virtual Environment. Practical case KVALIVE. 2010. 39 p.

148 Matti Pajari. Prestressed hollow core slabs supported on beams. Finnish shear tests on floors in 1990–2006. 2010. 674 p.

149 Tommi Ekholm. Achieving cost efficiency with the 30% greenhouse gas emission reduction target of the EU. 2010. 21 p.

150 Sampo Soimakallio, Mikko Hongisto, Kati Koponen, Laura Sokka, Kaisa Manninen, Riina Antikainen, Karri Pasanen, Taija Sinkko & Rabbe Thun. EU:n uusiutuvien energialähteiden edistämisdirektiivin kestävyyskriteeristö. Näkemyksiä määritelmistä ja kestävyyden todentamisesta. 130 s. + liitt. 7 s.

151 Ian Baring-Gould, Lars Tallhaug, Göran Ronsten, Robert Horbaty, René Cattin, Timo Laakso, Michael Durstewitz, Antoine Lacroix, Esa Peltola & Tomas Wallenius. Wind energy projects in cold climates. 2010. 62 p.

152 Timo Laakso, Ian Baring-Gould, Michael Durstewitz, Robert Horbaty, Antoine Lacroix, Esa Peltola, Göran Ronsten, Lars Tallhaug & Tomas Wallenius. State-of-the-art of wind energy in cold climates. 2010. 69 p.

153 Teemu Tommila, Juhani Hirvonen & Antti Pakonen. 2010. Fuzzy ontologies for retrieval of industrial knowledge – a case study. 54 p. + app. 2 p.

154 Raili Alanen. Veneiden uudet energiajärjestelmät. 2010. 82 s.

157 Tero Sundström, Ari Kevarinmäki, Stefania Fortino & Tomi Toratti. Shear resistance of glulam beams under varying humidity conditions. 2011. 125 p. + app. 12 p.

ISBN 978-951-38-7498-8 (URL: http://www.vtt.fi/publications/index.jsp)
ISSN 1459-7683 (URL: http://www.vtt.fi/publications/index.jsp)